

Nagasaki Symposium on  
Nano-Dynamics 2009  
(NSND-2009)

January 27, 2009

General Education and Research Building  
Nagasaki University, Nagasaki, Japan

Organizing Committee

Nano-Dynamics Group, Nagasaki University

# Program Overview

| Time                     | Title etc.  | Authors & Affiliation  |
|--------------------------|---|--|
| 9:20-9:40                | Welcome Address<br><br>About Nano-Dynamics Project in Nagasaki  | Dr. Shigeru Katamine (President of Nagasaki Univ.)<br><br>Prof. Takamasa Sagara (Leader of Research Project, Nagasaki Univ.) |
| <b>Invited Lecture 1</b> |   |  |
| 9:40-10:30               | Functionalization of Hydrogen/Deuterium-Terminated and Oxidized Diamond, and Layer-by-Layer Growth of Polymer/Nanodiamond Multilayers as Applied to Separation Science        | Prof. Matthew R. Linford (Brigham Young Univ., USA)  |
| 10:30-11:00              | Si Nanowires FET Prepared by Ion-implantation   | Prof. Sang-Kwon Lee (Chonbuk Nat'l Univ., Korea)   |
| 11:15-12:05              | NO <sub>x</sub> Adsorption on SnO <sub>2</sub> Nanoparticles: Dynamics of the Surface Reactions in Correlation with SnO <sub>2</sub> Sensing Properties                       | Prof. Marie-Isabelle Baraton (Univ. of Limoges & CNRS, SPCTS, France)  |
| 12:05-12:35              | Application of Ion Migration at Solid-solid Microcontact  | Dr. Kai Kamada (Nagasaki Univ., Japan)   |
| 12:35-14:00              | Lunch Time  |  |
| <b>Invited Lecture 2</b> |   |  |
| 14:00-14:50              | Molecular Metal Wires and Molecular Switches  | Prof. Shie-Ming Peng (Nat'l Taiwan Univ., Taiwan)  |
| 14:50-15:20              | Carbon Nanotube Infiltration: a Versatile Approach for Fabricating High Aspect Ratio Microstructures Using Carbon Nanotube Frameworks   | Prof. Robert C. Davis (Brigham Young Univ., USA)   |
| 15:20-15:30              | Coffee Break  |  |
| 15:30-16:40              | <b>Poster Presentation Short Talks</b>  |  |
| 16:40-18:15              | <b>Poster Session</b>   |  |
| 18:20-18:30              | Closing Remarks<br><br>Prof. Toru Shigechi (Dean of Faculty of Engineering, Nagasaki Univ.)<br><br>Prof. Hideaki Nakata (Dean of Graduate School of Sci&Tech, Nagasaki Univ.) |  |
| 18:50-20:20              | Scientific mixer for research plan exchange in Student Union (Sei-kyo 2F) (Students Poster Prize Winner Celebration)  |  |

# Symposium Organization

## HONORED SYMPOSIUM CHAIRS

|                        |   |
|------------------------|---|
| Prof. Shigeru Katamine | President of Nagasaki Univ.                                       |
| Prof. Toru Shigechi    | Dean of Faculty of Engineering, Nagasaki Univ.                    |
| Prof. Hideaki Nakata   | Dean of Graduate School of Science and Technology, Nagasaki Univ. |

## ORGANIZING COMMITTEE CHAIR

|                       |                   |
|-----------------------|-------------------|
| Prof. Takamasa Sagara | Applied Chemistry |
|-----------------------|-------------------|

## PROGRAM CHAIRS

|                        |                                       |
|------------------------|---------------------------------------|
| Prof. Takamasa Sagara  | Applied Chemistry                     |
| Prof. Yasuhiro Shimizu | Materials Science and Engineering     |
| Prof. Isamu Moriguchi  | Applied Chemistry                     |
| Prof. Masaki Nakano    | Electrical and Electronic Engineering |

## ADVISORY BOARD

|                          |                                   |
|--------------------------|-----------------------------------|
| Prof. Masakazu Iwamoto   | Tokyo Institute of Technology     |
| Prof. Kunihiro Koumoto   | Nagoya University                 |
| Prof. Masayoshi Onishi   | Applied Chemistry                 |
| Prof. Masatomo Iwao      | Applied Chemistry                 |
| Prof. Makoto Egashira    | Materials Science and Engineering |
| Prof. Mutsuhisa Furukawa | Materials Science and Engineering |
| Prof. Masayuki Hasaka    | Materials Science and Engineering |
| Prof. Yasuo Uchiyama     | Materials Science and Engineering |
| Prof. Akio Kagawa        | Materials Science and Engineering |

## SYMPOSIUM COMMITTEE

|                            |                                       |
|----------------------------|---------------------------------------|
| Prof. Hiroshi Fujiyama     | Electrical and Electronic Engineering |
| Prof. Hirotohi Fukunaga    | Electrical and Electronic Engineering |
| Dr. Masanori Shinohara     | Electrical and Electronic Engineering |
| Prof. Tomomitsu Hatakeyama | Applied Chemistry                     |
| Dr. Keisuke Umakoshi       | Applied Chemistry                     |
| Dr. Hiroto Murakami        | Applied Chemistry                     |
| Dr. Masanari Kimura        | Applied Chemistry                     |
| Dr. Tsutomu Fukuda         | Applied Chemistry                     |
| Dr. Yoshiyuki Egami        | Applied Chemistry                     |
| Dr. Shuji Tanabe           | Materials Science and Engineering     |
| Dr. Guo-Bin Zheng          | Materials Science and Engineering     |
| Dr. Takeshi Ohgai          | Materials Science and Engineering     |
| Dr. Ken Kojio              | Materials Science and Engineering     |
| Dr. Kai Kamada             | Materials Science and Engineering     |
| Dr. Takeo Hyodo            | Materials Science and Engineering     |

# Contents

|  |   |
|--|---|
| <b>Preface</b>   | 1 |
| <b>Materials Science Based on Nano-Dynamics in Nagasaki University</b> | 3 |

## Invited Lecture

|       |   |    |
|-------|---|----|
| [I01] | Functionalization of Hydrogen/Deuterium-Terminated and Oxidized Diamond, and Layer-by-Layer Growth of Polymer/Nanodiamond Multilayers as Applied to Separation Science  | 5  |
|       | <i>M. R. Linford<sup>1</sup>, R. C. Davis<sup>1</sup>, Li Yang<sup>1</sup>, G. Saini<sup>1</sup>, N. Shirahata<sup>2</sup>, R. B. Blake<sup>1</sup>, L. Wiest<sup>1</sup>, D. Jensen<sup>1</sup>, A. Dadson<sup>3</sup>, M. A. Vail<sup>3</sup></i><br>( <sup>1</sup> Brigham Young Univ., USA, <sup>2</sup> NIMS, Japan, <sup>3</sup> U.S. Synthetic Corp., USA) |    |
| [I02] | Si Nanowires FET Prepared by Ion-implantation   | 6  |
|       | <i>S.-K. Lee (Chonbuk Nat'l Univ., Korea)</i>   |    |
| [I03] | NOx Adsorption on SnO <sub>2</sub> Nanoparticles: Dynamics of the Surface Reactions in Correlation with SnO <sub>2</sub> Sensing Properties   | 7  |
|       | <i>M.-I. Baraton (Univ. of Limoges &amp; CNRS, SPCTS, France)</i>   |    |
| [I04] | Application of Ion Migration at Solid-solid Microcontact  | 9  |
|       | <i>K. Kamada (MSE, Nagasaki Univ., Japan)</i>   |    |
| [I05] | Molecular Metal Wires and Molecular Switches  | 11 |
|       | <i>S.-M. Peng (Nat'l Taiwan Univ., Taiwan)</i>  |    |
| [I06] | Carbon Nanotube Infiltration: a Versatile Approach for Fabricating High Aspect Ratio Microstructures Using Carbon Nanotube Frameworks   | 12 |
|       | <i>D. N. Hutchison, N. B. Morrill, Q. Aten, B. W. Turner, B. D. Jensen, L. L. Howell, R. R. Vanfleet, R. C. Davis (Brigham Young Univ., USA)</i>  |    |

## Poster Presentation

|       |   |    |
|-------|---|----|
| [P01] | Luminescent Heteropolynuclear Complexes of 3,5-Dimethylpyrazolate [Pt <sub>2</sub> Au <sub>2</sub> M <sub>2</sub> (Me <sub>2</sub> pz) <sub>8</sub> ] (M = Ag, Cu) Showing Synergetic Effect of Three Transition Elements in the Excited State  | 14 |
|       | <i>K. Umakoshi<sup>1</sup>, K. Saito<sup>1</sup>, Y. Arikawa<sup>1</sup>, M. Onishi<sup>1</sup>, S. Ishizaka<sup>2</sup>, N. Kitamura<sup>2</sup>, Y. Nakao<sup>3</sup> and S. Sakaki<sup>3</sup> (<sup>1</sup>Nagasaki Univ., <sup>2</sup>Hokkaido Univ., <sup>3</sup>Kyoto Univ.)</i> |    |
| [P02] | Synthesis and Reactivities of a Nitrosoethane Complex having a Hydrotris (pyrazol-1-yl)borato Ligand  | 15 |
|       | <i>S. Tashita, H. Miyahara, Y. Arikawa, K. Umakoshi and M. Onishi (AC, Nagasaki Univ.)</i>  |    |
| [P03] | Physical and Mechanical Properties of Polyurethanes Crosslinked by [3]Rotaxane  | 17 |
|       | <i>S. Ohira<sup>1</sup>, R. Kusano<sup>1</sup>, K. Kojio<sup>2</sup>, M. Furukawa<sup>2</sup>, T. Sagara<sup>1</sup> and H. Murakami<sup>1</sup> (<sup>1</sup>AC and <sup>2</sup>MSE, Nagasaki Univ.)</i>   |    |

|       |   |    |
|-------|---|----|
| [P04] | Convenient Synthesis of Pyrrolidine by Amphiphilic Allylation<br><i>K. Tohyama, Y. Yamaguchi and M. Kimura (AC, Nagasaki Univ.)</i>   | 19 |
| [P05] | Regulated Optical Properties of Single-walled Carbon Nanotubes via Redox Reaction<br><i>Y. Tanaka, K. Hirayama, T. Fujigaya, Y. Niidome and N. Nakashima (Kyushu Univ.)</i>   | 21 |
| [P06] | Electrochemical behaviors of fructose dehydrogenase immobilized onto UV-ozone-treated carbon nanotubes modified electrode<br><i>S. Kaneko, H. Yamaguchi, S. Sakamoto, T. Nishimura, M. Tominaga and I. Taniguchi (Kumamoto Univ.)</i>   | 22 |
| [P07] | Anti-oxidation Property of CNT/PyC/SiC Coating for Carbon/Carbon Composites<br><i>Y. Mukojima, H. Sano, G.-B. Zheng and Y. Uchiyama (MSE, Nagasaki Univ.)</i>   | 24 |
| [P08] | Growth of Carbon Nanotubes on Carbon Nanofibers<br><i>S. Muranaka, H. Sano, G.-B. Zheng and Y. Uchiyama (MSE, Nagasaki Univ.)</i>   | 26 |
| [P09] | Preparation of Mesoporous and Meso-macroporous Tin Dioxide Powders and Their Application to Sensor Materials<br><i>L. Yuan, T. Hyodo, Y. Shimizu and M. Egashira (MSE, Nagasaki Univ.)</i>  | 28 |
| [P10] | Hydrogen Sensing Properties of Anodized TiO <sub>2</sub> Film Sensors Equipped with Pd and Pt Electrodes in Different Structure<br><i>M. Nakaoka, T. Hyodo, Y. Shimizu and M. Egashira (MSE, Nagasaki Univ.)</i>  | 30 |
| [P11] | Preparation of Pore Filling Membrane with Pd Nanoparticles<br><i>A. Tominaga, O. Nakagoe and S. Tanabe (MSE, Nagasaki Univ.)</i>  | 32 |
| [P12] | Preparation of Au-Pd Core-shell Nanoparticles Supported TiO <sub>2</sub> Photocatalyst with Sonochemical Technique<br><i>H. Ejima, O. Nakagoe, N. Shima, A. Tominaga and S. Tanabe (MSE, Nagasaki Univ.)</i>  | 34 |
| [P13] | Substrate Bias Effect on Deposition Process of Amorphous Carbon Films<br><i>T. Inayoshi<sup>1</sup>, H. Kawazoe<sup>1</sup>, M. Shinohara<sup>1</sup>, Y. Matsuda<sup>1</sup>, H. Fujiyama<sup>1</sup>, Y. Nitta<sup>2</sup> and T. Nakatani<sup>2</sup><br/>(<sup>1</sup>EEE, Nagasaki Univ., <sup>2</sup>Toyo Adv. Tech. Co., Ltd.)</i> | 36 |
| [P14] | Source Molecular Effect on Amorphous Carbon Film Deposition<br><i>H. Kawazoe<sup>1</sup>, T. Inayoshi<sup>1</sup>, M. Shinohara<sup>1</sup>, Y. Matsuda<sup>1</sup>, H. Fujiyama<sup>1</sup>, Y. Nitta<sup>2</sup> and T. Nakatani<sup>2</sup><br/>(<sup>1</sup>EEE, Nagasaki Univ., <sup>2</sup>Toyo Adv. Tech. Co., Ltd.)</i>           | 38 |
| [P15] | Surface Modification due to Solution Plasma<br><i>Z. Shuai, K. Akaki, K. Shimizu, K. Kotani, M. Shinohara, Y. Matsuda and H. Fujiyama (EEE, Nagasaki Univ.)</i>   | 40 |
| [P16] | Monitoring of Chemical Vapor Deposition Process of Hydrocarbon Thin Films by Optical Reflectance Interferometry<br><i>K. Uehara, M. Shinohara and Y. Matsuda (EEE, Nagasaki Univ.)</i>  | 42 |
| [P17] | Influence of Hydrogen Addition on Electric and Optical Properties of Sputter-deposited Aluminum-doped Zinc Oxide Thin Films<br><i>R. Kan, T. Iwata, T. Shibasaki, M. Shinohara and Y. Matsuda (EEE, Nagasaki Univ.)</i>   | 44 |

|       |  |    |
|-------|--|----|
| [P18] | Porous V <sub>2</sub> O <sub>5</sub> /Carbon Nano-composites Electrodes for Rechargeable Power Sources with Large Capacity and High Power<br><i>I. Moriguchi, K. Matsuo and H. Yamada (AC, Nagasaki Univ.)</i>   | 46 |
| [P19] | Proton Conducting Membrane Prepared from Organic-Inorganic Hybrid Precursor for Intermediate Temperature Fuel Cells<br><i>H. Yamada, S. Aono and I. Moriguchi (AC, Nagasaki Univ.)</i>   | 48 |
| [P20] | Coupled Dynamics of Au-nanoparticles and Surfactants Driven by Potential Control on a Au(111) Electrode Surface<br><i>K. Izumi and T. Sagara (AC, Nagasaki Univ.)</i>  | 50 |
| [P21] | Spectroelectrochemical Study for Dyes Adsorbed on Gold Nano-Rings Immobilized on an ITO Electrode<br><i>G. Imasaki and T. Sagara (AC, Nagasaki Univ.)</i>  | 52 |
| [P22] | Spatio-Temporal Observation of Potential-driven Dynamics of <i>n</i> -Hexadecane Liquid Thin Layer on a Au(111) Electrode by Fluorescence Microscopic Imaging and Electroreflectance Measurements<br><i>D. Goto, H. Nagatani and T. Sagara (AC, Nagasaki Univ.)</i>  | 54 |
| [P23] | Structural Change Effect of Ferritin on the Electrode Reaction<br><i>M. Tominaga, K. Nakao and I. Taniguchi (Kumamoto Univ.)</i>   | 56 |
| [P24] | One Dimensional Kramers-Grote-Hynes-based Reaction Rate Analysis on Thermally Bleaching Process of Spirooxazines<br><i>Y. Shigemitsu<sup>1</sup> and Y. Ohga<sup>2</sup> (<sup>1</sup>Ind. Tech. Center of Nagasaki, <sup>2</sup>Oita Univ.)</i>   | 58 |
| [P25] | First-principles Study on Electron Transport Property through Graphene Strips<br><i>Y. Egami<sup>1</sup>, T. Ono<sup>2</sup> and K. Hirose<sup>2</sup> (<sup>1</sup>AC, Nagasaki Univ., <sup>2</sup>Osaka Univ.)</i>   | 60 |
| [P26] | Surface Molecular Mobility of Crosslinked Polyurethane by Scanning Force Microscopy<br><i>T. Osajima, S. Matsumura, S. Motokucho, K. Kojio and M. Furukawa (MSE, Nagasaki Univ.)</i>   | 62 |
| [P27] | Temperature Dependent Atomic Force Microscopic Study of Microphase-separated Structure of Polyurethane Elastomers<br><i>Y. Nishino, S. Motokucho, K. Kojio and M. Furukawa (MSE, Nagasaki Univ.)</i>   | 63 |
| [P28] | Absorption Measurement of Zn Atom Density during ICP-assisted Magnetron Sputter-deposition of Al-doped ZnO Thin Films<br><i>T. Iwata, R. Kan, T. Shibasaki, M. Shinohara and Y. Matsuda (EEE, Nagasaki Univ.)</i>  | 64 |
| [P29] | Observation of Arcing in DC Magnetron Sputtering of AZO Target<br><i>K. Komine, M. Shinohara and Y. Matsuda (EEE, Nagasaki Univ.)</i>  | 66 |
| [P30] | Inner Wall DLC Coating of Narrow Tubes by Using the 2nd Harmonic ECR Micro Plasma<br><i>K. Yan<sup>1</sup>, Y. Nitta<sup>2</sup>, T. Nakatani<sup>2</sup>, K. Okamoto<sup>2</sup>, M. Shinohara<sup>1</sup> and H. Fujiyama<sup>1</sup> (<sup>1</sup>EEE, Nagasaki Univ., <sup>2</sup>Toyo Adv. Tech. Co., Ltd.)</i>         | 68 |
| [P31] | CVD•PVD Hybrid DLC Coating to Extra Fine Wire by Quadrupole Magnetron Plasmas<br><i>S. Yoshitsune<sup>1</sup>, S. Nishiyama<sup>2</sup>, N. Iwamoto<sup>2</sup>, Y. Tokunaga<sup>2</sup>, M. Shinohara<sup>1</sup> and H. Fujiyama<sup>1</sup> (<sup>1</sup>EEE, Nagasaki Univ., <sup>2</sup>Japan Fine Steel Co., Ltd.)</i> | 70 |

AC: Department of Applied Chemistry

MSE: Department of Materials Science and Engineering

EEE: Department of Electrical and Electronic Engineering

in Nagasaki University

- [P32] Generation of Micro Plasma Surrounded by Solid Wall for Sub-ECR Condition 72  
*A. Yukishige, M. Shinohara and H. Fujiyama (EEE, Nagasaki Univ.)*
- [P33] Magnetic Property of Electrodeposited Ni-W, Ni-Mo and Ni-Cr Alloys 74  
*T. Fujimaru<sup>1</sup>, T. Ohgai<sup>1</sup>, K. Takao<sup>1</sup>, M. Mizumoto<sup>1</sup>, A. Kagawa<sup>1</sup>, Y. Tanaka<sup>2</sup>  
 and S. Sumita<sup>2</sup> (<sup>1</sup>MSE, Nagasaki Univ., <sup>2</sup>TDK Corp.)*
- [P34] Electrodeposition Process of Zn-Te Compound Semiconductors 76  
*Y. Kawanaka<sup>1</sup>, T. Ohgai<sup>1</sup>, K. Takao<sup>1</sup>, M. Mizumoto<sup>1</sup>, A. Kagawa<sup>1</sup>, Y. Tanaka<sup>2</sup>  
 and S. Sumita<sup>2</sup> (<sup>1</sup>MSE, Nagasaki Univ., <sup>2</sup>TDK Corp.)*
- [P35] Electrochemical Synthesis of Zn-Al-based Layered Double Hydroxides 78  
 Intercalated with 4-hydroxy-3-methoxy Cinnamic Acid as a UV-ray Absorbent  
*N. Hario, K. Kamada, T. Hyodo, Y. Shimizu and M. Egashira  
 (MSE, Nagasaki Univ.)*

|   |                        |
|---|------------------------|
| AC: Department of Applied Chemistry<br>MSE: Department of Materials Science and Engineering<br>EEE: Department of Electrical and Electronic Engineering | in Nagasaki University |
|---|------------------------|

## Preface

### **For the Development of Research Project “Materials Science Based on Nano-Dynamics” to Make Nagasaki be a Hot-Spot of New Trends of Interdisciplinary Nano-Science**

Takamasa Sagara<sup>1,2\*</sup>

<sup>1</sup>*Department of Applied Chemistry, Faculty of Engineering, Nagasaki University*

<sup>2</sup>*Leader of the “Nano-Dynamics” Research Project*

Over two years have passed since our project entitled “Materials Science Based on Nano-Dynamics” (formally, “Fusional Science of Materials Based on Nano-Dynamics”) was kicked off as one of the Nagasaki University Priority Research Projects. Our project emphasizes both challenging fundamental research by outstanding young chemists and physicists and advanced applied research for the development of material fabrication technologies. We are targeting the core issue of nano-science, namely, understanding of spatio-temporal dynamics in nano-world and its application.

Our concept of nano-dynamics, looking ahead to the future of nano-science and technology, incorporates the following three main points:

1. Development of unique spatio-temporal functions based on highly controlled and reversible movements of nano-units and entities.
2. Establishment of fabrication processes and techniques for producing special nano-structures by utilizing the dynamic motions of molecules, assemblies and clusters, and for preparing nano-regulated reaction media such as “nano-spaces”.
3. Functionalization of advanced materials to a high level based on nano-scale changes of state and movements of nano-entities.

The research is now ongoing in Departments of Electrical and Electronic Engineering, Materials Science and Engineering, and Applied Chemistry in Faculty of Engineering as well as in Graduate School of Science and Technology.

The first international symposium of our project, “Nagasaki Symposium on Nano-Dynamics 2008 (NSND2008)”, was successfully held on January 29, 2008. Seven scientific lectures, including four by invited oversea speakers, and 42 poster presentations attracted 134 participants [1]. On December 2, 2008, “Memorial Symposium on Nano-Dynamics” was held on the basis of the agreement on academic cooperation between Nagasaki University and University of Bari, Italy. Three



delegates from Italy made a courtesy call on President Katamine and gave lectures in front of 97 audiences.

Following these international symposia, it is pleased for us to hold “Nagasaki Symposium on Nano-Dynamics 2009 (NSND2009)” on January 27, 2009.

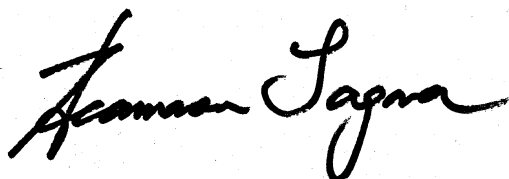
The chief objective of the symposium in 2009 is to provide a forum for researchers working in the many and expanding fields of nano-science and nano-technology in relation to a keyword of “**dynamics**”, including, for example, basic and applied chemistry, materials science and technology, nano-bio/organic/inorganic science, and electric and magnetic technologies.

Furthermore, the research project team has intention, by organizing this symposium and through the development and activation of the new concept of “nano-dynamics”, to found a center of excellence. Our Nagasaki-based research center should be regarded as a hot-spot of new trends of interdisciplinary nano-science. For example, we should be able to display a flag advertising the project by mapping down “*Visit Nagasaki to get meeting with the science and technology of nano-dynamics*”. The hot-spot should serve the meeting ground for youths of vision in nano-science, achieve unprecedented results of research, and foster and secure young investigators who can fly high ahead to future global development of Chemistry and Materials Science. The symposium is designed to harness and dynamize more effective network among researchers across various fields and to provide a broader and international range of opportunities for discussions and presentations of all topics.

Join in the discussion in the second NSND and find hints to impact the future of interfacial nano-science.

[1] see <http://naosite.lb.nagasaki-u.ac.jp/dspace/handle/10069/9871>

**Acknowledgement:** This symposium is financially supported by the Nagasaki University president’s discretionary fund for Priority Research Projects, for which we are most grateful. We are also indebted to University president and headquarters, Deans of Faculty of Engineering and Graduate School of Science and Technology for the highest encouragements.



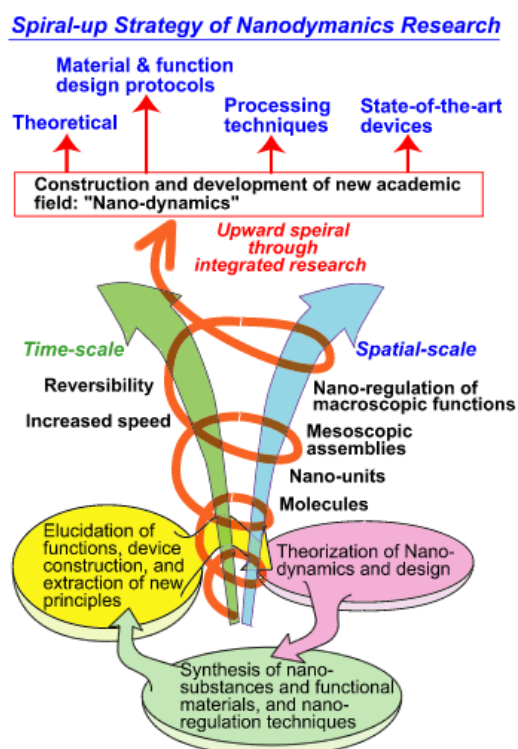
Takamasa Sagara  
**Organizing Committee Chair**

## Materials Science Based on Nano-Dynamics

In the burgeoning field of nanoscale science, especially in the fields of chemistry and materials science, the main emphasis has so far been on constructing novel and unique nanostructures and functionalizing of specific substances. However, the investigation of *nanoscale dynamic processes* has received less attention, even though it is a critical aspect of nanoscience in both physics and chemistry. Our understanding of the spatiotemporal dynamism of molecules and clusters has not yet been theoretically deepened; thus, there is a lack of potential applications in nano-processes and nanomaterial preparations. With the novel and indispensable concept of “*Nano-dynamics*”, we will develop the theoretical aspects of this field as a foundation for integrated nanoscience research enterprise and material innovation. We will emphasize both challenging fundamental research by outstanding young materials chemists and physicists and the development of material fabrication technologies with regard to explicit target applications. We will maintain a clear strategy of integrating research resources in order to investigate new areas in nanoscience and nanotechnology. This strategy involves an upward spiral of theorization, materials synthesis, and device construction, in addition to complementary development of nanomaterial hierarchies on both temporal and spatial scales, leading to the establishment of the new academic and technological field of nano-dynamics.

Our concept of nano-dynamics, looking ahead to the future of nanoscience and technology, incorporates the following three main points: (i) Development of unique spatiotemporal functions based on highly controlled and reversible movements of nano-units and entities, (ii) Establishment of fabrication processes and techniques for producing special nanostructures by utilizing the dynamic motions of molecules, assemblies and clusters, and for preparing nano-regulated reaction media such as “nano-spaces”, and (iii) Functionalization of advanced materials to a high level based on nanoscale changes of state and movements of nano-entities.

*The intellectual discipline of “Nano-dynamics” will make possible a number of unprecedented achievements*



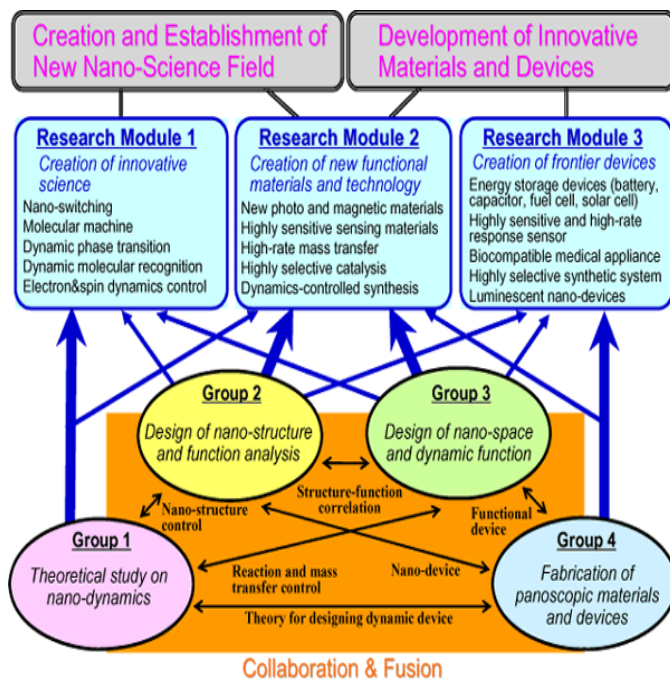
in structural design, materials processing, and production of state-of-the-art devices. This discipline will breathe fresh life into nanotechnology research by unifying the currently scattered fields of materials nanoscience. We will try to sweep away disciplinary boundaries, to focus researchers' strengths, and to visualize an abundance of goals. We aim at creating and establishing a new field of nanoscience for developing advanced functional materials and innovative frontier devices. Therefore, we will be established via interdisciplinary collaborative and integrated research. The research projects will be developed based on an upward-spiral strategy; that is, (1) theoretical study of nano-dynamics → (2) design and creation of new substances and materials based on nano-dynamics → (3) fabrication of functional materials and devices → and then back to (1). Three research modules will be set up on an ad hoc basis in view of concrete targets as shown in the figure, while the research targets will be achieved by four specialized research groups working in close cooperation:

• **Group 1: Theoretical study of nano-dynamics:** Understanding, theory, and realization of highly controlled movement of nano-entities; elucidation of the origin of dynamics and nano-level phase separation; amplification to macroscopic signals and application to molecular machines.

• **Group 2: Design of nanostructure and function analysis:** Control and design of unique nano-fields for chemical reactions; molecular recognition by specially designed functional nanostructures; creation of new functions via analysis of dynamic transformation of substances at nanostructure surfaces.

• **Group 3: Design of nano-space and dynamic functions:** Innovative synthesis using nano-spaces, novel nano-column synthetic systems and metal complex supra-structures; development of advanced energy storage devices with extremely high-rate charging-discharging function via control of mass-transfer dynamics in nano-space.

• **Group 4: Fabrication of panoscopic materials and devices:** Construction and analysis of panoscopic materials by computer simulation; plasma nano-coatings for functional thin films; design and synthesis of novel micro-machines comprising panoscopic materials.



# Invited Lecture

## Si Nanowires FET Prepared by Ion-implantation

Sang-Kwon Lee

*Department of Semiconductor Science and Technology, Chonbuk National University*

*664-14 Deokjin, Deokjin-Ku, Jeonju, KOREA*

*Tel: +82-63-270-3973, Fax: +82-63-270-3585, E-mail: sk\_lee@chonbuk.ac.kr*

Nanowire devices have received considerable attention for use in integrated nanoscale electronics as well as high performance sensors, owing to their one dimensional structure, high surface-to-volume ratio, and small size. In this study, current and on-going research activities of nano-sensor and device laboratory (NSDL) at Chonbuk National University were reviewed. Especially, research works on the fabrication and electrical characteristics of n- and p-channel Si nanowires FET (SiNW FET), which were prepared by both boron and phosphorus ion implantation, were reviewed. The ion implantation was performed on randomly-dispersed intrinsic Si NWs without any implantation mask under the conditions of dose of  $1 \times 10^{13} \sim 1 \times 10^{11}$  ions/cm<sup>2</sup> and a fixed energy of 10 keV. The experimental current-voltage characteristics of the B- and P-implanted SiNW FET exhibited excellent FET behavior which corresponded well with a 2D numerical simulation. The influence of activation annealing on the electric characteristics of B-implanted Si NW FETs were also discussed. In addition, some research works were also presented on high-brightness GaN nanowire UV-blue LEDs prepared using two assembly techniques, random dispersion (RD) and dielectrophoresis assisted assembly deposition (DAAD).

## **NO<sub>x</sub> Adsorption on SnO<sub>2</sub> Nanoparticles: Dynamics of the Surface Reactions in Correlation with SnO<sub>2</sub> Sensing Properties**

Marie-Isabelle Baraton

*University of Limoges & CNRS,*

*SPCTS, Faculty of Sciences, 123 Avenue Albert Thomas, F-87060 Limoges, France*

*Tel: +33 555 457348, Fax: +33 555 778100, E-mail: m-isabelle.baraton@unilim.fr*

### **Abstract**

This work reports a FTIR study of NO<sub>x</sub> adsorption on semiconductor tin oxide nanosized particles in relation with the sensing properties of the material. The chemical reactions are monitored *in situ* simultaneously with the electrical conductivity variations. A different dynamics was found between the main surface reactions and the changes in the SnO<sub>2</sub> electrical conductivity. Thanks to our investigation technique developed in earlier works, the chemical reactions solely responsible for the variations of the SnO<sub>2</sub> electrical conductivity have been tentatively determined.

### **Introduction**

Semiconductor chemical gas sensors detect gases through the variations of the semiconductor electrical conductivity induced by chemical reactions or interactions occurring at the semiconductor surface under gas adsorption. The correlation between the surface reactions and the changes in the electrical conductivity is not always straightforward because the reactions can be multiple generating several kinds of surface chemical species differently linked to the surface. Moreover, apparent discrepancies may be observed between the dynamics of the reactions and the response time of the sensor.

In previous works [1,2], we have proved that Fourier transform infrared (FTIR) spectroscopy is a high-performance tool to follow *in situ* the chemical reactions at the surface of semiconductor nanosized particles and to simultaneously monitor the induced changes in the electrical conductivity. This technique is applied to investigate the adsorption of NO<sub>x</sub> on the SnO<sub>2</sub> surface in order to identify the specific reaction(s) responsible for the NO<sub>x</sub> detection by SnO<sub>2</sub>-based chemical sensors.

## Results and discussion

The infrared surface spectrum of SnO<sub>2</sub> shows that, under the first adsorption of NO<sub>x</sub> on the fresh SnO<sub>2</sub> surface, the newly formed prominent surface species are nitrate groups coordinated in the bidentate and bridged geometries. Additionally, a broad negative band is due to the decrease of the free carrier absorption generated by a decrease of the electrical conductivity. An infrared analysis versus time shows that the decrease of the free electron density, that is the decrease of the electrical conductivity is almost completed within the first 2 minutes under NO<sub>x</sub> adsorption. Then, after the first 2 minutes, nitrate groups continue to form with practically no change in the electrical conductivity. The formation of nitrate groups is a relatively slow process whereas changes in the electrical conductivity are quite fast. Therefore, nitrate groups cannot be responsible for the response of the sensor to NO<sub>x</sub>. Nitrate groups are not reversible under desorption and thus the SnO<sub>2</sub> surface remains contaminated after the first NO<sub>x</sub> adsorption/desorption cycle.

During subsequent NO<sub>x</sub> adsorption/desorption cycles under similar conditions, the surface reactions and their dynamics are different from those observed during the first cycle. No formation of new nitrate groups is detected. The species formed under the subsequent NO<sub>x</sub> adsorptions are mainly gaseous species (NO<sub>2</sub>, N<sub>2</sub>O<sub>4</sub>) and are eliminated by evacuation. Concomitantly, reversible effects and smaller changes in the free electron absorption are observed. It is proposed that the formation of (NO<sub>x</sub><sup>-</sup>) nitrosyl anion, resulting from the adsorption of NO<sub>x</sub> on surface oxygen vacancies, would trap free electrons into localized states, thus leading to a decrease of the electrical conductivity. The dynamics of NO<sub>x</sub><sup>-</sup> formation is compatible with the response time of the sensor.

## Perspectives

The ultimate role of FTIR spectroscopy in the optimization of chemical gas sensors is to identify the surface reactions responsible for the reversible reactions generating the reversible changes in the electrical conductivity. This is achieved through several gas adsorption/desorption cycles to check the reversibility of the reactions and through an analysis of the reactions dynamics to check the compatibility with the sensor response.

## References

1. M.-I. Baraton and L. Merhari, *Scripta Materialia*, **44**, 1643-1648 (2001).
2. M.-I. Baraton and L. Merhari, *Synthesis and Reactivity in Inorganic, Metal-Organic and Nano-Metal Chemistry*, **3**, 733-742 (2005).

## Application of Ion Migration at Solid-Solid Microcontact

Kai Kamada

*Department of Materials Science and Engineering, Faculty of Engineering,  
Nagasaki University, 1-14 Bunkyo-machi, Nagasaki 852-8521, Japan*

*\* E-mail: [kkamada@nagasaki-u.ac.jp](mailto:kkamada@nagasaki-u.ac.jp)*

### Introduction

As solid state ionics deals with rapid ionic motion in solid materials, it focuses on materials showing ionic or mixed (ionic – electronic) conduction, so-called solid electrolytes or ion conductors. Ion migration is equivalent to charge transfer. Thus, it is significant to evaluate electrical characters of ion conductors. The microelectrode technique, already established in liquid state electrochemistry, has recently been employed to measure the electrical properties of ion conductors. The advantages of the microelectrode technique in the solid electrochemical system include an improved space resolution, the rapid attainment of steady state, and so on. For instance, microelectrodes play a significant role in the measurements of local conductivities in ceramic materials, transference numbers in mixed conductors, and in the determination of redox potentials in metal oxides.

### Pinpoint doping using metal ion conductors

Our group has developed the pinpoint doping technique of metal ions into solid materials such as glass and ceramics by applying a dc bias to the microcontact of metal ion conductors with the doping target [1]. The study shows that a simple reduction of the contact area enables pioneering research on ion conductors. We were able to demonstrate pinpoint doping into glass and superconducting ceramics on a  $10^{1-2}$   $\mu\text{m}$  scale using a  $\beta''\text{-Al}_2\text{O}_3$  microelectrode. Moreover, scanning a  $\beta''\text{-Al}_2\text{O}_3$  microelectrode under an applied electric field caused a fine-patterned dopant distribution on the target surface [2].

### Solid electrochemical micromachining

As another application, we also proposed the micromachining technique for metal substrates through solid electrochemical reaction of metal ion conductors [3,4]. The proposed method involves an anodic electrochemical reaction at the microcontact between the metal substrate and ion conductor. More concretely, the metal substrate is



locally incorporated into the ion conductor in the form of metal ions via the microcontact under a dc bias. The electrochemical micromachining can be achieved as a result of consumption of the metal only at the microcontact.

#### References

1. K. Kamada et al., *Electrochem. Solid-State Lett.*, **5**, J1-J3 (2002).
2. K. Kamada et al., *J. Mater. Chem.*, **13**, 1265-1268 (2003).
3. K. Kamada et al., *Chem. Mater.*, **17**, 1930-1932 (2005).
4. K. Kamada et al., *Electrochim. Acta*, **52**, 3739-3745 (2007).

## Molecular Metal Wires and Molecular Switches

Shie-Ming Peng\*

Department of Chemistry, National Taiwan University, Taipei, Taiwan

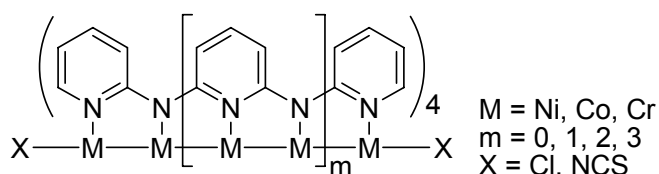
Tel.: 886-2-23638305; Fax.: 886-2-83693765

Email: smpeng@ntu.edu.tw

Keywords: Metal-Metal Bonds, Metal String Complexes, Molecular Metal Wires, Molecular Switches

### I. Linear Metal String Complexes<sup>1,2,3</sup>

- \* Synthesis, Structure, Bonding



### II. Potential Application as Molecular Metal Wires & Molecular Switches<sup>4</sup>

- \* STM Study on the Conductivity of Metal Strings
- \* C-AFM Measurements of Single Metal String Molecules
- \* Comparative Study on the I-V Characteristics (Theory V.S. Experiment)

### III. Tuning of the Metal Strings<sup>5,6</sup>

- \* Naphthyridyl Amino Ligands: Low Oxidation Mixed Metal Strings
- \* Asymmetrical Ligands: Toward Molecular Rectifier
- \* Heteronuclear Metal String Complexes

### IV. Conclusion

#### Reference:

1. C.-Y. Yeh, C.-C. Wang, Y.-H. Chen and S.-M. Peng, in *Redox Systems Under Nano-Space Control*, Ed: T. Hirao, Springer, Germany, 2006, Ch. 5.
2. S.-Y. Lai, T.-W. Lin, Y.-H. Chen, C.-C. Wang, G.-H. Lee, M.-H. Yang, M.-K. Leung and S.-M. Peng, *J. Am. Chem. Soc.*, **1999**, 121, 250.
3. S.-J. Shieh, C.-C. Chou, G.-H. Lee, C.-C. Wang and S.-M. Peng, *Angew. Chem. Int. Ed. Engl.*, **1997**, 36, 56.
4. I.-W. P. Chen, M.-D. Fu, W.-H. Tseng, J.-Y. Yu, S.-H. Wu, C.-J. Ku, C.-H. Chen, and S.-M. Peng, *Angew. Chem. Int. Ed. Engl.*, **2006**, 5414.
5. (a) C.-H. Chien, J.-C. Chang, C.-Y. Yeh, G.-H. Lee, J.-M. Fang and S.-M. Peng, *Dalton Trans.*, **2006**, 2106. (b) C.-H. Chien, G.-H. Lee, Y. Song and S.-M. Peng, *Dalton Trans.*, **2006**, 3249.
6. M.-M. Rohmer, I. P.-C. Liu, J.-C. Lin, M.-J. Chiu, C.-H. Lee, G.-H. Lee, M. Benard, X. Lopez, S.-M. Peng, *Angew. Chem. Int. Ed. Engl.*, **2007**, 46, 3533.



Born 1949. B.S., 1970, National Taiwan Univ.; Ph.D., 1975, Univ. of Chicago. Research Associate, 1975-76, Northwestern Univ. Associate Professor, 1976-80; Professor, 1980-; Chairman, 1987-90, Dept. of Chemistry, NTU. Humboldt Research Fellow of Germany, 1983-84. Research Fellow, 1982-; Acting Director, 1985-87, Institute of Chemistry, Academia Sinica; Academician, 1998, Academia Sinica. Vice President, 1999-2002, National Taiwan University.

# Poster Presentation

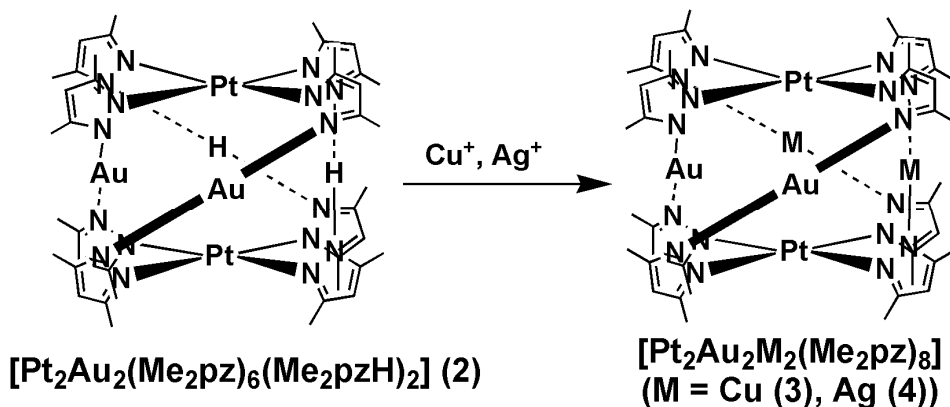
## Luminescent Heteropolynuclear Complexes of 3,5-Dimethylpyrazolate [Pt<sub>2</sub>Au<sub>2</sub>M<sub>2</sub>(Me<sub>2</sub>pz)<sub>8</sub>] (M = Ag, Cu) Showing Synergetic Effect of Three Transition Elements in the Excited State

Keisuke Umakoshi,<sup>†,\*</sup> Keizo Saito,<sup>†</sup> Yasuhiro Arikawa,<sup>†</sup> Masayoshi Onishi,<sup>†</sup> Shoji Ishizaka,<sup>‡</sup> Noboru Kitamura,<sup>‡</sup> Yoshihide Nakao,<sup>§</sup> and Shigeyoshi Sakaki<sup>§</sup>

<sup>†</sup>Department of Applied Chemistry, Faculty of Engineering, Nagasaki University, Bunkyo-machi, Nagasaki 852-8521, Japan, <sup>‡</sup>Division of Chemistry, Graduate School of Science, Hokkaido University, Kita-ku, Sapporo 060-0810, Japan, <sup>§</sup>Department of Molecular Engineering, Graduate School of Engineering, Kyoto University, Nishikyo-ku, Kyoto 615-8510, Japan

\*Tel/Fax: +81-95-819-2672, E-mail: kumks@nagasaki-u.ac.jp

Heteropolynuclear transition metal complexes have been attracting much attention, because they are expected to exhibit specific interactions and cooperative effects between the transition elements, which provide novel functions that are unobtainable through the individual elements. One of the best probes to investigate the metal-metal interactions is luminescence, because it is very sensitive to the change of the energies of ground and excited states. Much effort has been devoted to the study on the photophysical properties of heteropolynuclear complexes, though these studies are limited to the complexes composed of two transition elements and ligands. It is thus very interesting to study the photophysical properties arising from the metal-metal interactions among three transition elements. Here, we wish to report the synthesis of luminescent heteropolynuclear complexes containing three transition elements, [Pt<sub>2</sub>Au<sub>2</sub>M<sub>2</sub>(μ-Me<sub>2</sub>pz)<sub>8</sub>] (M = Cu (3), Ag (4)), which exhibit synergetic effect of the three transition elements.



## Physical and Mechanical Properties of Polyurethanes Crosslinked by [3]Rotaxane

Shinji Ohira<sup>2</sup>, Ryosuke Kusano<sup>2</sup>, Ken Kojio<sup>3</sup>, Mutsuhisa Furukawa<sup>1,3</sup>,  
Takamasa Sagara<sup>4</sup> and Hiroto Murakami<sup>1,4\*</sup>

<sup>1</sup>*Department of Materials Science, Graduate School of Science and Technology,*

<sup>2</sup>*Department of Materials Engineering and Molecular Science, Graduate School of Science and Technology*

<sup>3</sup>*Department of Materials Science and Engineering, Faculty of Engineering,*

<sup>4</sup>*Department of Applied Chemistry, Faculty of Engineering,  
Nagasaki University, 1-14 Bunkyo, Nagasaki 852-8521, Japan*

\*Tel&FAX: +81-95-819-2688, E-mail: hiroto@nagasaki-u.ac.jp

### Abstract

We report here physical and mechanical properties of three polyurethanes (**PU11**, **PU33** and **PU0**) with and without azobis(dibenzo-24-crown-8 ether) **ABC**, which acts as a mechanical bonding cross-link point possessing a [3]rotaxane structure.

### Introduction

One of the most interesting properties of rotaxanes arising from a mechanical bond is that the ring molecule can move freely along the axis molecule since no covalent bond exists between the ring and axis molecules (Fig. 1).<sup>1,2)</sup> It is

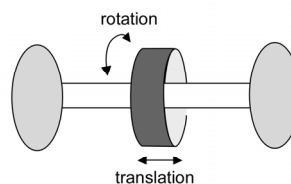


Figure 1. Schematic draws of a rotaxane.

expected that introduction of the mechanical bonding crosslink instead of the hydrogen bonding one into the hard segments of PU elastomers (PUEs) leads to control the mechanical properties and development of novel functions of PUEs.

In this presentation, we describe characterization of three PUs with and without a [3]rotaxane as a mechanical bonding crosslink point by spectral, thermal, and mechanical measurements.

### Results and Discussions

Glass transition temperatures ( $T_g$ ) of the soft segment chains in **PU0**, **PU11** and **PU33** were observed at  $-62$ ,  $-61$  and  $-59$  °C, respectively. The  $T_g$  values are gradually shifted to higher temperature with increasing the content of **ABC** while the difference was small. The shift would be expected that the decrease of the formation of hydrogen

bonding between the PU chains induced by the introduction of **ABC** would involve decreasing both the hard-segment and pure soft-segment phases. In fact, the ATR-FT-IR spectra of the PUs revealed that relative intensity ratios of the carbonyl groups ( $I_{\nu(\text{C}=\text{O})\text{H-bond}}/I_{\nu(\text{C}=\text{O})\text{free}}$ ) of the PUs decreased with increasing the content of **ABC**.

Figure 2 shows the stress-strain curves for the **PU0**, **PU11** and **PU33**. Young's moduli for **PU0** and **PU33** were 11.1 and 10.8 MPa, respectively, whereas that for **PU11** was 1.8 MPa. Remarkably, **PU33**

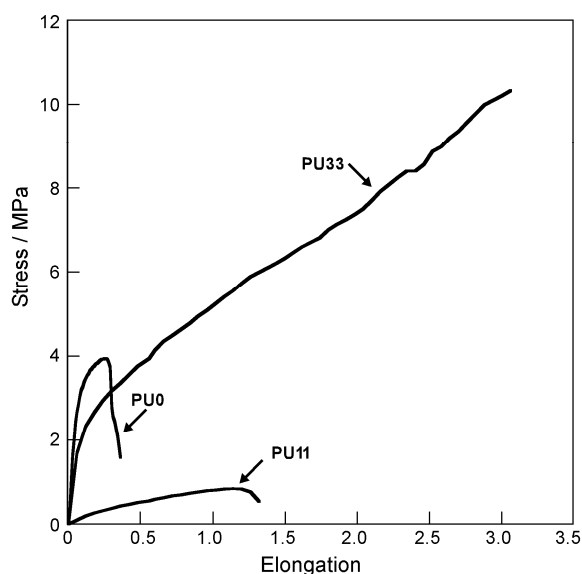


**Figure 2.** Stress vs. elongation curves for **PU0**, **PU11** and **PU33** at 20 °C.

possesses the best tensile strength and strain at break. Even if the interaction between a crown unit of **ABC** and an ammonium unit of **Ax** is broken by tension, the crown unit can slide on the chain and interact with neighbor ammonium unit of **Ax**. Therefore, we believe that this sliding behavior causes the unique tensile properties. These tensile strength and elongation properties are the evidence for the existence of the mechanical bond crosslink point via the rotaxane in the structure of **PU33**.

## Conclusions

The content of 33 % for **ABC** in **PU33**, in which some of them act as the mechanical bond crosslink point, is enough to develop the properties originated from the mechanical bond crosslink point. In fact, incorporation of the enough amount of the mechanical bond crosslink point via the rotaxane structure causes the best tensile strength and elongation among the PUs. In contrast, the content of 11 % for **ABC** in **PU11** is unsatisfying to form the network structure.

## References

1. J. F. Stoddart et al., *J. Am. Chem. Soc.*, **113**, 5131-5133 (1991).
2. K. Ito et al., *Adv. Mater.*, **13**, 485-487 (2001).

## Convenient Synthesis of Pyrrolidine by Amphiphilic Allylation

Katsumi Tohyama<sup>1</sup>, Yumi Yamaguchi<sup>2</sup>, Masanari Kimura<sup>2\*</sup>

<sup>1</sup>Graduate School of Science and Technology,

<sup>2</sup>Department of Applied Chemistry, Faculty of Engineering,

Nagasaki University, 1-14 Bunkyo-machi, Nagasaki 852-8521, Japan

\*Tel: +81-95-819-2679, Fax: +81-95-819-2683, E-mail: masanari@nagasaki-u.ac.jp

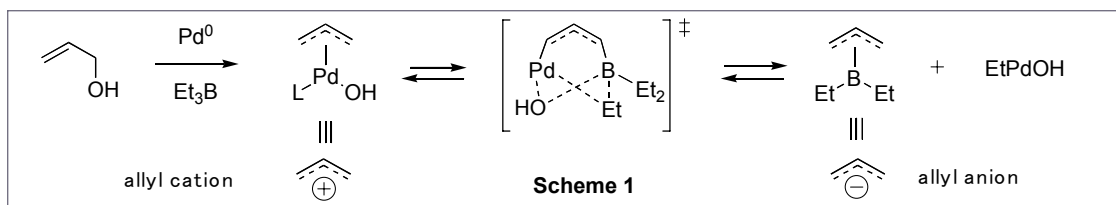
Key Words; Palladium, Triethylborane, Aldimine, Pyrrolidine, Amphiphilic Allylation

### Abstract

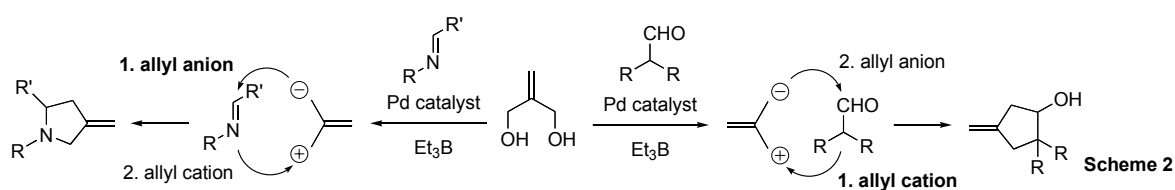
The combination of Pd(0) catalyst and triethylborane promotes the amphiphilic allylation of aldimine with 2-methylenepropane-1,3-diol in the order of nucleophilic-electrophilic attack to provide pyrrolidine in one-pot under mild conditions.

### Introduction

We have developed that a combination of Pd-catalyst and Et<sub>3</sub>B activates allyl alcohol as an allyl cation and an allyl anion species for allylic alkylations (Scheme 1). Et<sub>3</sub>B promoted allyl alcohol to undergo the oxidative addition of a Pd(0) species via coordination to the hydroxy group to form  $\pi$ -allylpalladium, which serves as an allyl cation equivalent toward a variety of soft nucleophiles to cause electrophilic allylation (Tsuji-Trost type reaction).<sup>1</sup> In the absence of nucleophiles,  $\pi$ -allylpalladium is subjected to an allyl-ethyl exchange reaction, providing allyl diethylborane as an allyl anion equivalent, which reacts with benzaldehyde and aldimines to provide homoallyl alcohols and homoallylamines,<sup>2</sup> respectively (umpolung of  $\pi$ -allylpalladium). Furthermore, the similar catalytic system accelerates the amphiphilic allylation of alkyl aldehydes with 2-methylenepropane-1,3-diol to provide 3-methylenecyclopentanol via electrophilic–nucleophilic allylation (Scheme 2).<sup>3</sup>



Here we would like to report the sequential amphiphilic allylation of aldimines with 2-methylenepropane-1,3-diol in the order of nucleophilic-electrophilic allylation to provide 3-methylenepyrrolidines under similar catalytic system.<sup>4</sup> Notably, the order of the amphiphilic allylation of aldimines is apparently opposite to that of aldehydes.

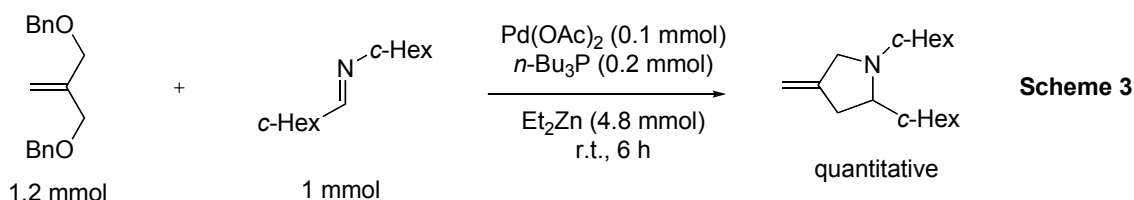


## Experimental

The reaction was conducted as follows: in situ formation of aldimines prepared from aldehydes and amines via azeotropic distillation of THF-H<sub>2</sub>O two times, and exposure of the aldimines residue to a mixture of 2-methylenepropane-1,3-diol, Pd(OAc)<sub>2</sub>, *n*-Bu<sub>3</sub>P, and Et<sub>3</sub>B at 50 °C under nitrogen atmosphere.

## Results and Discussions

The reaction tolerates a wide variety of aldimines generated from aromatic and aliphatic aldehydes and primary amines to provide 3-methylenepyrrolidines in high yields. Et<sub>2</sub>Zn is also effective for the amphiphilic allylation of aldimines with 1,3-dibenzyloxy-2-methylenepropane under similar Pd catalytic system. On the contrary to the result of 2-methylenepropane-1,3-diol with Et<sub>3</sub>B, Et<sub>2</sub>Zn promotes the amphiphilic allylation of the aldimine composed of cyclohexanecarboxyaldehyde and cyclohexylamine to provide 3-methylenepyrrolidine at room temperature in quantitative yield (Scheme 3).



## Conclusions

The catalytic system of Pd catalyst and triethylborane promotes aldimines to undergo the sequential amphiphilic allylation with 2-methylenepropane-1,3-diols. This reaction would be utilized for the efficient synthesis of physiologically active molecules, pyrrolidines and proline derivatives.

## References

1. M. Kimura and Y. Tamaru et al., *Tetrahedron Lett.*, **41**, 3627 (2000).
2. M. Kimura and Y. Tamaru et al., *Org. Lett.*, **7**, 637 (2005).
3. M. Kimura and Y. Tamaru et al., *J. Am. Chem. Soc.*, **126**, 11138 (2004).
4. M. Kimura, and K. Tohyama, et al., *Angew. Chem. Int. Ed. Engl.*, **47**, 5803 (2008).



## Regulated Optical Properties of Single-walled Carbon Nanotubes via Redox Reaction

Yasuhiko Tanaka, Kohei Hirayama, Tsuyohiko Fujigaya,

Yasuro Niidome and Naotoshi Nakashima\*

*Department of Applied Chemistry, Graduate School of Engineering,*

*Kyushu University, 744 motooka, Fukuoka 819-0395, Japan*

\*Tel & Fax: +81-92-802-2840, E-mail: nakashima-tcm@mail.cstm.kyushu-u.ac.jp

Carbon nanotubes (CNTs) have been in the forefront of nanoscience and nanotechnology because of their many unique properties. However, their insolubility in solvents has hindered chemical approaches using CNTs. We have reported the fundamental properties and applications of soluble carbon nanotubes in aqueous and organic systems<sup>1-3</sup>. Individually dissolved CNTs show the inherent properties of the CNTs that are not seen in bundled ones.

Single walled carbon nanotubes (SWNTs) exhibit interesting optical properties via redox reactions<sup>4-6</sup>. Here, we report the finding that near IR absorption and photoluminescence spectra of individually dissolved SWNTs in aqueous micellar solution are regulated by the addition of a chemical reducing agent. The details will be reported at the presentation.

### References

- 1 N. Nakashima, T. Fujigaya, H. Murakami, *Soluble Carbon Nanotubes*. American Scientific Publisher: California, **2008**, p 113-128.
- 2 H. Murakami, N. Nakashima, *J. Nanosci. Nanotechnol.* **2006**, *6*, 16-27.
- 3 N. Nakashima, *Int. J. Nanosci.* **2005**, *4*, 119-137.
- 4 M. Zheng, B. A. Diner, *J. Am. Chem. Soc.* **2004**, *126*, 15490-15494.
- 5 M. J. O'Connell, E. E. Eibergen, S. K. Doorn, *Nature Mater.* **2005**, *4*, 412-418.
- 6 G. Dukovic, B. E. White, Z. Zhou, F. Wang, S. Jockusch, M. L. Steigerwald, T. F. Heinz, R. A. Friesner, N. J. Turro, L. E. Brus, *J. Am. Chem. Soc.* **2004**, *126*, 15269-15276.

## Electrochemical behaviors of fructose dehydrogenase immobilized onto UV-ozone-treated carbon nanotubes modified electrode

*Shiori Kaneko, Hiroyuki Yamaguchi, Shingo Sakamoto, Toshihumi Nishimura,  
Masato Tominaga, Isao Taniguchi*

*Graduate School of Science and Technology, Kumamoto University  
2-39-1, Kurokami, Kumamoto 860-8555, Japan  
Tel: +81-96-342-3656, Fax: +81-96-342-3656,  
E-mail: masato@gpo.kumamoto-u.ac.jp*

### Abstract

Carbon nanotubes (CNTs) were synthesized onto a gold electrode. Fructose dehydrogenase (FDH) was immobilized onto the UV-ozone-treated CNTs on gold electrode (UV-CNT/Au). Catalytic oxidation currents based on the direct electron transfer reactions of FDH were observed at FDH modified UV-CNT/Au electrode. The observed catalytic oxidation currents strongly depended on the UV-ozone treatment time.

### Introduction

The increasing interest in direct electron transfer (DET) reaction type enzyme is driven by its important applications as biosensors, biofuel cells and bioreactors. CNTs are used as an electrode for DET reactions with enzymes, because CNTs have a high conductivity and small diameter. However, the influence of surface conditions of CNTs on the DET reactions with enzymes has not been investigated. In this study, we found, for the first time, that the DET reaction of enzymes at CNT surface was strongly influenced with the surface structural defects of CNTs.

### Experimental

CNTs were synthesized onto a gold electrode surface by using chemical vapor deposition method using Co-Mo alloy nanoparticles as a catalyst. From Raman spectroscopic results and TEM image (Fig. 1) the diameters of synthesized CNTs were evaluated to be ca. 1~1.5 nm. To induce a surface structural defect onto the CNTs, UV-ozone treatment was performed for 1 and 5 min. D-fructose dehydrogenase (FDH, EC 1.1.99.11) was purchased from Toyobo Co., Japan, and used without further purification. FDH is consisted from three subunits including flavin and heme c as prosthetic group. To immobilize FDH onto the CNT surface, the CNTs modified gold (CNT/Au) electrode was immersed into phosphate solution (pH 5) of 1 unit  $\mu\text{l}^{-1}$  FDH for 1 min.

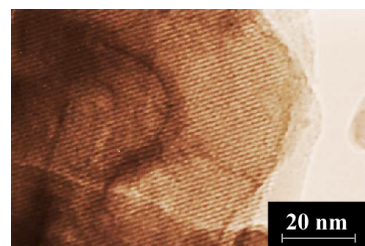


Fig. 1 TEM image for CNTs grown on a gold electrode.

## Results and Discussion

Fig. 2 shows the X-ray photoelectron spectroscopic (XPS) results at the UV-ozone-treated CNT/Au (UV-CNT/Au) electrode in the C(1s) region. Ratio of peaks corresponding to the oxidized carbon species such as C-O, C=O and O-C=O (ca. 286-290 eV) were increased with UV-ozone treatment time. These results indicated that the surface structural defects of CNTs were induced by UV-ozone treatment. Fig. 3 show typical cyclic voltammograms at FDH-modified and -unmodified CNT/Au electrodes. Catalytic oxidation currents were observed from ca. -0.1 V in a phosphate solution (pH 5) in the presence of 0.1 M fructose. On the other hand, no catalytic oxidation current was observed at the unmodified CNT/Au electrode. These results indicate that the observed catalytic oxidation current based on the DET reactions of FDH immobilized onto the CNT/Au electrode. The UV-ozone-treated CNT for 1 min was most suitable electrode for DET reaction with FDH in comparison with other electrodes. To clarify the reason, we evaluated the surface excess of FDH on the CNT/Au electrode by using fluorescent measurement. The surface excess of FDH was evaluated to be  $4.5 (\pm 1.0) \times 10^{-11} \text{ mol cm}^{-2}$ , which did not depend on the UV-ozone treatment time. These results indicate that the difference in the catalytic current values was not due to the surface excess of FDH. It is well known that the molecular orientation of the enzyme on the electrode surface is one of the most important requirements for fast DET reactions, because the redox center of the enzyme is buried deeply within the protein shell. The proper orientation of FDH on an electrode surface is also important for successful its DET reactions [1]. From the fact that the catalytic oxidation current based on the DET reaction of FDH increased from ca. -0.1 V, the DET reaction of FDH at the electrode surface occurred at the heme c-containing subunit [1]. From the result of the observation of catalytic oxidation from -0.1 V together with the fact that surface excess of FDH did not depend on UV-ozone treatment time, the difference in the observed catalytic current values at the UV-CNT/Au electrodes was came from the difference in the proper orientation of FDH on the CNT surface.

1 M. Tominaga, C. Shirakihara, and I. Taniguchi, *J. Electroanal. Chem.*, **610**, 1-8 (2007).

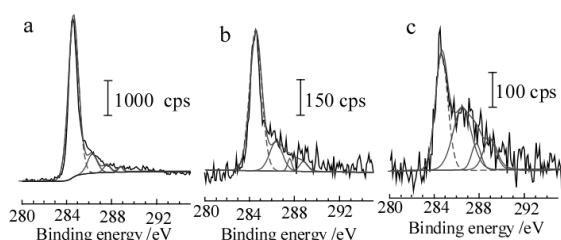


Fig. 2 XPS results in the C(1s) region at CNT/Au electrodes treated with UV-ozone for 0 (a), 1 (b) and 5 min (c).

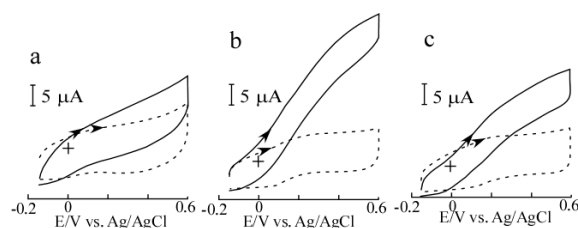


Fig. 3 Cyclic voltammograms at the UV-ozone treated (a: 0, b: 1 and c: 5 min) CNT/Au electrodes modified with FDH in a phosphate solution (pH 5) in the presence (solid line) and the absence (broken line) of 0.1 M fructose. Potential sweep rate:  $5 \text{ mV s}^{-1}$ . Electrode area:  $0.25 \text{ cm}^2$ .

## Anti-oxidation property of CNT/PyC/SiC coating for Carbon/Carbon composites

Yuji Mukojima<sup>1</sup>, Hideki Sano<sup>2</sup>, Guo-Bin Zheng<sup>2\*</sup> and Yasuo Uchiyama<sup>2</sup>

<sup>1</sup>*Graduate School of Science and Technology,*

<sup>2</sup>*Department of Materials Science and Engineering, Faculty of Engineering,*

*Nagasaki University, 1-14 Bunkyo-machi, Nagasaki 852-8521, Japan*

*\*Tel: +81-95-819-2657, Fax: +81-95-819-2656, E-mail: gbzheng@nagasaki-u.ac.jp*

### Introduction

Ceramic coating, such as SiC, is required to prevent the oxidation of the C/C, since C/C composites are prone to oxidize above 723K in air. However, due to mismatch of coefficient of thermal expansion (CTE) between C/C composites and ceramic coating, cracks formed in the ceramic coating on cooling from high temperature.

In order to suppress the cracking in coating, CNT/PyC/SiC coatings were produced by chemical vapor deposition of pyrolytic carbon (PyC) and SiC into CNT layer, which was dip-coated on C/C surface. CNT and PyC were used to suppress cracks and reinforce the bonding between C/C composites and SiC coating. In our previous study, CNT layer was prepared by direct growth of CNTs on C/C substrate. However, this process is too difficult to control the quality of CNTs and thickness of CNT layer. Therefore, in this study, CNT layer was prepared using dip-coating. The effect of CNT layers on the anti-oxidation property of CNT/SiC and CNT/PyC/SiC coating was investigated.

### Experimental

CNTs were treated with mixed solution of sulfuric acid and nitric acid at 110°C for 2 hours. Then, CNTs layer was prepared by dip-coating of C/C in CNT dispersion. The deposition of PyC was performed using propane as carbon source at 1150°C, under a pressure of 5 kPa for 1, 3, 5 min. Subsequently, the source was switched to CH<sub>3</sub>SiCl<sub>3</sub> for deposition of SiC, under a pressure of 4 kPa for 60min. SiC coating, CNT/SiC coating and CNT/PyC/SiC coating (X denoted deposition time of PyC) were prepared. The microstructure of the coating was observed using SEM. Isothermal oxidation tests were carried out at 1200°C for 2 hours in air of 30ml/min using TG.

### Results and Discussion

CNTs used in this experiment were MWNTs with an average diameter of 20 nm. Fig.1 shows SEM images of cross-section of CNT layer, CNT/PyC coating, CNT/PyC/SiC coating. From Fig.1 a), it can be seen that thickness of the CNT layer

varied from 5 to 20  $\mu\text{m}$  with an average of 10  $\mu\text{m}$ . From Fig.1 b), PyC deposited into small space among CNTs, but still left large pores among CNT aggregates. From Fig.1 c), It can be seen that, CNT/PyC3/SiC coating consisted of two layers with the inner CNT/PyC/SiC layer and the outer SiC layer with coating thickness ranging from 20-30  $\mu\text{m}$ . CNT pullout could be observed from the fracture surface of the coating, suggesting reinforcement effect of CNT. However, the coating was not very dense due to formation of whisker-like SiC.

Fig.2 shows the results of isothermal oxidation test at 1200°C for 2 hours. Compared with the SiC coated C/C composites, the CNT/SiC coated samples exhibited an obvious improvement of oxidation resistance. While compared with the CNT/SiC coated samples, the CNT/PyC/SiC coated samples showed a better anti-oxidation property. Among them, The CNT/PyC3/SiC coatings with PyC deposited for 3 min showed the best anti-oxidation property. It is believed that the better anti-oxidation property of CNT/PyC/SiC coated C/C samples was primarily due to less the cracking in coating by CNT. However, complete anti-oxidation is not achieved yet. Further researches are carried out to improve the coating.

### Conclusions

CNTs have intense effect on the oxidation property of the SiC coating on the C/C composites. The CNT/PyC/SiC coatings with PyC deposited for 3 min showed best anti-oxidation property.

### References

1. Yu-Lei Zhang, He-Jun Li et al. Surface & Coatings Technology 201 (2006) 3491-3495

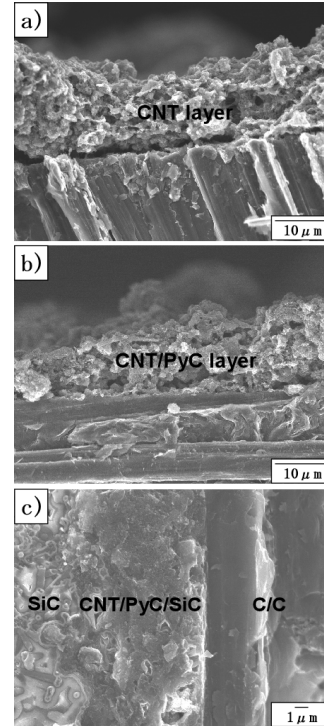


Fig.1 SEM image of cross-section of samples. a) CNT b) CNT/PyC c) CNT/PyC3/SiC

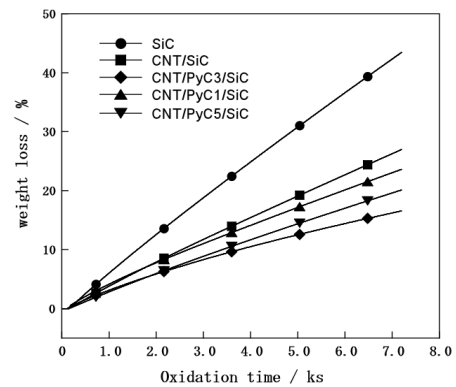


Fig.2 Isothermal oxidation test of C/C composites with CNT/PyC/SiC coating.

## Growth of carbon nanotubes on carbon nanofibers

Sho Muranaka, Hideaki Sano, Guo-Bin Zheng, and Yasuo Uchiyama  
*Department of Materials Science and Engineering, Faculty of Engineering,  
Nagasaki University, 1-14 Bunkyo-machi, Nagasaki 852-8521, Japan*

*\*Tel: +81-95-819-2657, Fax: +81-95-819-2656, E-mail: gbzheng@nagasaki-u.ac.jp*

### Introduction

CNTs, which have extremely small diameter and high aspect ratio, have superior electrical and thermal conductivity and mechanical strength. CNTs are expected to be used as functional filler to improve the conductivity and mechanical properties of plastics and ceramics. In this study, we develop three-dimensional CNT@CNF by growing CNTs on carbon nanofibers, which are expected to further improve electrical conductivity and strength in composites as well as in electrode.

### Experimental

CNFs(VGCF, Shouwa Denko) with average diameter of 150 nm and fiber length of 10-20  $\mu\text{m}$  were used. Catalyst particles for growth of CNTs were adhered on CNFs by two methods. In surfactant method, catalytic precursor solution consisted of Co nitrate or Ni nitrate with addition of dodecylbenzenesulfonic acid(DBA) or dodecylsodium sulfate (SDS). CNFs were dispersed the precursor solution and filtered by anodized alumina membrane. In chemical precipitation process, the CNFs, which were treated in  $\text{HNO}_3$  at  $110^\circ\text{C}$  for 2h, were dispersed in aqueous solution of Co nitrate. Ammonia solution was added into the solution to adjust pH value to 9.5. The CNFs were then separated and washed using centrifuge. The growth of CNTs on CNFs was carried out at  $600^\circ\text{C}$  for 20 min in  $\text{N}_2$ ,  $\text{H}_2$  and  $\text{C}_2\text{H}_2$ .

### Result and discussion

Fig. 1(a, b) shows the images of CNTs grown on CNFs from Co-DBA and Ni-SDS catalyst precursors. It can be seen that CNTs formed around the CNFs. The average diameter of CNTs from Co-DBA is 18 nm, and that of CNTs from Ni-SDS is 15 nm. Since DBA and SDS is anion surfactant, hydrophilic group is ion exchanged by  $\text{Co}^{2+}$  or  $\text{Ni}^{2+}$  while hydrophobic group adhered on CNFs surface. After drying and decomposition, small nanoparticles were formed on the CNF surface. However, CNFs aggregated severely due to the presence of DBA or SDS.

Fig. 1(c, d) shows the images of the catalyst particles obtained by chemical precipitation process, and the corresponding CNTs. The CNTs showed higher growth density than those obtained from Co-DBA and Ni-SDS. The CNTs has average diameter of 20 nm and CNT@CNF has maximum diameter of 750 nm. From Fig. 1c, it is seen that many nanoparticles adhered on the surface of CNF. The precipitation of cobalt

hydroxide generated by pH adjustment combined with - OH and - COOH of the CNFs surface, and thus the nanoparticles adhered to CNFs [1].

Fig. 2 shows the comparison of the catalyst particles and CNTs when Co-DBA or chemical precipitation process was used. The average catalyst particle size after reduction for Co-DBA was 22 nm, while the catalyst particle size for chemical precipitation process was 12 nm. It indicates that the chemical precipitation process is more adequate method to synthesize small and uniformly-distributed nanoparticles on CNFs.

Although the catalyst particles obtained from chemical precipitation process was smaller, the CNTs had similar diameter to those from Co-DBA. It is probably because many large particles did not contribute to the growth of CNTs in Co-DBA. Both kinds of CNTs had the curved morphology.

### Conclusions

Treatment in Co-DBA or Ni-SDS precursor solution could adhere nanoparticles on CNFs. However, chemical precipitation process was a better method to adhere catalyst particles on CNFs, and CNTs with high growth density were formed on CNFs.

### Reference

[1] Z. Dong, K. Ma, K. He, Mater. Lett 62 (2008) 4059-4061.

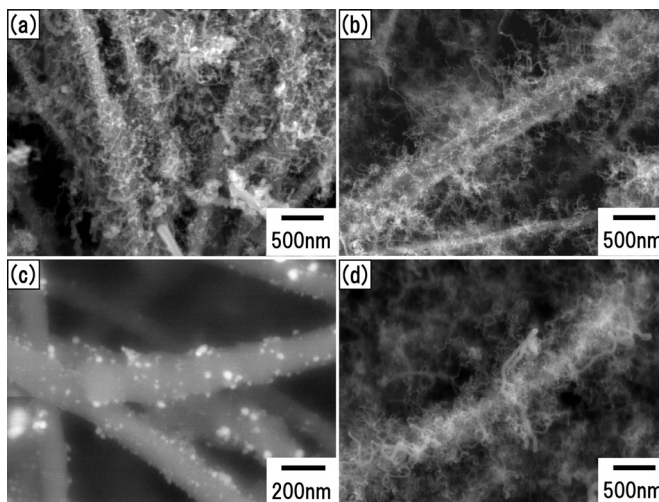


Fig.1. SEM images of CNTs grown on CNFs by Co-DBA (a) and Ni-SDS (b) treatment, (c) Co catalyst adhered on CNFs by chemical precipitation process, (d) CNTs grown from (c).

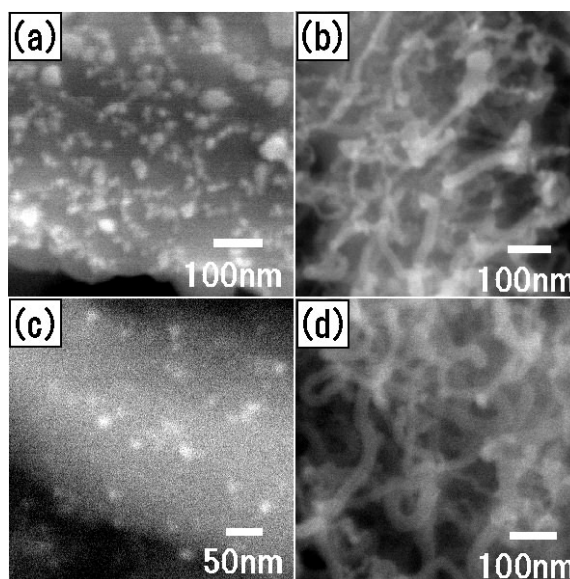


Fig2. SEM images of (a)Co catalyst obtained by Co-DBA, (b) CNTs synthesized from (a), (c) Co catalyst obtained by chemical precipitation process, and (d) CNTs synthesized from (c).

## Preparation of Mesoporous and Meso-macroporous Tin Dioxide Powders and Their Application to Sensor Materials

O Luyang YUAN<sup>a</sup>, Takeo HYODO<sup>a</sup>, Yasuhiro SHIMIZU<sup>b</sup> and Makoto EGASHIRA<sup>b</sup>

<sup>a</sup>Graduate School of Science and Technology, <sup>b</sup>Faculty of Engineering,  
Nagasaki University, 1-14 Bunkyo-machi, Nagasaki 852-8521

Mesoporous SnO<sub>2</sub> (mp-SnO<sub>2</sub>) and meso-macroporous SnO<sub>2</sub> (m·mp-SnO<sub>2</sub>) powders were prepared by employing SnCl<sub>4</sub>·5H<sub>2</sub>O as a Sn source. Mesoporous structure was controlled by C<sub>20</sub>H<sub>37</sub>O<sub>7</sub>SNa (AOT), while macroporous structure was controlled by polymethylmethacrylate (PMMA) microspheres. The mp- and m·mp-SnO<sub>2</sub> powders with and without SiO<sub>2</sub> and Sb<sub>2</sub>O<sub>5</sub> additives were also prepared. Gas sensing properties of mp- and m·mp-SnO<sub>2</sub> pellet-type sensors to 1000 ppm H<sub>2</sub> were measured in the temperature range of 300 - 500°C. The addition of 9 wt% SiO<sub>2</sub> was effective for enhancing the specific surface area (SSA), but the simultaneous addition of Sb<sub>2</sub>O<sub>5</sub> resulted in a decrease in SSA. The addition of Sb<sub>2</sub>O<sub>5</sub> up to 10 wt% was found to reduce the sensor resistance in air, but beyond that it led to an increase in resistance. Among the sensors tested, mp-SnO<sub>2</sub> added with only 5 wt% Sb<sub>2</sub>O<sub>5</sub> showed the highest H<sub>2</sub> response at 400°C.

### 1. Introduction

In recent years, a particular focus is currently being given to nano-structured SnO<sub>2</sub> powders as sensor materials. The present study is, therefore, directed to preparing thermally stable mp-SnO<sub>2</sub> and m·mp-SnO<sub>2</sub> powders aiming at improving their gas sensing properties. The effects of the addition of SiO<sub>2</sub> and Sb<sub>2</sub>O<sub>5</sub> on the microstructure and H<sub>2</sub> gas sensing properties have also been examined.

### 2. Experimental

mp-SnO<sub>2</sub> and m·mp-SnO<sub>2</sub> powders were prepared by employing SnCl<sub>4</sub>·5H<sub>2</sub>O as a Sn source. Mesoporous structure was controlled by AOT, while macroporous structure was controlled by PMMA microspheres with a diameter of 800 nm.

Table 1 Preparation conditions and specific surface area of m·mp-SnO<sub>2</sub>.

| Sample  | The amount of MO added to SnO <sub>2</sub>                    |                                   | SnCl <sub>4</sub> ·5H <sub>2</sub> O | Mesopore template (AOT) | Macropore template | pH adjusted | SSA (m <sup>2</sup> g <sup>-1</sup> ) |       |
|---------|---|-----------------------------------|--------------------------------------|-------------------------|--------------------|-------------|---------------------------------------|-------|
|         | MO: Sb <sub>2</sub> O <sub>5</sub> (using SbCl <sub>3</sub> ) | MO: SiO <sub>2</sub> (using TEOS) |                                      |                         |                    |             |                                       |       |
| A       | non   | non                               | 1.753 g                              | 4.452 g                 | non                | non         | 152.1                                 |       |
| A-P     |   |                                   |                                      |                         |                    |             | 143.2                                 |       |
| A-PT    |   |                                   |                                      |                         |                    |             | 262.7                                 |       |
| A-PTS1  | 1 wt%   | 9 wt%                             |                                      |                         | 0.35 g             | 8.5         | 253.2                                 |       |
| A-PTS5  | 5 wt%   | non                               |                                      |                         |                    |             | 220.8                                 |       |
| A-S5    |   |                                   |                                      |                         | non                | 8.5         | 164.3                                 |       |
| A-TS5   |   |                                   |                                      |                         |                    |             | 9 wt%                                 | 200.2 |
| A-PS5   |   |                                   |                                      |                         |                    |             | non                                   | 150.2 |
| A-PTS10 | 10 wt%  | 9 wt%                             |                                      |                         | 0.35 g             | 8.5         | 218.2                                 |       |
| A-PTS17 | 17 wt%  |                                   |                                      |                         |                    |             | 172.1                                 |       |
| A-PTS33 | 33 wt%  |                                   | 171.6                                |                         |                    |             |                                       |       |
| A-PTS50 | 50 wt%  |                                   | 168.9                                |                         |                    |             |                                       |       |

Typical preparation procedure of mp-SnO<sub>2</sub> and m·mp-SnO<sub>2</sub> was as follows. A given amount of each constituent listed in Table 1 was mixed in 400 ml of ultrapure water and the pH value of the resulting mixture was adjusted by adding an NH<sub>3</sub> aqueous solution to be 8.5 in some cases. As for tetraethoxysilane (TEOS) and SbCl<sub>3</sub>, the amounts necessary to produce the given amounts of SiO<sub>2</sub> and Sb<sub>2</sub>O<sub>5</sub> were added to the solution. The mixed solution was kept at 20°C for 3 days. The solution was evaporated to dryness in an oven at 80°C overnight. The resultant powder was then treated with a 0.1 mol m<sup>-3</sup> phosphoric acid solution for about 2 h.



The powder was molded into the pellet at a pressure of 1000 kg cm<sup>-2</sup>. Then the pellet was calcined in air at 600°C for 5 h. A pair of Pt electrodes was prepared on the pellet surface by screen printing. Hereafter each sample and sensor will be expressed by the abbreviations listed in Table 1. The gas sensing properties of the mp- and m·mp-SnO<sub>2</sub> pellet-type sensors to 1000 ppm H<sub>2</sub> were measured at a flow rate of 0.1 dm<sup>3</sup> min<sup>-1</sup> in the temperature range of 300 - 500°C. Magnitude of the response was defined as the ratio ( $R_a/R_g$ ) of sensor resistance in air ( $R_a$ ) to that in 1000 ppm H<sub>2</sub> balanced with air ( $R_g$ ).

### 3. Results and Discussion

Table 1 shows the specific surface area (SSA) of all the samples prepared. The SSA remained almost unchanged by the PMMA addition (compare A and A-P), but increased significantly by the 9 wt% SiO<sub>2</sub> addition (see A-PT). However, SSA decreased clearly with increasing the amount of Sb<sub>2</sub>O<sub>5</sub> (see a series of A-PTS10 to A-PTS50).

Figure 1 shows variations in resistance of m·mp-SnO<sub>2</sub> sensors (A-PTS series) with the Sb<sub>2</sub>O<sub>5</sub> amount added. It was revealed that the addition of Sb<sub>2</sub>O<sub>5</sub> up to 10 wt% was found to reduce the sensor resistance in air. But, beyond that, it led to an increase in resistance with increasing the Sb<sub>2</sub>O<sub>5</sub> additive amount, probably due to the solubility limit of Sb<sub>2</sub>O<sub>5</sub>. Thus, the A-PTS10 sensor showed the lowest resistance in air at 400°C. The resistance decrease can be explained by the valency control, i.e. partial substitution of Sn<sup>4+</sup> sites with Sb<sup>5+</sup> ions, producing free electrons, as described in Eq. (1).

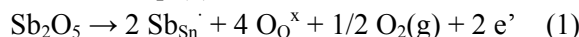


Figure 2 shows the temperature dependence of response to 1000 ppm H<sub>2</sub> of sensors. Among the sensors fabricated by the addition of Sb<sub>2</sub>O<sub>5</sub> from 0 wt% to 50 wt%, A-TS5, i.e. m·mp-SnO<sub>2</sub> added with 9 wt% SiO<sub>2</sub> plus 5 wt% Sb<sub>2</sub>O<sub>5</sub>, showed the highest H<sub>2</sub> response (see Fig. 2 (a)). Fig. 2(b) compares the effect of introduction of macropores on the H<sub>2</sub> sensing properties of sensors added with 5 wt% Sb<sub>2</sub>O<sub>5</sub> as well as 9 wt% SiO<sub>2</sub> plus 5 wt% Sb<sub>2</sub>O<sub>5</sub>. A-S5, i.e. mp-SnO<sub>2</sub> added with 5 wt% Sb<sub>2</sub>O<sub>5</sub> showed the highest H<sub>2</sub> response among all the sensors tested. By comparing A-PS5 and A-PTS5, or A-S5 and A-PS5, the introduction of macropores was confirmed to be effective for shortening the recovery time.

From these results, it was revealed that the addition of SiO<sub>2</sub> was found to increase the SSA of the m·mp-SnO<sub>2</sub> powder. The sensor resistance in air could be reduced by the addition of Sb<sub>2</sub>O<sub>5</sub>. The recovery time could be reduced by the introduction of macropores.

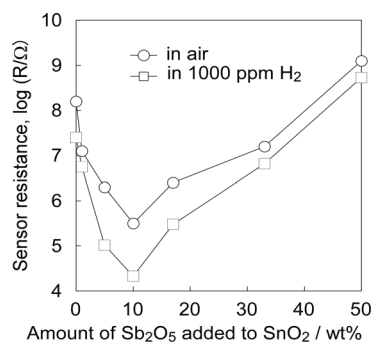


Fig. 1 Variations in resistance of m·mp-SnO<sub>2</sub> sensors (A-PTS series) with the Sb<sub>2</sub>O<sub>5</sub> amount added.

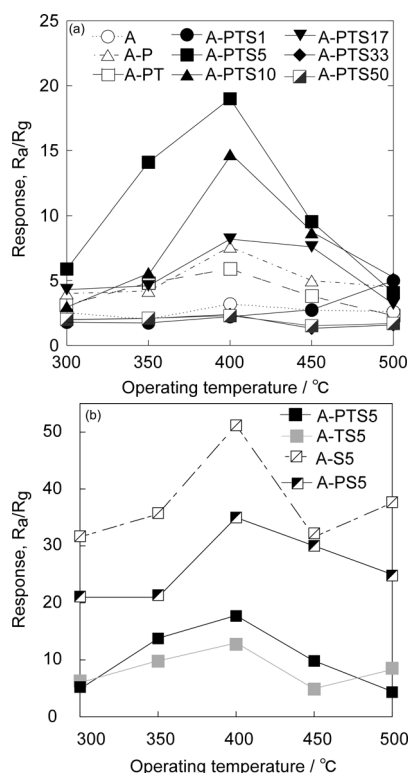


Fig. 2 Temperature dependences of response of sensors to 1000 ppm H<sub>2</sub>.

## Hydrogen Sensing Properties of Anodized TiO<sub>2</sub> Film Sensors Equipped with Pd and Pt Electrodes in Different Structure

Masaki Nakaoka<sup>1</sup>, Takeo Hyodo<sup>1</sup>, Yasuhiro Shimizu<sup>2</sup> and Makoto Egashira<sup>2\*</sup>

<sup>1</sup>Graduate School of Science and Technology,

<sup>2</sup>Department of Materials Science and Engineering, Faculty of Engineering,  
Nagasaki University, 1-14 Bunkyo-machi, Nagasaki 852-8521, Japan

\*Tel: +81-95-819-2642, Fax: +81-95-819-2643, E-mail: \*egashira@nagasaki-u.ac.jp

### Abstract

H<sub>2</sub> sensing properties of diode-type gas sensors fabricated with anodized TiO<sub>2</sub> films equipped with Pd and Pt electrodes in different structure have been investigated. In air atmosphere, the H<sub>2</sub> response of a TiO<sub>2</sub> sensor with Pd-Pt alloy electrodes fabricated by simultaneous sputtering of Pd and Pt (Pt-Pd/TiO<sub>2</sub>) was larger than those of sensors with layered electrodes of Pd(upper layer)/Pt(lower layer) or Pt(upper layer)/Pd(lower layer), which will be referred to be Pd/Pt/TiO<sub>2</sub> and Pt/Pd/TiO<sub>2</sub>, respectively, fabricated by successive sputtering of constituent metals. On the other hand, all sensors showed much larger H<sub>2</sub> responses in N<sub>2</sub> than those in air, and the magnitude of H<sub>2</sub> response was quite comparable to each other among three kinds of sensors in N<sub>2</sub>. These result show that adsorbed oxygen and/or thin oxide layers on the surface of Pd have a great influence on the H<sub>2</sub> sensing behavior.

*Keywords:* Anodic oxidation; TiO<sub>2</sub>; Diode-type sensor; H<sub>2</sub>

### Introduction

Our previous studies have revealed that a TiO<sub>2</sub> thin film having sub-micron pores could be fabricated by anodic oxidation of a Ti plate and that the anodized TiO<sub>2</sub> thin film equipped with a Pd top electrode and the Ti plate bottom electrode exhibited high H<sub>2</sub> response in a wide range of H<sub>2</sub> concentration as a diode-type sensor under flowing both air and N<sub>2</sub> atmospheres (1, 2). In this study, H<sub>2</sub> response properties of three kinds of sensors equipped with Pd-Pt electrodes, but in different structure, fabricated by r.f. magnetron sputtering were studied to evaluate the role of each noble metal.

### Experimental

A half part of a Ti plate (5.0 × 10.0 × 0.5 mm) was anodically oxidized in a 0.5 M H<sub>2</sub>SO<sub>4</sub> aqueous solution at 20°C for 30 min at a current density of 50 mA cm<sup>-2</sup>. A pair of electrode (3.0 × 3.0 mm) was fabricated on the TiO<sub>2</sub> thin film and the Ti plate by radio-frequency magnetron sputtering of Pd (300 W, 7 min) and Pt (200 W, 7 min) simultaneously (Pd : Pt = 36 : 64 (wt%)) or successively (See Fig. 1 and Table 1). The electrical contact to Au lead wires was achieved by application of a Pt paste and then was ensured by subsequent firing at 600°C for 1 h in dry air. A dc voltage of 1 mV was applied to the sensors under forward bias conditions, and the H<sub>2</sub> sensing properties were measured at 250°C to 8000 ppm H<sub>2</sub> balanced with air or N<sub>2</sub>. The H<sub>2</sub> response properties of the sensor subjected to the additional treatment in dry N<sub>2</sub> at 600°C for 1 h were also measured. For easy comparison, air- and N<sub>2</sub>-treatments are expressed as T<sub>air</sub> and T<sub>N<sub>2</sub></sub>, respectively, and



Fig. 1 Schematic sensor structure.

Table 1 Electrode structure of sensors.

| No. | Sensor                 | Electrode            |             |
|-----|------------------------|----------------------|-------------|
|     |                        | Upper layer          | Lower layer |
| 1   | Pd-Pt/TiO <sub>2</sub> | Pd-Pt (single layer) |             |
| 2   | Pt/Pd/TiO <sub>2</sub> | Pt                   | Pd          |
| 3   | Pd/Pt/TiO <sub>2</sub> | Pd                   | Pt          |

measurements in air and in N<sub>2</sub> atmosphere are indicated as M<sub>air</sub> and M<sub>N<sub>2</sub></sub>, respectively.

## Results and Discussions

Figure 2 shows response transients of three kinds of sensors to 8000 ppm H<sub>2</sub> at 250°C. Under the T<sub>air</sub>-M<sub>air</sub> conditions, the H<sub>2</sub> response of Pd-Pt/TiO<sub>2</sub> was the largest among the three kinds of sensors, probably due to the largest amount of dissolved H species into the alloy electrode. On the other hand, the H<sub>2</sub> response of Pt/Pd/TiO<sub>2</sub> was extremely smaller than those of Pd/Pt/TiO<sub>2</sub> and Pd-Pt/TiO<sub>2</sub>. This phenomenon may arise from higher H<sub>2</sub> oxidation activity of Pt than Pd, leading to a smaller amount of H<sub>2</sub> molecules capable of reaching at the surface of the under-laying Pd, especially in the case of Pt/Pd/TiO<sub>2</sub>. In contrast, all sensors showed much larger H<sub>2</sub> responses under the T<sub>N<sub>2</sub></sub>-M<sub>N<sub>2</sub></sub> conditions than those observed under the T<sub>air</sub>-M<sub>air</sub> conditions. This fact indicates that less amounts of oxygen adsorbate at the electrode surfaces as

well as in oxygen-free environment facilitate the dissolution of H species into the electrodes. In addition, Pt/Pd/TiO<sub>2</sub> showed faster response speed in comparison with Pd-Pt/TiO<sub>2</sub> and Pd/Pt/TiO<sub>2</sub> in air. This result can be explained by the less oxidative nature of Pt than Pd, namely the shorter time necessary for reducing the oxidized electrode surface. Actually, all sensors showed fast response speeds in N<sub>2</sub>. However, recovery speeds of all sensors in N<sub>2</sub> were terribly slower than those observed in air. This result implies that the existence of gaseous oxygen in the environment is essential for achieving fast extraction of H species dissolved into the electrodes, and therefore it takes a longer time for the complete extraction in N<sub>2</sub>.

## Conclusions

H<sub>2</sub> sensing properties of diode-type gas sensors of Pd-Pt/TiO<sub>2</sub>, Pt/Pd/TiO<sub>2</sub> and Pd/Pt/TiO<sub>2</sub> have been investigated. The magnitude of H<sub>2</sub> response and the response speed were largely dependent on the structure of the electrodes in air. On the other hand, the magnitude of H<sub>2</sub> response in N<sub>2</sub>, which was much larger than that in air, and H<sub>2</sub> response and recovery speeds were almost independent of the electrode structure. These results reveal that the adsorbed oxygen and/or thin oxide layers have a great influence on the H<sub>2</sub> sensing behavior.

## References

1. Y. Shimizu et al., *Sens. Actuators B*, **83**, 195 (2002).
2. H. Miyazaki et al., *Sens. Actuators B*, **108**, 467 (2005).

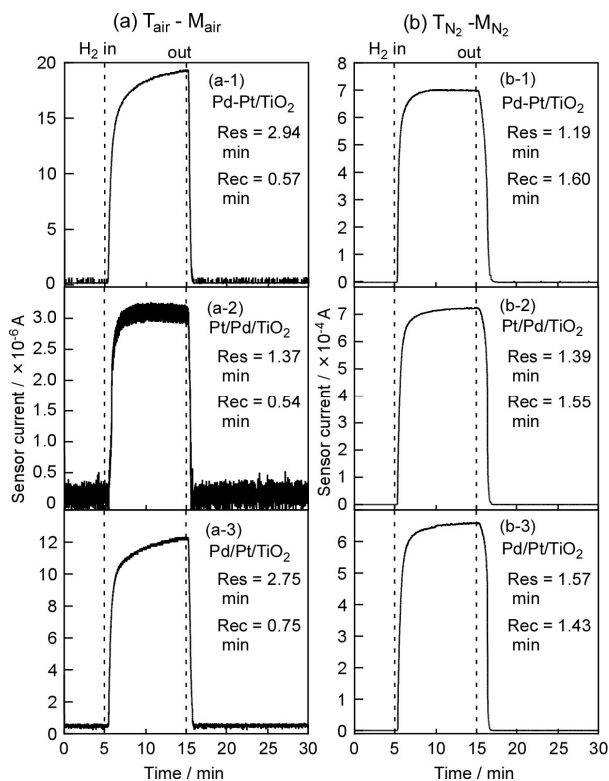


Fig. 2 Response transients of three kinds of sensors to 8000 ppm H<sub>2</sub> in (a) air and (b) N<sub>2</sub> at 250°C. The sensors were pretreated at 600°C for 1 h in (a) air and (b) N<sub>2</sub>.

## Preparation of Pore Filling Membrane with Pd Nanoparticles

Aki Tominaga<sup>1</sup>, Osamu Nakagoe<sup>2</sup> and Shuji Tanabe<sup>1\*</sup>

<sup>1</sup>Graduate School of Science and Technology,

<sup>2</sup>Department of Materials Science and Engineering,

Nagasaki University, 1-14 Bunkyo-machi, Nagasaki 852-8521, Japan

\*Tel: +81-95-819-2659, Fax: +81-95-819-2661, E-mail: s-tanabe@nagasaki-u.ac.jp

### Abstract

Hydrogen perm-selective membranes were composed Pd nanoparticles. The nanoparticles were prepared by sonochemical reduction from Pd<sup>II</sup> ions. Then the nanoparticles deposited on a substrate disc with electrophoresis technique. These electrophoretic membranes have shown high performance of perm-selectivity for H<sub>2</sub> with separation factor  $\alpha=3.85$ , under room temperature.

### Introduction

To realize the H<sub>2</sub> permeable membrane with high permeance rate, thinner metallic membrane has to be required<sup>1)</sup>. Thinner and denser membranes are required because of higher permeance rate of H<sub>2</sub>.

In this work, Pd nanoparticles were prepared with sonochemical reduction technique. The nanoparticles were precipitated on anodic oxidation alumina disc, and then the perm-selective membranes were created successfully using electrophoresis technique. Permeances of H<sub>2</sub> were measured with a closed circulation system at room temperature.

### Experimental

Pd nanoparticles were prepared from Pd<sup>II</sup> solution (0.4mM) with ultrasonic reduction under Ar atmosphere for 20 min<sup>2)</sup>. Formation of nanoparticles was confirmed by UV-vis spectra. Morphology of nanoparticles was observed by high-resolution transmission electron microscope (HR-TEM). The prepared Pd nanoparticles were deposited on the surface of anodic aluminum oxide (AAO, pore size : 20nm) substrates by electrophoresis (electrophoresis condition : 500V, 3min). The morphologies of the deposited membrane were observed by field emission scanning electron microscope (FE-SEM).

Permiations of N<sub>2</sub> and H<sub>2</sub> were evaluated by monitoring the pressure on both sides of membrane using a vacuum line under ambient temperature.

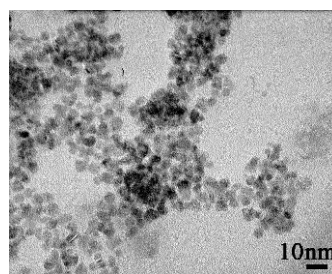


Fig.1 TEM photograph of Pd nanoparticles. (average particle size =  $4.04 \pm 1.28$  nm)

Volume of permeation ( $q$  [ $\text{cm}^3$ ]), permeability coefficient ( $R$  [ $\text{cm}^3 (\text{cm}^2 \cdot \text{mmHg} \cdot \text{sec})^{-1}$ ]), and separation factor ( $\alpha$ ) were calculated by equations described as follows,

$$q = R(p_1 - p_2)A\Delta t,$$

$$\alpha = R_{\text{H}_2} / R_{\text{N}_2},$$

where  $P$  is transmission coefficient [ $\text{cm}^3 \cdot \text{cm} (\text{cm}^2 \cdot \text{cmHg} \cdot \text{sec})^{-1}$ ],  $(p_1 - p_2)$  is differential pressure [ $\text{cmHg}$ ],  $A$  is membrane area [ $\text{cm}^2$ ],  $t$  is differential time [ $\text{sec}$ ],  $l$  [ $\text{cm}$ ] is membrane thickness.

## Results and Discussions

Table 1. Gas permeation properties of obtained membrane

| Membrane               | Permeation gas | $R$ [ $\text{cm}^3 (\text{cm}^2 \cdot \text{cmHg} \cdot \text{sec})^{-1}$ ] | $\alpha$ [-] |
|------------------------|----------------|---|--------------|
| Before electrophoresis | H <sub>2</sub> | $1.97 \times 10^{-6}$   | 2.90         |
|                        | N <sub>2</sub> | $6.77 \times 10^{-7}$   |              |
| After electrophoresis  | H <sub>2</sub> | $9.37 \times 10^{-8}$   | 3.85         |
|                        | N <sub>2</sub> | $2.43 \times 10^{-8}$   |              |

From Fig. 1, average size of Pd nanoparticles was ca. 4.0 nm in diameter. Table 1 shows photographs of AAO substrates before and after electrophoresis of Pd nanoparticles. It was clear that Pd nanoparticles were fixed on the surface of substrate because AAO substrate colored to black after the electrophoresis. These data indicate that Pd nanoparticles were filled in nano pores of AAO substrate. This membrane has separation factor of hydrogen  $\alpha = 3.85$ .

## Conclusions

In summary, we developed new preparation procedure which could make the very thin hydrogen perm-selective membrane. The procedure consisted of two preparation steps, one was the preparation of nanoparticles by sonochemical reduction and the other was deposition of the particles on a substrate by the electrophoresis method. The hydrogen permeance rate and hydrogen-nitrogen separation factor of the obtained membrane showed very high performance at the room temperature.

## References

1. Lu. G. Q et al., *Colloid. Int. Sci.*, **314**, 589-603 (2007).
2. K. Okitsu et al, *Chem. Mater.* **8**, 315-317 (1996).

## Preparation of Au-Pd core-shell nanoparticles supported TiO<sub>2</sub> photocatalyst with sonochemical technique

Hiroaki Ejima<sup>1</sup>, Osamu Nakagoe<sup>2</sup>, Naoki Shima<sup>1</sup>, Aki Tominaga<sup>1</sup> and Shuji Tanabe<sup>1\*</sup>

<sup>1</sup>*Graduate School of Science and Technology,*

<sup>2</sup>*Department of Materials Science and Engineering, Faculty of Engineering,  
Nagasaki University, 1-14 Bunkyo-machi, Nagasaki 852-8521, Japan*

\**Tel: 095-819-2659, Fax: 095-819-2661, E-mail: s-tanabe@nagasaki-u.ac.jp*

### Abstract

TiO<sub>2</sub> Photocatalysts fixed with Au core Pd shell (Au@Pd) nanoparticle were prepared and evaluated these catalytic activities. Au@Pd Nanoparticles were prepared by ultrasound irradiation toward aqueous solutions containing HAuCl<sub>4</sub>·4H<sub>2</sub>O, PdCl<sub>2</sub>·2NaCl·3H<sub>2</sub>O and surfactant (PEG-MS: polyethylene glycol-monostearate). The photocatalytic activities were evaluated from H<sub>2</sub> formation on ethanol decomposition. It was found from the results that Pd shell thickness on the Au@Pd nanoparticles strongly affected the activity of H<sub>2</sub> formation.

### Introduction

TiO<sub>2</sub> Photocatalyst is applied to the various fields because it has high activity for decomposition of the organic compounds. To improve the activity, it is necessary to inhibit recombination of electron-hole pair which is formed by photo excitation. The immobilization of noble metal nanoparticles on TiO<sub>2</sub> surface is one of the promising ways to suppress recombination of electron-hole pair due to modification of its electronic state. The electronic state of bimetallic nanoparticles was strongly depended on its structure. Especially, we have already reported the bimetallic nanoparticle with core-shell structure, which has one metal core covered with another metal as a shell, show high activity. In this paper, we report the preparation of bimetallic nanoparticles with core-shell structure supported on TiO<sub>2</sub> by ultrasound reduction and photocatalytic activity for H<sub>2</sub> formation from ethanol decomposition.

### Experimental

Au@Pd Nanoparticles were prepared by ultrasound irradiation (200 kHz, 6 W/cm<sup>2</sup>) of aqueous solution containing HAuCl<sub>4</sub>·4H<sub>2</sub>O, PdCl<sub>2</sub>·2NaCl·3H<sub>2</sub>O and PEG-MS. To control the thickness of the shell, the solutions included the different Pd/Au atomic ratio were used as starting materials. The Au@Pd nanoparticles were immobilized on the TiO<sub>2</sub> surface by adding to TiO<sub>2</sub> powder in the colloidal solution followed with ultrasound irradiation. In order to elucidate the correlation between geometric structure in the nanoparticle and catalytic activity, mixture of Au and Pd nanoparticles were also

immobilized on TiO<sub>2</sub> photocatalyst (Pd atomic ratio = 0.25, 0.5 and 0.75, denoted as Au+Pd). Formation of core-shell structure was confirmed with UV-vis spectra. The shape and diameter of noble metal nanoparticles were measured by HR-TEM. Photocatalytic activity of Au@Pd/TiO<sub>2</sub> and Au+Pd/TiO<sub>2</sub> was evaluated by H<sub>2</sub> formation from ethanol decomposition.

## Result and Discussions

UV-vis Spectra indicated that absorption peaks corresponded to surface plasmon resonance were observed in Au+Pd solutions, whereas the peaks disappeared in the Au@Pd solutions because Au nanoparticles were covered with Pd nanoparticles completely. It was suggested that Au@Pd core-shell nanoparticles formed. TEM Images and average diameter of noble metal nanoparticles indicated that the diameter decreased with increasing initial Pd concentration. Fig.1 shows the comparison of photo catalytic activities between Au@Pd and Au+Pd nanoparticles on TiO<sub>2</sub> powder. The result indicated that the activities of all of the Au@Pd supported TiO<sub>2</sub> photocatalysts were higher activity than those of Au+Pd/TiO<sub>2</sub> catalysts and the H<sub>2</sub> evolution from Au@Pd had the maximum at 0.52 of Pd atomic ratio. In addition, the shell thickness and core diameter of Au@Pd nanoparticles strongly depend on Pd atomic ratio as shown in Table 1. These results led us to the conclusion that noble metal nanoparticles with core-shell structure probably inhibited a recombination of electron-hole pair, and that Pd shell thickness strongly influenced the catalytic activities.

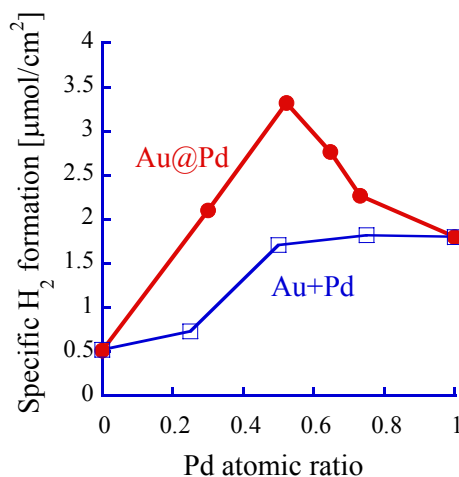


Fig.1 The dependence of specific amount of H<sub>2</sub> formed on Pd atomic ratio in Au/Pd bimetallic nanoparticles.

## Conclusions

TiO<sub>2</sub> Photocatalysts fixed with Au@Pd nanoparticles were successfully prepared with sonochemical procedure. The catalytic activities of ethanol decomposition on Au@Pd/TiO<sub>2</sub> were higher than those of Au+Pd/TiO<sub>2</sub> catalysts. The thickness of Pd shell strongly affected the catalytic activities due to the specific H<sub>2</sub> formation decreased with increasing Pd shell thickness.

Table 1 Core size and shell thickness of Au@Pd calculated from TEM observation

| Pd Atomic ratio | Core nm | Shell nm | Surface area cm <sup>2</sup> |
|-----------------|---------|----------|------------------------------|
| 0               | -       | -        | 58                           |
| 0.52            | 5.2     | 0.65     | 84                           |
| 0.64            | 4.6     | 0.80     | 96                           |
| 0.73            | 3.9     | 0.95     | 108                          |
| 1               | -       | -        | 155                          |

## Substrate Bias Effect on Deposition Process of Amorphous Carbon Films

Takanori Inayoshi<sup>1</sup>, Hiroki Kawazoe<sup>1</sup>, Masanori Shinohara<sup>2\*</sup>

Yoshinobu Matsuda<sup>2</sup>, Hiroshi Fujiyama<sup>1</sup>, Yuki Nitta<sup>3</sup> and Tatsuyuki Nakatani<sup>3</sup>

<sup>1</sup>*Graduate School of Science and Technology, Nagasaki University*

<sup>2</sup>*Department of Electrical and Electronic Engineering, Nagasaki University*

*1-14 Bunkyo-machi, Nagasaki 852-8521, Japan*

<sup>3</sup>*Toyo Advanced Technologies Co., Ltd.,*

*5-3-38 Ujina-higashi Ninami-ku Hiroshima, 734-8501, Japan.*

\*E-mail: [sinohara@nagasaki-u.ac.jp](mailto:sinohara@nagasaki-u.ac.jp)

### Abstract

Substrate bias effects on the deposition process of amorphous carbon films were investigated by using infrared spectroscopy in multiple internal reflection geometry (MIR-IRAS). The density of the sp-CH species was increased in amorphous carbon films with substrate bias; on the other hand, the density of the sp<sup>3</sup>-CH<sub>X</sub> (X=1~3) species was decreased in amorphous carbon films with substrate bias.

### Keywords:

Acetylene plasma, Amorphous carbon film, Deposition process, Infrared spectroscopy, Substrate bias

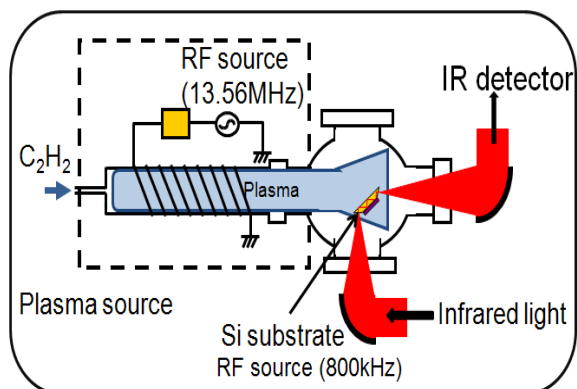
### Introduction

An amorphous carbon film has been one of promising materials because it has unique properties such as mechanical hardness, chemical inertness, bio-compatibility, and changeable electrical property. Additionally, it can be synthesized at low temperature by plasma process. So, it is widely used in the industry. Now, it is often deposited by using acetylene (C<sub>2</sub>H<sub>2</sub>) gas as a source gas. To obtain the desirable film properties, it is important to control the film deposition process. Then, the deposition process has to be understood. In fact, the detailed deposition has not been understood, because there are a lot of parameters in this process. One of important process parameters is substrate bias. We have investigated the substrate bias effect on deposition process of amorphous carbon films by using infrared spectroscopy in multiple internal reflection geometry (MIR-IRAS).



## Experiments

We observed deposition process of amorphous carbon films by using “in-situ” and “real time” infrared spectroscopy in multiple internal reflection geometry (MIR-IRAS). The film thickness during deposition was estimated from the deposition rate. The film deposition rate was calculated from the deposition time and the thickness after the deposition measured with the profilometer. Plasma was generated by 13.56 MHz RF power. The substrate bias was fed by 800kHz RF power.



Plasma was generated by 13.56 MHz RF power. The substrate bias was fed by 800kHz RF power.

## Results and Discussions

Compared the substrate bias of 0V with that of -200V, we observe a similar spectra when the film thickness is 1nm. As the film grows thicker, the deference grew larger. At the substrate bias of 0V, the intensity of the peak around  $2900\text{cm}^{-1}$ , which corresponds with the  $\text{sp}^3\text{-CH}_x$  species, was increased more than that of the peak located around  $3360\text{cm}^{-1}$ , which corresponds with the  $\text{sp-CH}$  species. On the other hand, at the bias of -200V, the peak intensity of the  $\text{sp-CH}$  and that of the  $\text{sp}^3\text{-CH}_x$  grew at almost the same rate.

This phenomenon is considered as follows: at the bias of 0V, the  $\text{sp-CH}$  deposited on the film reacts with H species in plasma. Then, the density of the  $\text{sp}^3\text{-CH}_x$  species was increased. On the other hand, at the bias of -200V, in addition of this effect, the effect of drawing the  $\text{sp-CH}$  species into the film grew also larger.

## Conclusions

Substrate bias effects on the deposition process of amorphous carbon films have been investigated by using infrared spectroscopy in multiple internal reflection geometry (MIR-IRAS). Owing to the substrate bias, the density of the  $\text{sp-CH}$  species was increased in amorphous carbon films.

## Acknowledgements

This research was partially supported by a Grant-in-Aid for Young Scientists (A), No. 20684027 (2008-2011) from the Ministry of Education, Culture, Sports, Science and Technology (MEXT) of Japan

## Source Molecular Effect on Amorphous Carbon Film Deposition

Hiroki Kawazoe<sup>1</sup>, Takanori Inayoshi<sup>1</sup>, Masanori Shinohara<sup>2\*</sup>

Yoshinobu Matsuda<sup>2</sup>, Hiroshi Fujiyama<sup>1</sup>, Yuki Nitta<sup>3</sup> and Tatsuyuki Nakatani<sup>3</sup>

<sup>1</sup>Graduate School of Science and Technology, Nagasaki University

<sup>2</sup>Department of Electrical and Electronic Engineering, Nagasaki University

1-14 Bunkyo-machi, Nagasaki 852-8521, Japan

<sup>3</sup>Toyo Advanced Technologies Co., Ltd.,

5-3-38 Ujina-higashi Ninami-ku Hiroshima, 734-8501, Japan.

\*E-mail: sinohara@nagasaki-u.ac.jp

### Abstract

We investigated deposition process of amorphous carbon films using acetylene and methane as a source molecule, by using infrared spectroscopy in multiple internal reflection geometry (MIR-IRAS). We found that deposited film structures were different due to source molecules.

### Keywords:

Acetylene, Methane, Plasma, Amorphous carbon film, Deposition process, Infrared spectroscopy

### Introduction

An amorphous carbon film is used in many fields because it has various useful characteristics. The films were often deposited by using acetylene ( $C_2H_2$ ) as a source gas as well as by using methane. We think the film structures have a relation with the structure of source molecule. Then, we investigate the difference of deposition process of the films due to source molecules: acetylene ( $C_2H_2$ ) and methane ( $CH_4$ ). We used “in-situ” and “real-time” infrared spectroscopy in multiple internal reflection geometry (MIR-IRAS).

### Experiments

Figure 1 shows the experimental setup used in this study. Source gases,

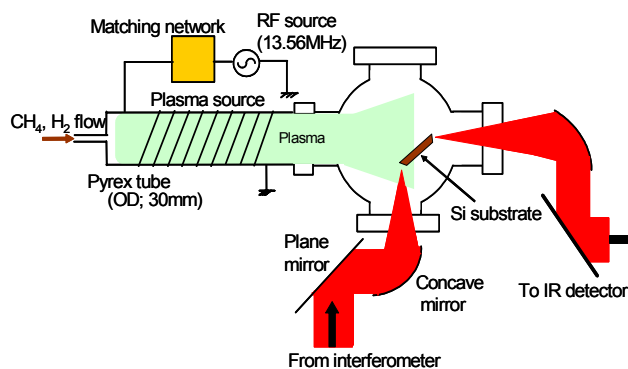


Fig 1. Experimental setup

such as  $C_2H_2$  or  $CH_4$ , were introduced from the glass tube into the vacuum chamber. Plasma excitation was accomplished by RF power (13.56 MHz) to the coil wrapped around the glass tube via the matching box. Si substrate ( $10 \times 40$  mm) that grinds the short edges to 45 degrees is mounted as shown in the figure. The infrared light traveled into the Si sample with internal multiple reflections. This MIR-IRAS has high sensitivity to the surface reaction even during plasma.

## Results and Discussions

When  $CH_4$  was used as a source gas, we observed the large peaks due to the  $sp^3-CH_x$  ( $x=1 \sim 3$ ) species and the small peaks due to the  $sp^2-C$  species. On the other hand, when  $C_2H_2$  was used, we observed the large peaks due to the  $sp-CH$  species, the  $sp-C$  species, the  $sp^2-C$  species, and the  $sp^3-CH_x$  species, in addition to the peak due to the  $sp^3-CH_x$  species.

These results indicated that the  $sp$ - species is easily formed when  $C_2H_2$  was used. We considered that a  $CH_4$  molecule is composed of  $sp^3-CH$  bond in itself; on the other hand, a  $C_2H_2$  molecule contains an  $sp$ -bond in itself. This difference leads to the film structures. It means that the decomposition of source molecules during plasma is also different.

## Conclusions

Deposition process of amorphous carbon films using acetylene and methane as a source molecule was investigated by using infrared spectroscopy in multiple internal reflection geometry (MIR-IRAS). Films deposited using acetylene contained a lot of the  $sp$ -species such as the  $sp-C$ ,  $sp-CH$  species. On the other hand, films deposited using methane contained a lot of  $sp^3-CH_x$  species and less the  $sp$ -species.

## Acknowledgements

This research was partially supported by a Grant-in-Aid for Young Scientists (A), No. 20684027 (2008-2011) from the Ministry of Education, Culture, Sports, Science and Technology (MEXT) of Japan

## Surface Modification due to Solution Plasma

Z. Shuai<sup>1</sup>, K. Akaki<sup>2</sup>, K. Shimizu<sup>2</sup>, K. Kotani<sup>2</sup>, M. Shinohara<sup>2\*</sup>,  
Y. Matsuda<sup>2</sup>, and H. Fujiyama<sup>1</sup>

<sup>1</sup>*Graduate School of Science and Technology,*

<sup>2</sup>*Department of Electrical and Electronic Engineering, Faculty of Engineering,  
Nagasaki University, 1-14 Bunkyo-machi, Nagasaki 852-8521, Japan*

\*Tel: +81-95-819-2542, Fax: +81-95-819-2542, E-mail: [sinohara@nagasaki-u.ac.jp](mailto:sinohara@nagasaki-u.ac.jp)

### Abstract

We succeeded in the generation of two types of solution plasmas: one was generated in the ultrasonic bubbles by feeding DC power or commercial AC 60Hz power for the etching of silicon substrate. The other plasma was generated by low frequency power for the film deposition inside tubes. Now we are optimizing the plasma generation condition for each application.

**Keyword:** solution plasma, etching, deposition, amorphous carbon film

### Introduction

Solution plasma indicates plasma in liquid phase. This solution plasma is not widely utilized, in a comparison with regular plasmas in gas phase. Although nowadays it was utilized as water clarification, fabrication of nanoparticles, sterilization, and so on, we consider such applications were not sufficient. This is because we believe the possibilities of solution plasma were not fully utilized.

Then we expect one of the promising challenges is for material surface treatments, like plasma etching and plasma deposition using regular gas-phase plasma. Solution plasma has some advantages of the material processing: the experimental setup is very cheap. Furthermore, the solution plasma can be generated in a very small area. Then, it can be used for film coating and etching on a small area, with low cost. Especially it is suitable to the film coating on the inside area of fine tubes. The cheap tubes can be changed to high-value tubes, by coating the functional films inside the tubes. Moreover, the plasma can be generated in various solvents. Then, the film coating and etching techniques without hazardous acid or alkali solutions and hazardous or greenhouse gases will be developed: solution plasmas can help the establishments of the next-generation processes: they are required to be easy on the earth.

## **Experiments and Results**

For silicon-surface etching, solution plasma was generated by applying DC power or commercial AC power to the electrodes with special configurations during the bubbles in pure water. The bubbles were generated with an ultrasonic homogenizer (produced by Kaijo); the ultrasonic homogenizer has a stainless steel horn of 30 mm in diameter. Its power can be changed to 600W; its frequency is 20 kHz. We confirmed silicon etching with microscope and profilemeter.

For coating the functional films inside the fine tubes, the solution plasma was generated in the inside tube with applying 10 kHz power, but without ultrasonic bubble. We can deposit the carbon film in side the tube. The film was analyzed with FT-IR.

We will show the detailed present study in this presentation.

## **Acknowledgements**

This research was partially supported by Research for promoting technological seeds from JST (2008-2009) and a Grant-in-Aid for Scientific Research Nagasaki University (2007-2008).

## Monitoring of Chemical Vapor Deposition Process of Hydrocarbon Thin Films by Optical Reflectance Interferometry

Kazuishi Uehara<sup>1</sup>, Masanori Shinohara<sup>2</sup>, Yoshinobu Matsuda<sup>2</sup>

<sup>1</sup>Graduate School of Science and Technology, <sup>2</sup>Department of Electrical and Electronic Engineering, Nagasaki University, Bunkyo 1-14, Nagasaki 852-8521, Japan  
Tel: +81-95-819-2540, Fax: +81-95-819-2540, E-mail:ymat@nagasaki-u.ac.jp

### Abstract

Optical reflectance interference has been investigated during the deposition processes of hydrocarbon thin films. A clear oscillation in the laser power reflected from the substrate has been observed during the deposition. From the instantaneous oscillation amplitude, temporal change in the refractive index was evaluated.

### Introduction

The chemical vapor deposition (CVD) of hydrocarbon thin films including DLC films have been well established and widely used in many variety of industry so far. [1] It will be useful to establish an inexpensive and handy in-situ monitoring method. For the purpose, we have focused attention on the optical reflectance interference [2] using a small power cw laser. In this paper, experimental results of measurement of reflectance interference signal during CVD processes of hydrocarbon thin films are presented. In addition, possibility of in-situ monitoring of deposition rate and refractive index are discussed.

### Experimental

A single turn coil antenna with a diameter of 100 mm was arranged in the middle of the chamber to excite the inductive RF discharge. After the chamber was evacuated down to a pressure less than  $3 \times 10^{-6}$  Torr, working gases were introduced by mass flow controllers at the total flow rate of 10 sccm and the total working pressure was set at 5 mTorr. For the chemical vapor deposition of hydrocarbon thin films, mixed gas of 50 % argon and 50 % methane was used in 13.56MHz inductively coupled plasma.

To monitor the reflectance interference, 1 mW He-Ne laser beam was incident onto a polished surface of Si (001) substrate attached on a substrate holder located 5 cm behind the ICP center. The geometry was approximated to vertical incidence. Reflected beam was focused by a lens on the sensing area of a photodiode. Temporal change of the photodiode output was displayed and recorded on a PC.

## Results and Discussion

Figure 1 shows the temporal variation of photodiode output during hydrocarbon film deposition by Ar/CH<sub>4</sub>-ICP. The exact, integrated deposition time was 1866s. The film thickness after the deposition was measured by a stylus profiler. As a result, film thickness was found 2.8μm. In addition, the averaged refractive index of the deposited thin films was calculated as 1.7. This value is lower than the reported refractive indices for DLC films (1.8-2.4) which are usually fabricated with high substrate bias more than 100V, but corresponds to the values of hydrogenated carbon films fabricated under low substrate bias.

Here, we will make analysis by assuming the deposition rate is constant. By comparing the experimental instantaneous values read over each oscillation period, we can obtain the instantaneous refractive index at each different local minimum point. In addition, the experimental increment of optical path length over the oscillation period  $\Delta$  was read at each different local minimum point. Evaluated  $n_1$  and  $\Delta$  are plotted in Fig. 2. Figure.2 shows the instantaneous refractive index decreased from 2.0 to 1.3 during deposition. It is noted the calculated  $2n_1 \Delta$  is close to the laser wavelength  $\lambda=632.8$  nm over the entire deposition time.

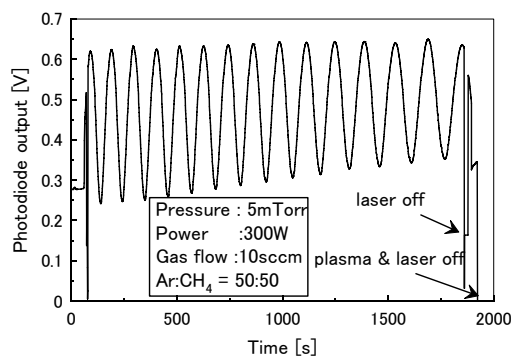


Fig. 1 Temporal variation of photodiode output during hydrocarbon film deposition

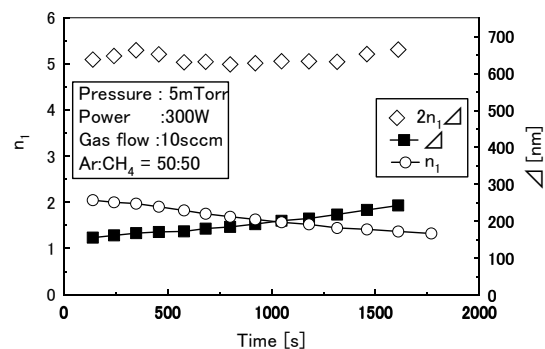


Fig. 2 Temporal variations of refractive index and the instantaneous increment

## Conclusions

Deposition process of hydrocarbon films was investigated by optical reflectance interference. By using several assumptions, temporal change in refractive index during deposition was obtained. It has to be cross-checked, but this technique has a potential for a simple process monitor.

## References

- [1] J.Robertson: Materials Science and Engineering, R 37 (2002) 129.
- [2] S. Yoshida and H. Yajima: "Optical Thin Films and Devices", University of Tokyo Press, Tokyo (1994) (in Japanese).

## Influence of hydrogen addition on electric and optical properties of sputter-deposited aluminum-doped zinc oxide thin films

Ryoji Kan<sup>1</sup>, Tadashi Iwata<sup>1</sup>, Takashi Shibasaki<sup>1</sup>, Masanori Shinohara<sup>2</sup>,  
and Yoshinobu Matsuda<sup>2\*</sup>

<sup>1</sup>*Graduate School of Science and Technology,*

<sup>2</sup>*Department of Electrical and Electronic Engineering,*

*Nagasaki University, Bunkyo-machi 1-14, Nagasaki 852-8521, Japan*

*\*Tel: +81-95-819-2540, Fax: +81-95-819-2540, E-mail: ymat@nagasaki-u.ac.jp*

### Abstract

We have investigated the influence of hydrogen addition on AZO thin films. The electric conductivity of the film was improved when a very small amount of hydrogen (0.25%) was added, but was decreased by adding excessive amount of hydrogen. The optical transmittance and the deposition rate were almost constant for a small amount of hydrogen addition of not more than 0.5%, but decreased by adding excessive amount of hydrogen.

### Introduction

For the last ten years, aluminum-doped zinc oxide (AZO) has been a focus of constant attention as a transparent conducting material that may take the place of tin-doped indium oxide (ITO). The inherent electric conductivity of AZO is lower than that of ITO, but the former has advantages over ITO in environment resistance and resource cost. To completely replace the ITO, a reproducible and highly-reliable fabrication process of good quality AZO thin films has to be developed. Recently, it has been reported that the electric conductivity of the AZO film was improved when hydrogen gas was added to working argon (Ar) gas.[1] Thus, we have investigated the effect of hydrogen addition on the electric conductivity, optical transmittance and deposition rate of the AZO thin films deposited by ICP assisted sputter-deposition.

### Experimental Setup and Procedure

A 2 wt % aluminum-doped ZnO target was used in the experiment. The distance between the target and the substrate was set 80mm. An internal coil antenna of 10cm in diameter covered with insulator was arranged between the substrate and the target. Argon mixed with a small amount of hydrogen was used for the working gas. The total gas pressure was fixed at 30 mTorr, and the amount of hydrogen addition was changed by setting the preset partial pressure of hydrogen before each deposition. The fraction of hydrogen defined by  $C_H(= [H_2]/([Ar]+[H_2]))$  was varied in steps 0, 0.25, 0.5 and 1%.



The ultimate pressure in the chamber was  $3 \times 10^{-6}$  Torr or less. The flow rate of Ar was adjusted to 50 sccm by using a mass flow controller. The sputtering power (target power) and the ICP assist power (ICP-RF power) were fixed at 44W and 200W, respectively. Deposition time was 30 minutes for all samples. The film thickness, the electric conductivity and the optical transmittance of the deposited AZO thin films were measured by a stylus profiler (Mitsutoyo, SV-400), a four-point probe and an optical fiber spectrometer (ocean optics, HR4000CG) for each piece, respectively.

## Results

Figures 1 and 2 show the change in resistivity, transmittance and deposition rate of ZnO films against the hydrogen mixture fraction. From Fig.1, it is found that the film conductivity was slightly improved; the minimum resistivity of  $1.8 \times 10^{-3} \Omega \text{cm}$  was obtained at  $C_H = 0.25\%$ . Excess addition of hydrogen more than 0.5%, however, decreased the film conductivity. Next, the transmittance and the deposition rate is shown in Fig. 2. The optical transmittance and the deposition rate decrease at  $C_H = 1.0 \%$ .

## Conclusions

By adding a small amount of hydrogen into the working argon gas, a slight improvement of film conductivity was confirmed in the ICP assisted sputter-deposition of aluminum doped ZnO. The lowest resistivity of  $1.8 \times 10^{-3} \Omega \text{cm}$  was obtained at 0.25% hydrogen addition. However, adding excessive amount of hydrogen of more than 0.5% deteriorated all the conductivity, the transmittance and the deposition rate of deposited AZO thin films.

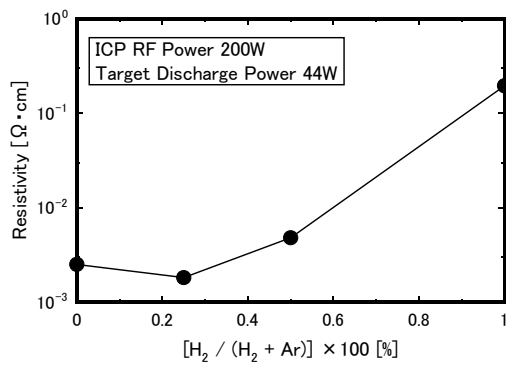


Fig1 Variations of resistivity of AZO films deposited under Ar + H<sub>2</sub> Plasma for different H<sub>2</sub> fraction

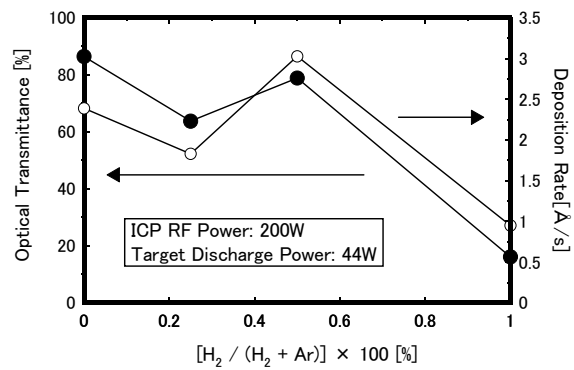


Fig.2 Variations of optical transmittance and deposition rate of AZO films deposited under Ar + H<sub>2</sub> Plasma for different H<sub>2</sub> fraction

## References

- [1] R. Das, K. Adhikary, and S. Ray: Jpn. J. Appl. Phys. 47 (2008) 1501.

## Porous V<sub>2</sub>O<sub>5</sub>/Carbon Nano-composites Electrodes for Rechargeable Power Sources with Large Capacity and High Power

Isamu Moriguchi<sup>1,\*</sup>, Keisuke Matsuo<sup>2</sup> and Hirotohi Yamada<sup>1</sup>

<sup>1</sup>*Faculty of Engineering,*

<sup>2</sup>*Graduate School of Science and Technology,*

*Nagasaki University, 1-14 Bunkyo-machi, Nagasaki 852-8521, Japan*

*\*Tel/Fax: +81-95-819-2669, E-mail: mrgch@nagasaki-u.ac.jp*

### Abstract

Nanoporous composite electrodes for rechargeable power sources were successfully fabricated by coating porous carbon with thin V<sub>2</sub>O<sub>5</sub> gel layers. Their electrochemical properties were demonstrated, which took after both lithium ion batteries and electrochemical double layer capacitors. The nanoporous V<sub>2</sub>O<sub>5</sub>/carbon composites exhibited large capacity of more than 100 mAh (g-composite)<sup>-1</sup> and good rate capability of 80% at 5.0 A (g-composite)<sup>-1</sup>. The good performance is explained by electric double layer capacitance of large surface area and high rate lithium insertion to thin V<sub>2</sub>O<sub>5</sub> gel layers.

### Introduction

Rechargeable power sources with both large capacity and high power are strongly demanded for their potential application to power sources for electric vehicles (EVs). Electric double layer capacitors (EDLCs) and lithium ion batteries (LIBs) are the most promising candidates. EDLCs exhibit good rate capability but low capacity. On the other hand, capacity of LIBs are relatively high but their power density is not enough for EVs. In this study, composite electrodes based on concepts of both EDLCs and LIBs were synthesized.<sup>1)</sup> We prepared V<sub>2</sub>O<sub>5</sub>/carbon nanoporous composites that utilize capacitance of both double layer and pseudo capacitance of lithium insertion into V<sub>2</sub>O<sub>5</sub>. The structure and the electrochemical properties of the composite electrodes are reported.

### Experimental

Ordered porous carbons that are employed as frameworks of composite electrodes were synthesized by using colloidal crystals of SiO<sub>2</sub> (particle size: 110 nm) as templates. The detailed procedure was reported elsewhere.<sup>2)</sup> The porous carbons were dispersed in a V<sub>2</sub>O<sub>5</sub> sol that were prepared by dissolving vanadium powder in hydrogen peroxide.<sup>3)</sup>

After stirring, carbons were collected by filtration and dried. This coating process was repeated several times.  $V_2O_5$ -coated carbon thus obtained is hereafter abbreviated as  $V_2O_5[n]/C$ , where  $n$  is the number of the coating process. Surface areas and porous structure of  $V_2O_5[n]/C$  were investigated by  $N_2$  ad-/desorption isotherms and TEM, respectively. Electrochemical properties of  $V_2O_5[n]/C$  were investigated by cyclic voltammetry and galvanostatic charging/discharging in 1 M  $LiClO_4$  (PC + DME).

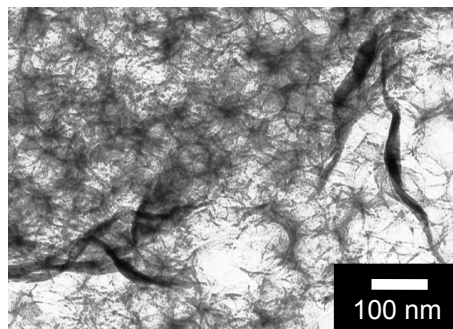


Fig. 1. TEM image of porous  $V_2O_5[9]/C$ .

### Results and Discussions

TEM images revealed the porous carbons had ordered spherical pores with a diameter of 110 nm, and was coated with  $V_2O_5$  for  $V_2O_5[n]/C$  (Fig. 1). The amounts of loaded  $V_2O_5$  increased almost linearly with repeating the coating process, and about 34 wt-% of  $V_2O_5$  was loaded after 11th cycle. In cyclic voltammograms (Fig. 2), for pristine carbon, almost rectangular voltammograms were obtained due to charging/discharging of double layer capacitance, which was calculated to be about  $80 \text{ F g}^{-1}$ .

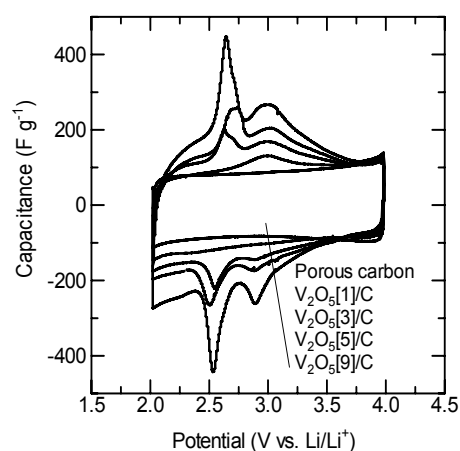


Fig. 2. Cyclic voltammograms of porous carbon and  $V_2O_5[n]/C$  nanoporoues composites.

Coating  $V_2O_5$  layers on carbons resulted in appearance of two pairs of red-ox peaks at 2.6 V and 2.9 V, indicating lithium insertion to and extraction from amorphous  $V_2O_5$ .  $V_2O_5[n]/C$  exhibited large capacity of  $50 - 100 \text{ mAh (g-composite)}^{-1}$  between 2.0 – 4.0 V vs.  $Li/Li^+$ , and 80% of capacity was retained at a high charge rate of  $5.0 \text{ A g}^{-1}$ . In summary, large capacity and high rate capability of  $V_2O_5$ /carbon nanoporous composites were successfully demonstrated.

### References

1. H. Yamada, et al., *J. Phys. Chem. C.*, **111**, 8397-8402 (2007).
2. I. Moriguchi, et al., *Electrochem. Solid-State Lett.*, **7**, A221-A223 (2004).
3. T. Kudo, et al., *Solid State Ionics*, **152-153**, 833-841 (2002).

## Proton Conducting Membrane Prepared from Organic-Inorganic Hybrid Precursor for Intermediate Temperature Fuel Cells

Hirotohi Yamada<sup>1,\*</sup>, Shintaro Aono<sup>2</sup> and Isamu Moriguchi<sup>1</sup>

<sup>1</sup>*Faculty of Engineering,*

<sup>2</sup>*Graduate School of Science and Technology,*

*Nagasaki University, 1-14 Bunkyo-machi, Nagasaki 852-8521, Japan*

*\*Tel/Fax: +81-95-819-2861, E-mail: h-yama@nagasaki-u.ac.jp*

### Abstract

Proton conducting membranes were prepared by using epoxy-resin-silica hybrid polymer as flexible matrix and Cs-doped phosphotungstic acid PWA (Cs-PWA) as proton conducting networks. Cs-PWA was well dispersed and the membranes exhibited good flexibility. Thermogravimetric analysis indicated that the membranes were stable at temperatures up to about 230°C. Proton conductivity of the membrane with a weight ratio of Cs-PWA/E201=1.6 were about  $8.1 \times 10^{-4} \text{ Scm}^{-1}$  at 160°C and 80% relative humidity. Their conductivity was improved by increasing volume fraction of Cs-PWA, which was successful after Cs-PWA was ground to nano-sized particles.

### Introduction

In many researches on Polymer electrolyte membrane fuel cells (PEMFCs), protonic conducting membranes that work at above 100°C have been strongly required in order to solve the inactivation of Pt catalyst by CO, to reduce the amount of Pt, and to improve the quality of exhaust gas as heat sources. Protonic conducting membranes consisting of organic-inorganic composites are attractive because of their flexibility of organic matrix and high protonic conductivity at elevated temperatures of inorganic materials. In this study, we employed an organic-inorganic compound “Compoceran E201®” consisting of epoxy monomer and siloxane (E201, Arakawa Chemical Industries, LTD.) as matrix. With E201, better dispersion of inorganic materials in the matrix is expected because siloxane part exhibits affinity to inorganic materials. We report the preparation and proton conductivity of membranes synthesized by dispersing Cs doped phosphotungstic acid (Cs-PWA) as inorganic proton conductors in E201.

### Experimental

Cs-PWA was synthesized by mechanochemical reaction of  $\text{Cs}_2\text{SO}_4$  and PWA by using a ball-mill.<sup>1)</sup> Cs-PWA was dispersed and well stirred in E201 dissolved in acetone.

After 2-ethyl-4-methylimidazol was added as a hardener of epoxy parts of E201, the solution was spread on PTFE dish and heated at 60°C for 4 hours to form a membrane. The membrane thus obtained is denoted as Cs-PWA:E201( $x$ ) where  $x$  is the weight ratio of Cs-PWA to E201. The dispersion of Cs-PWA was observed by using FE-SEM. Thermalgravimetry analysis (TGA) was conducted to study the thermal stability of and the composition the membranes. The proton conductivity of the membranes were investigated by measuring a.c. impedance in the frequency range from 10<sup>6</sup> to 0.1 Hz at 80-160°C with a relative humidity of 20 to 80%.

## Results and Discussions

Membranes Cs-PWA:E201( $x$ ) exhibited good homogeneity, smoothness and flexibility up to  $x = 1.6$ . FE-SEM observation revealed Cs-PWA particles were well dispersed in the matrix. TGA confirmed the thermal stability up to 230°C. Table 1 shows the weight and volume fraction of Cs-PWA in the membranes that were estimated from the results of TGA and density. Figure 1 shows temperature dependence of proton conductivity of Cs-PWA:E201( $x$ ). The proton conductivity was independent of Cs-PWA composition for  $x \leq 0.5$ , while was enhanced by about one order of magnitude for  $x = 1.6$ . As listed in table 1, at  $x = 1.6$ , the volume fraction of Cs-PWA in the membrane was 27% and close to the threshold of percolation network. This means the partial network of Cs-PWA was formed for  $x = 1.6$ . In order to obtain higher proton conductivity, higher incorporation of Cs-PWA is required, which was successfully achieved by increasing the amount of Cs-PWA that were nano-sized by ball milling to improve the dispersion in the matrix. The results on the membrane consisting of the nano-sized Cs-PWA will be reported in the poster.

Table 1. Weight fraction and volume fraction of Cs-PWA in Cs-PWA:E201( $x$ ).

| $x$ | Weight fraction (wt%) | Volume fraction (vol%) |
|-----|-----------------------|------------------------|
| 0.1 | 6.5                   | 1.6                    |
| 0.3 | 28.2                  | 8.6                    |
| 0.5 | 37.1                  | 12                     |
| 1.6 | 61.1                  | 27                     |

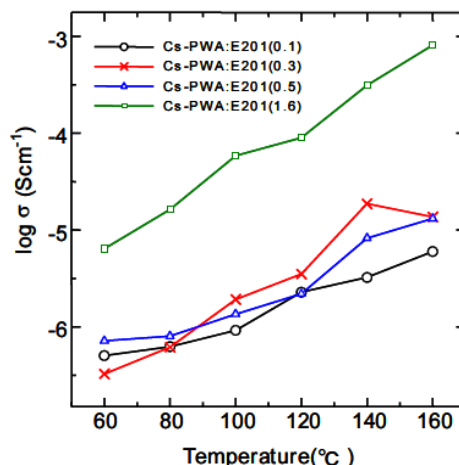


Fig. 1. Temperature dependence of the conductivity for Cs-PWA:E201( $x$ ) under R.H. of 80%.

## References

1. A. Matsuda, et al, *Solid State Ionics*, **178**, 723-727 (2007).

## Coupled dynamics of Au-nanoparticles and surfactants driven by potential control on a Au(111) electrode surface

Kenji Izumi<sup>1</sup>, Takamasa Sagara<sup>2\*</sup>

<sup>1</sup>*Department of Materials Engineering and Molecular Science,  
Graduate School of Science and Technology,*

<sup>2</sup>*Department of Applied Chemistry, Faculty of Engineering,  
Nagasaki University, 1-14 Bunkyo-machi, Nagasaki 852-8521, Japan  
Tel: +81-95-819-2676, E-mail: sagara@nagasaki-u.ac.jp*

### Introduction

Au-nanoparticles (Au-NPs) exhibit various physicochemical and optical characteristics in contrast to bulk Au. If we can regulate reversible changes of assembling structure of Au-NPs on an electrode surface by potential control, the changes may be applicable to novel functions of nano-devices that can electrochemically switch, for example, charging-state and locally-enhanced optical electric field. We previously reported potential-driven dynamic processes of a Au-NP, the surface of which is modified with an adsorption-desorption active terminal group, on a Au(111) electrode [1].

It is known that some surfactants exhibit potential-driven phase transitions of their monolayer-level adsorption layers on a Au single crystal electrode surface [2]. If the phase transition can be coupled with the movements of Au-NPs in coexistence, we may realize enhanced and synchronized dynamics of Au-NPs. In this work, we aim at providing alkanethiol-protected Au-NPs with dynamic interfacial behavior by potential control in the presence of a water-insoluble neutral surfactant or water-soluble anionic one. We describe herein the preliminary examination of aforementioned coupled behavior using the results of electrochemical and spectroelectrochemical measurements.

### Experimental

We used a hexanethiol monolayer-protected Au-NP with a 3.1 nm-average diameter. As the surfactants, octadecanol (C<sub>18</sub>OH) and sodium dodecylsulfate (SDS) were used. An anneal-cooled Au(111) single crystal electrode was brought into horizontal contact with Ar gas/0.05 M KClO<sub>4</sub> solution interface and set in a hanging meniscus (H-M) configuration to make electrochemical and electroreflectance (ER) measurements. These measurements were carried out by the use of a Ag/AgCl/sat-KCl reference electrode in Ar gas atmosphere at room temperature.

## Results and Discussions

For a Au(111) electrode covered with a Au-NP/C<sub>18</sub>OH mixed film, interfacial differential capacitance-potential curve (*C-E* curve) and ER voltammogram (ERV) are shown in Fig. 1. In Fig. 1-A, *C-E* curve shows low capacitances at  $E > 0.0$  V regardless of the existence of Au-NP, indicating that C<sub>18</sub>OH forms a compact adsorbed phase near the potential of zero charge (pzc) of the Au(111) electrode. Small ER signals in this potential region (Fig. 1-B), presumably due to the potential induced change of surface electron density, are in line with the low capacitance. In the range of  $-0.2$  V  $< E < 0.2$  V, a drastic change of *C* value and appearance of an ERV peak reflect the phase transition of C<sub>18</sub>OH adsorbed layer. Even in the coexistence of Au-NPs, capacitance reaches the same value as that for a bare electrode at  $-0.7$  V, indicating simultaneous desorption of Au-NPs with C<sub>18</sub>OH from the electrode surface.

For the Au-NP/SDS system, desorption of both Au-NPs and SDS at negative potentials were observed as in the case of Au-NP/C<sub>18</sub>OH. In contrast, a step increase of capacitance, exceeding the value of the bare electrode, was observed from 0.2 V to more positive potentials in the presence of SDS. This is likely due to charging-discharging of the Au-NPs. Interestingly, this critical onset potential lies in between two phase transition potentials of SDS on a Au(111) electrode.

In summary, movements of Au-NPs directly associated with original phase transition behavior of two different surfactants were not clearly observed. The majority of Au-NPs used in this work may be beyond the smaller size limit exhibiting measurable plasmon absorption. Although ER methods enabled us to shed light in more depth on the interfacial behavior, additional methods to directly track the dynamics of small Au-NPs should be explored.

## References

- [1] T. Sagara, M. Kokubu, *e-J. Surf. Sci. Nanotech.*, **3**, 141 (2005). [2] I. Burgess, C. A. Jeffrey, X. Cai, G. Szymanski, Z. Galus, J. Lipkowski, *Langmuir*, **15**, 2607 (1999).

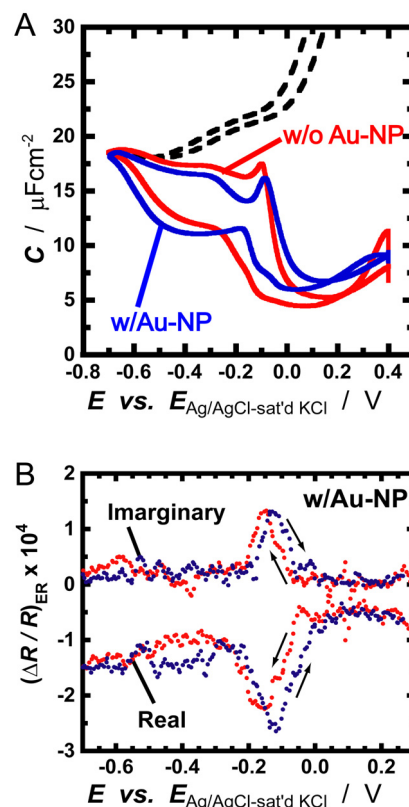


Fig. 1. Response of Au-NP/C<sub>18</sub>OH system at a Au(111) electrode: *C-E* curve (A) and ER voltammogram [ $\lambda = 500$  nm,  $f = 14$  Hz] (B).

## Spectroelectrochemical Study for Dyes Adsorbed on Gold Nano-Rings Immobilized on an ITO Electrode

Gyotaro Imasaki<sup>1</sup>, Takamasa Sagara<sup>2</sup>

<sup>1</sup>*Department of Materials Engineering and Molecular Science,  
Graduate School of Science and Technology*

<sup>2</sup>*Department of Applied Chemistry Faculty of Engineering  
Nagasaki University, 1-14 Bunkyo-machi, Nagasaki 852-8521, Japan  
Tel: +81-95-819-2676, E-mail: sagara@nagasaki-u.ac.jp*

### Introduction

Nobel metal nano-structures exhibit characteristic optical absorption so-called plasmon resonance, resulting in excitation of collective oscillation of free electrons. This absorption is accompanied by enhancement of electromagnetic field in close proximity of the nano-structure. A gold nano-ring is one of the candidate structures which produce enhanced electric fields in both inner and outer ring surface regions independently [1].

The optical properties of nano-structures are affected by surrounding media (*eg.* surface protectants, solvents, and inter-structure interaction) and the charge densities on the structures. When metal nano-structures are immobilized on an electrode surface, one can control the optical properties of the modified electrode by potential [2]. We expect that an electrode/metal-nano-structure/electrolyte solution system forms a specific double-layer electric field, inducing unique Stark effects of coexisting dyes.

In this study, we synthesized gold nano-rings and immobilized them onto an ITO electrode. Spectroelectrochemical measurements such as a constant potential transmission spectral measurement were conducted for tracking the spectral response of the ITO electrode/gold-nano-ring/dye system.

### Experimental Section

A gold nano-ring was synthesized via replacement reaction of a silver nano-plate by gold using  $\text{AuCl}_4^-$  as a precursor ( $3\text{Ag}^0 + \text{AuCl}_4^- \rightarrow \text{Au}^0 + 3\text{Ag}^+ + 4\text{Cl}^-$ ). A silver nano-plate was synthesized by reduction of silver nitrate by sodium borohydride in the aqueous solution containing with polyvinylpyrrolidone (PVP), trisodium citrate, and hydrogen peroxide. Preparation of gold nano-ring was made by addition of  $\text{HAuCl}_4$  aqueous solution to the silver nano-plate dispersion under vigorous stirring. Thus



obtained gold nano-rings were immobilized on an ITO electrode covered with a monolayer of (3-mercaptopropyl)trimethoxysilane by immersing it in the gold nano-ring dispersion. Electrochemical measurements were conducted using a Ag/AgCl/sat-KCl reference electrode and a coiled Au wire counter electrode.

## Results and Discussions

Gold nano-rings synthesized in this study were smaller than 50 nm with circular and triangular shapes (Fig. 1). The dispersion solution contained other shapes as well, such as spherical particle and coin with inner hole of a reduced diameter. Presumably, small gold nano-rings shrank to spherical structures, and replacement reaction occurred at both edge and top faces of silver nano-plate resulted in the reduction of the inner hole diameter.

Spectroelectrochemical response of the ITO/gold nano-ring system was measured in 0.1 M phosphate buffer solution (pH 7.0). As shown in Fig. 2, gold nano-rings on an ITO electrode exhibited a spectral change as a function of the electrode potential. Absorption band around 550 nm was shifted to blue and its absorbance became greater at more negative potentials. This behavior indicates that charging-discharging of the gold nano-ring takes place [2,3].

In the presentation, spectroelectrochemical response of the ITO/gold nano-ring/dye system will be discussed.

## Reference

- [1] J. Aizpurua, P. Hanarp, D. S. Sutherland, M. Käll, G. W. Bryant, F. J. García de Abajo, *Phys. Rev. Lett.*, **90**, 57401 (2003).
- [2] A. Toyota, N. Nakashima, T. Sagara, *J. Electroanal. Chem.*, **565**, 335 (2004).
- [3] M. Giersig, P. Mulvaney, *Langmuir*, **12**, 788 (1996).

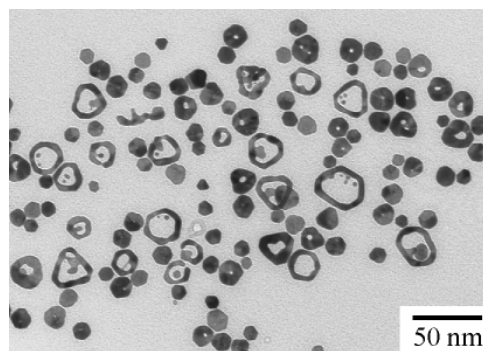


Fig. 1. TEM image of gold nano-ring synthesized in this study. Acceleration voltage: 100 kV.

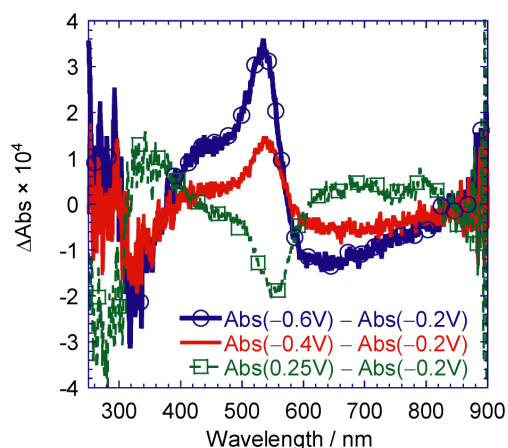


Fig. 2. Difference extinction spectra for an ITO/Au nano-ring electrode at three different constant potentials (base potential: -0.20 V).

**Spatio-temporal observation of potential-driven dynamics of  
*n*-hexadecane liquid thin layer on a Au(111) electrode  
by fluorescence microscopic imaging  
and electroreflectance measurements**

Daisaku Goto<sup>1</sup>, Hirohisa Nagatani<sup>2</sup>, Takamasa Sagara<sup>\*,2</sup>

<sup>1</sup>*Department of Materials Science and Engineering,  
Graduate School of Science and Technology,*

<sup>2</sup>*Department of Applied Chemistry, Faculty of Engineering,  
Nagasaki University, 1-14 Bunkyo-machi, Nagasaki 852-8521, Japan  
Tel: +81-95-819-2676, E-mail: sagara@nagasaki-u.ac.jp*

### **Introduction**

Control of electrode potential drives not only the changes of two-dimensional (2D) molecular distribution on an electrode surface but also the collective movements of the molecules to the direction normal to the surface [1]. Until now, among such dynamic processes as above, behavior of surfactant molecules has been engaged main interest. It has been usually accepted that the potential-driven behavior is largely determined by the interaction between the head group of the surfactant and the electrode surface, because the potential dependence of the behavior is in harmony with that of the constituent molecule of the head group [2,3]. On the contrary, the potential-dependent interaction of a long alkyl chain with the electrode surface has not been directly considered as one of the determining factors. It is of importance to shed light in more depth into the potential dependent behavior of alkanes that can be regarded as the surfactant long alkyl chain constituent molecule.

This work is devoted to the characterization of the potential-driven behavior of long-chain *n*-hexadecane (HD) using *in situ* epi-fluorescence microscopic imaging techniques and electroreflectance (ER) measurements.

### **Experimental**

1,6-diphenyl-1,3,5-hexatriene (DPH) was dissolved in HD as a fluorescent probe. An Au(111) electrode with a HD + DPH deposit was set in a hanging-meniscus (H-M) configuration at Ar gas/0.05 M KClO<sub>4</sub> solution interface in a newly home-designed quartz cell equipped with a bottom optical window. Fluorescence images were captured by CCD camera at 30 frame/s under simultaneous recording of differential

capacitance-potential ( $C-E$ ) curves. ER measurements were conducted at a H-M configuration with a normal incidence by irradiating the incident probe light to the electrode surface.

## Results and Discussions

An order-disorder phase change was observed in  $C-E$  curves for Au(111)/HD/solution interface in the potential range from  $-0.2$  V to  $0.1$  V (**Fig. 1**). Fluorescence images showed a number of bright spots of *ca.*  $20\ \mu\text{m}$  diameters in the dark background around  $-0.7$  V at which  $C$ -value reached that of a bare Au(111) electrode level. It is likely that HD desorbed from the Au(111) surface as micro-droplets and their top height reached the distance being insusceptible to fluorescence quenching by the metal surface. The steep decrease of area-integrated brightness of the image ( $I_{\text{FL}}$ ) was obviously observed in the positive potential scan from the desorption potential, while the change of  $C$ -value in this potential range was subtle. The ER voltammogram exhibited a peak at  $-0.4$  V only in the imaginary part in the positive potential scan when a modulation frequency was as low as 7 Hz. This fact indicates a presence of chemically-reversible but very sluggish process responsive to the low frequency potential modulation. These results of spectroelectrochemical measurements reveal that potential driven dynamic processes of HD are clearly observable as spectroscopic signals even when the processes are silent in electrochemical data. This may reflect dynamic behavior of HD layer extending far away from the electric-double layer region to the bulk of the solution.

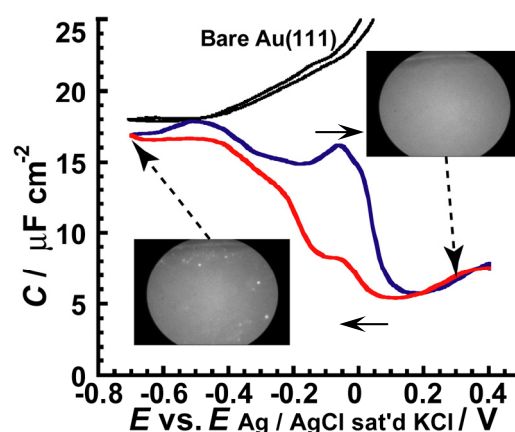


**Fig. 1.**  $C-E$  curve for a Au(111) electrode covered with HD + DPH in 0.05 M  $\text{KClO}_4$  solution at a hanging-meniscus configuration, together with two typical montage images taken from time-lapse epi-fluorescence microscope movie.

## References

- [1] V. Zamylny, I. Zawisza, J. Lipkowski, *Langmuir*, **1995**, *11*, 2242.
- [2] D. Bizzotto, A. M. Alees, J. Lipkowski, R. M. Crindle, *Langmuir*, **1995**, *11*, 3243.
- [3] B. Pettinger, J. Lipkowski, M. Hoon-Koshla, *J. Electroanal. Chem.*, **2001**, *500*, 471.

## Structural Change Effect of Ferritin on the Electrode Reaction

Masato Tominaga, Kota Nakao, Isao Taniguchi

*Graduate School of Science and Technology, Kumamoto University, 2-39-1, Kurokami,  
Kumamoto 860-8555, Japan*

*Tel: +81-96-342-3656, Fax: +81-95-342-3656,*

*E-mail: masato@gpo.kumamoto-u.ac.jp*

### Abstract

The biphasic behavior of peak current vs. temperature in cyclic voltammograms of ferritin immobilized onto poly(L-lysine)(PLL)-modified ITO electrodes was observed. The results of CD and fluorescent measurements indicated that the fine phase transition of ferritin structure occurred around 25 °C. The biphasic behavior of peak current of ferritin would be caused by the fine phase transition of ferritin structure induced by temperature.

### Introduction

Ferritin is an iron-storage protein found in most animals and plants. The outside diameter of ferritin is *ca.* 12 nm, and the cavity diameter is *ca.* 8 nm. The iron uptake and release mechanisms of ferritin are caused by the oxidation and reduction of iron ions (Fe(II)/Fe(III)) in the protein cavity. We have been investigating the redox reaction of ferritin immobilized onto a functionalized electrode surface [1,2]. In the present study, we investigated the effect of the structural change on the electrode reaction of ferritin immobilized onto PLL-modified ITO electrode.

### Experimental

Horse spleen ferritin (Sigma) was purified by size exclusion chromatography to remove free iron ions using a Sephadex G-25 column. Ferritin immobilized PLL-modified ITO electrodes were prepared according to previous reports [1]. Electrochemical measurements were carried out in a phosphate buffer solution (pH 7) under argon atmosphere. An Ag/AgCl (saturated KCl) electrode and a platinum electrode were used as the reference and counter electrodes, respectively.

### Results and Discussion

The well-defined a couple of redox peak of ferritin immobilized PLL-modified electrode were observed at temperature region of 5~50 °C. The redox peak currents depended on temperature. The peak currents vs. temperature showed biphasic behaviors around *ca.* 25 °C, as shown in Fig. 1. The decrease tendency in the slope of current increasing was not due to desorption of ferritin from the electrode surface. It was expected that the biphasic behaviors of peak currents would be due to the structural change in ferritin. In fact, the fine structural change in ferritin was detected by CD and fluorescent measurements, although it is known well that the ferritin structure is significantly stable up to *ca.* 80 °C. From the CD measurements, the decrease in the peak corresponding to  $\alpha$ -helix of ferritin with increasing temperature was detected, which showed biphasic behavior around 25 °C. Furthermore, the intensity in the fluorescence emission peak corresponding to tryptophane of amino acid residue of ferritin with increasing temperature was also detected, which also showed biphasic behavior around 25 °C. The results of CD and fluorescent measurements indicated that fine phase transition of ferritin structure occurred around 25 °C.

Taken into account of redox reaction of ferritin, ion follow passing through the ion channels of ferritin would occur due to charge compensate in the ferritin cavity during the redox of ferritin core (Fig. 2) [2]. The iron flow would be rate-determining step of ferritin redox. The fine phase transition of ferritin structure induced by temperature would influence the iron flow through the ion channels of ferritin.

## References

1. M. Tominaga, K. Soejima, M. Matsumoto, I. Taniguchi, *J. Electroanal. Chem.*, **579**, 51 (2005).
2. M. Tominaga, K. Soejima, I. Taniguchi, *J. Electroanal. Chem.*, **617**, 78, (2008).

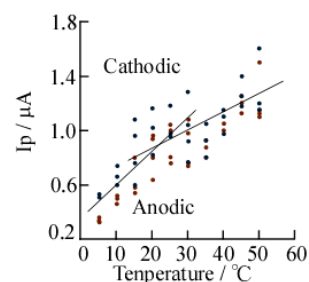


Fig. 1 Anodic and cathodic peak currents obtained from cyclic voltammograms of ferritin immobilized onto PLL-modified ITO electrode as a function of temperature. Potential sweep rate was 50 mV/s. Electrode area was 0.25 cm<sup>2</sup>.

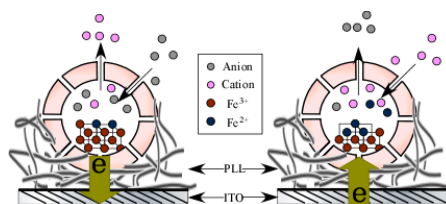


Fig. 2 Schematic representation of ferritin redox reaction on the electrode surface and ion flow during the redox processes.

## One dimensional Kramers-Grote-Hynes-based reaction rate analysis on thermally bleaching process of spirooxazines

Yasuhiro Shigemitsu<sup>1</sup> and Ysushi Ohga<sup>2</sup>

<sup>1</sup>Industrial Technology Center of Nagasaki, 2-1303-8 Omura Nagasaki 856-0026 Japan

<sup>2</sup>Department of Applied Chemistry, Oita University, 700 Danoharu Oita 870-1192 Japan

Tel: +81-957-52-1133, Fax: +81-957-52-1136, E-mail: shige@tc.nagasaki.go.jp

### I. Abstract

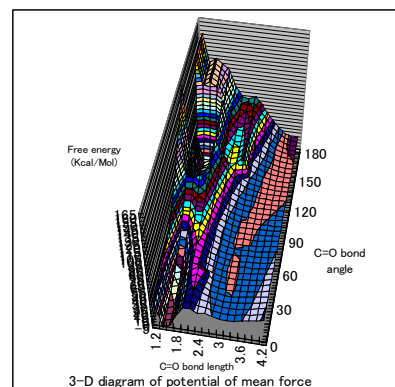
Photochromism of spirooxazines is initiated by fast photo-induced ring-opening reaction on the excited state potential energy surface (PES) accompanied with colouration, followed by slow thermally backward ring-closing reaction on adiabatic ground state PES. We herein report the analysis on the reaction rate using a variation of generalized-Langevin-equation models, i.e., Kramers-Grote-Hynes ( $k_{\text{KGH}}$ ) and Pollak-Grabert-Hanggi ( $k_{\text{PGH}}$ ) within one dimensional freedom. The aim of this presentation is to adequately describe the abnormal turnover incompatible with the Kramers turnover within one dimensional model.

### I. Introduction

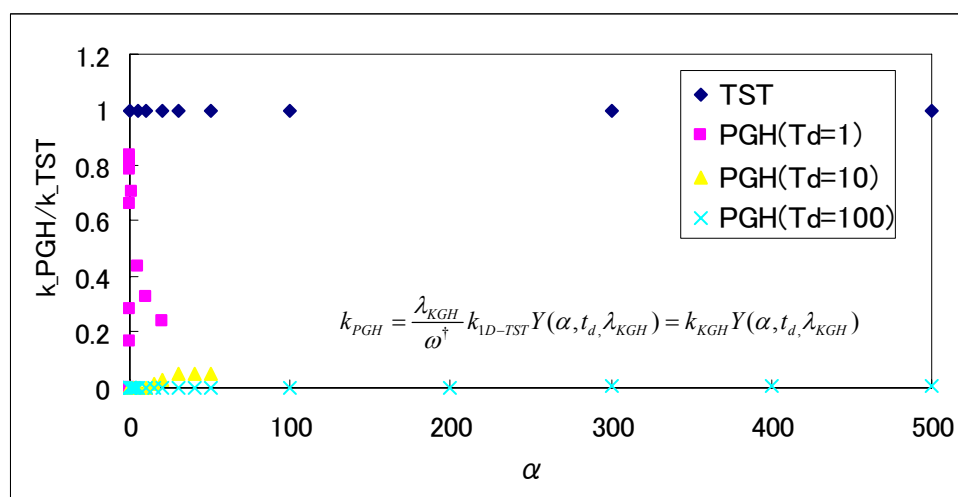
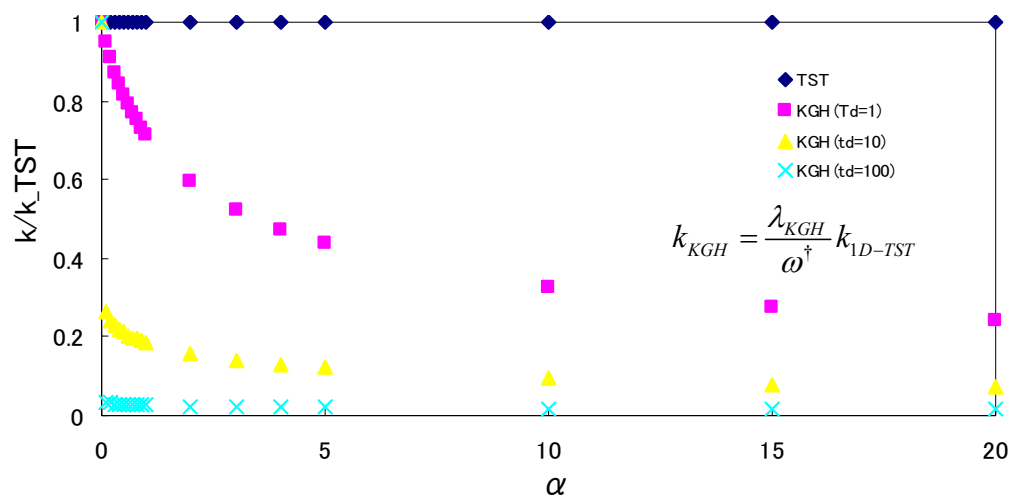
The thermal bleaching mechanism of spirooxazines has been extensively examined from both theoretical and experimental viewpoints. In condensed phase such as in the organic solvent, its reaction rate deviates from that of transition state theory ( $k_{\text{TST}}$ ) under a very high pressure with extremely strong solvent viscosity. Dating back to Kramers theory, the deviation has been analyzed on some theoretical models such as a variant of Fokker-Plank equation, where fast (solute vibration) and slow (solvent fluctuation) mode are independently treated to adequately describe the abnormal behavior of so-called Kramers turnover. Within this model, however, the diffusion equation is described by macroscopic parameters (simple model potential of mean force) and lacks the detailed information on molecular systems. The one dimensional model reported here include only one freedom along the reaction path coordinate and no consideration to decouple several freedom such as slow fluctuation or other non-reactive freedom. The reverse interconversion of spirooxazines is considered to hold strong solute-solvent coupling and expected to be well-described within one-dimensional model.

### II. Results and discussion

We solve the so-called Kramers and Grote-Hynes equations to evaluate the reaction rate. In PGH theory, we furthermore solve the depopulation factor to evaluate the reaction rate. As a solvent friction kernel, we use the Laplace transformed expression of Gaussian-type friction.



The magnitude of friction is regulated by varying the two parameters; the frequency ratio of solute- solvent at the saddle-point and a friction strength parameter ( $\alpha$ ). PGH is useful in uniformly describing the dependency of reaction rate on solvent friction from the range of low-pressure (increasing rate) to that of high pressure limit (decreasing rate). As a figure shows,  $k_{PGH}$  has bell-shaped structure as function of  $\alpha$ , which indicates the energy dissipation is important during the motion along the reaction path.



## References

- [1] H.Kono, Y.Ohga and T.Asano, et al, Phys.Chem.Chem.Phys., 6, 2260 (2004)
- [2] S.Tucker, M.Tuckerman and B.Berne, J.Chem.Phys., 95, 5809 (1991)

## First-principles study on electron transport property through graphene strips

Yoshiyuki Egami<sup>1,\*</sup>, Tomoya Ono<sup>2</sup> and Kikuji Hirose<sup>2</sup>

<sup>1</sup>*Department of Applied Chemistry, Faculty of Engineering, Nagasaki University, 1-14 Bunkyo-machi, Nagasaki 852-8521, Japan*

<sup>2</sup>*Department of Precision Science & Technology and Applied Physics, Graduate School of Engineering, Osaka University, 2-1 Yamada-oka, Suita, Osaka 562-0871, Japan*

\*Tel: +81-95-819-2703, E-mail: egami@nagasaki-u.ac.jp

### Abstract

We perform first-principles calculations for the electron-transport properties of graphene strips suspended between semi-infinite electrodes. The transport properties of graphene strips depending on the type of defects and the transport direction are investigated. The  $\pi$  states of carbon atoms play a main role in the electron transport, while the  $\sigma$  states also contribute to the transport through a graphene strip with a vacancy. Additionally, the electron-transport paths in the armchair direction are much affected by the existence of doped impurity atoms compared with those in zigzag direction.

### Introduction

The carbon-based materials, such as a carbon nanotube and fullerene, are promising for application to new electronic devices that will succeed conventional silicon-based devices, and the nanoelectronics with carbon-based materials is currently one of the rapidly-expanding fields in physics and chemistry. It is important to understand the structural and electronic properties of such materials. Graphene is also attracting interest. In this study, the first-principles electron-transport property calculations are carried out for defect-containing graphene suspended between semi-infinite electrodes and the effects of defects on electrons flowing through graphene are examined.

### Computational Scheme

The computational scheme is based on the real-space finite-difference (RSFD) method<sup>1</sup> within the framework of the density functional theory. The norm-conserving pseudopotential method and the local spin density approximation are employed to represent the ionic Coulomb potential and the exchange-correlation interactions between electrons, respectively. The transport properties of graphene strips sandwiched



between semi-infinite Au jellium electrodes (Fig. 1) are calculated by the overbridging boundary-matching method. The grid spacing is set to be 0.38 a.u., and the distances between the graphene strip and electrodes are taken to be 3.1 (2.8) a.u. for armchair-(zigzag-)direction transport.

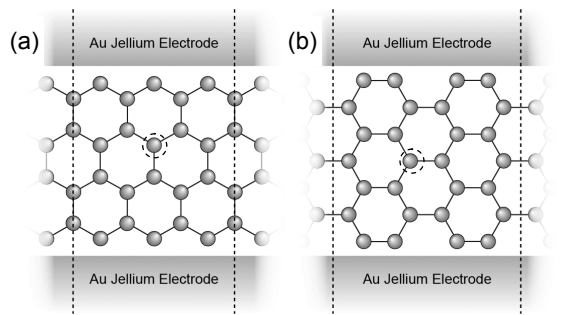


Fig. 1. Schematic view of computational models for (a) armchair-direction and (b) zigzag-direction transport. In calculations, a surrounded atom with dashed circle is replaced by a defect.

## Results and Discussions

In this study, one carbon atom in the graphene strips is replaced by a vacancy or an impurity atom (boron or nitrogen), and the effects of defects on the transport properties are analyzed by comparing the results with those of the perfect model without defects. In the case of the graphene strips without defects, the conductivity is mainly contributed to by the  $\pi$  orbitals, and the  $\sigma$  orbitals play a secondary role. For the graphene strip with a vacancy, a spin polarization is manifested and  $\sigma$ -orbitals of carbon atoms around the vacancy play an important role in the electron transport, although the  $\pi$ -orbitals of carbon atoms mainly contribute to the transport in the other models.

In the impurity-doped graphene strips, the spatial flowing paths of conducting electrons in the zigzag direction are less sensitive to the existence of defects than those in the armchair direction. However, the conductances of the zigzag-direction model are much affected by impurities as well as those of the armchair-direction one. This is caused by the robust features of the conductivities against disorders in the graphene for zigzag-direction transport. Consequently, the effects of impurities on the electron conductivity and transport path are clearly observed in the flowing path for the armchair-direction transport. On the other hand, for the zigzag-direction transport, the transmission probability becomes higher (lower) owing to increasing (decreasing) of  $\pi$  electrons which contribute to the electron transport in the nitrogen- (boron-)doped graphene strip while the current flowing path is insensitive to the impurity atom.

## References

1. K. Hirose, T. Ono, Y. Fujimoto and S. Tsukamoto, *First-principles Calculations in Real-Space Formalism, Electronic Configurations and Transport Properties of Nanostructures*, (Imperial College Press, London, 2005).
2. Y. Egami, *Journal of Computational and Theoretical Nanoscience*, *to be published*.

## Surface Molecular Mobility of Crosslinked Polyurethane by Scanning Force Microscopy

Takeshi Osajima<sup>1</sup>, Shun Matsumura<sup>1</sup>, Suguru Motokucho<sup>2</sup>,  
Ken Kojio<sup>2</sup> and Mutsuhisa Furukawa<sup>1</sup>

<sup>1</sup>Department of Materials and Science, Graduate School of Science and Technology,

<sup>2</sup>Department of Materials Science and Engineering, Faculty of Engineering,

Nagasaki University, 1-14 Bunkyo-machi, Nagasaki 852-8521, Japan

Phone&Fax: +81-95-819-2651 E-mail: furukawa@nagasaki-u.ac.jp

### Introduction

Surface properties of polymer materials are closely related to molecular mobility and chemical composition at the top surface. For the linear polymers, it is revealed that surface molecular mobility is activated in comparison with bulk. However, the study on crosslinked polymers has never done yet. It is inferred that another factors, for example, crosslinking density and dangling chain density, need to be thought to understand. In this study, surface molecular motion of the crosslinked polyurethanes was investigated in terms of their crosslinking density and the number of dangling chains.

### Experimental

Chemically crosslinked polyurethanes (PUs) with different crosslinking density were synthesized from poly(oxypropylene) triol (PPT) and, 4,4'-diphenylmethane diisocyanate (MDI) or tolylene-2,4-diisocyanate (TDI) by a one-shot method. Surface molecular mobility of PUs was investigated using lateral force microscope (LFM) at various temperatures.

### Results & Discussion

In differential scanning calorimetry (DSC) thermograms,  $T_g$  of bulk was clearly observed at around -60 °C for both PPT-TDI- and PPT-MDI-based PUs.  $\alpha$ -Relaxation of the PPT chains was detected in LFM measurement, and the relaxation temperature observed shifted to the lower temperature region in comparison with bulk measurement. This might be attributed to surface localization of dangling chains, decreasing crosslinking density and surface effect. Figure 1 shows temperature dependence of apparent activation energy for  $\alpha$ -relaxation of PUs. Apparent activation energy for surface was much lower than that for bulk. Therefore, it seems reasonable to conclude that the surface molecular mobility of crosslinked polyurethane is activated compared with the bulk one.

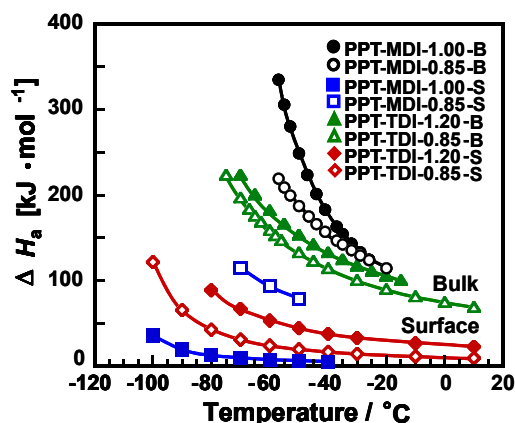


Figure 1. Apparent activation energy of PUs. Nomenclature denotes the name of polyol, diisocyanate, the ratio of  $K = [\text{NCO}]/[\text{OH}]$ . The symbol "S" and "B" represent data for surface and bulk, respectively.

## Temperature Dependent Atomic Force Microscopic Study of Microphase-separated Structure of Polyurethane Elastomers

Yuichi Nishino<sup>1</sup>, Suguru Motokuchō<sup>2</sup>, Ken Kojio<sup>2</sup> and Mutsuhisa Furukawa<sup>1</sup>

<sup>1</sup>*Department of Materials and Science, Graduate School of Science and Technology,*

<sup>2</sup>*Department of Materials Science and Engineering, Faculty of Engineering,*

*Nagasaki University, 1-14 Bunkyo-machi, Nagasaki 852-8521, Japan*

*Phone&Fax: +81-95-819-2651 E-mail: furukawa@nagasaki-u.ac.jp*

### Introduction

Block copolymers form a microphase-separated structure as the result of chain connectivity and the inherent thermodynamic incompatibility between the constituents of the copolymer. Microphase separation of block copolymers results in variety of applications, such as thermoplastic elastomers, compatibilizers, surface modifiers and photoresists. Polyurethane elastomers (PUEs), which are a multi-block copolymer, are widely used as thermoplastic elastomers, and their properties are related to the microphase-separated structure. The purpose of this study is observation of the microphase-separated structure of PUEs using temperature controllable atomic force microscope (AFM).

### Experimental

PUE was synthesized from poly(oxypropylene) glycol (PPG), 4,4'-diphenylmethane diisocyanate (MDI) and 1,4-buthane diol (BD) by a prepolymer method. Hard segment content was 24 wt%. The microphase-separated structure of PUE was investigated using AFM at various temperatures.

### Results & Discussion

Figure 1 shows AFM phase image of PPG-MDI-BD-based PUE at 27 and 117 °C in vacuo. At 27 °C, isolated darker dots surrounded with a brighter matrix were distinctly observed. Since the areal ratio of the darker dots is almost comparable with the hard segment content, it seems likely to consider that the darker and brighter regions correspond to the crystallized hard segment phase and soft segment one, respectively. With increasing temperature, the spherical hard segment domains were changed to a cylinder-like structure. This behavior implies short-range reorganization within the hard segment domains. Furthermore, the microphase-separated structure disappeared above 163 °C. This suggests melting of the hard segment domains.

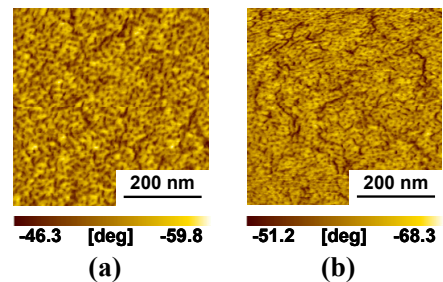


**Figure 1.** AFM phase image of PPG-MDI-BD-based PUE at (a) 27 and (b) 117 °C in vacuo.

## Absorption measurement of Zn atom density during ICP-assisted magnetron sputter-deposition of Al-doped ZnO thin films

Tadashi Iwata<sup>1</sup>, Ryouji Kan<sup>1</sup>, Takashi Shibasaki<sup>1</sup>,

Masanori Shinohara<sup>2</sup>, Yoshinobu Matsuda<sup>2\*</sup>

<sup>1</sup>Graduate School of Science and Technology,

<sup>2</sup>Department of Electrical and Electronic Engineering,

Nagasaki University, Bunkyo 1-14, Nagasaki 852-8521, Japan

\*Tel: +81-95-819-2540, Fax: +81-95-819-2540, E-mail: ymat@nagasaki-u.ac.jp

### Abstract

This paper reports the outlines of hollow cathode (HCD) lamp absorption system for the density measurement of sputtered metal atoms in the inductively coupled plasma (ICP) assisted sputter-deposition process of Al doped ZnO thin films. As a result, absorbance of about 6.5% was obtained, which corresponds to the Zn atom density of  $1.5 \times 10^{12} \text{ cm}^{-3}$ .

### Introduction

For the last few years, we have been investigating oxide thin film deposition process by using inductively coupled plasma (ICP) assisted sputtering, and we have succeeded in depositing high quality AZO thin films with resistivity of around  $10^{-3} \text{ } \Omega \text{ cm}$ . To understand the basic mechanism, however, a lot of information on the number density of gas phase species in various electronic states are required. This paper reports the outlines of HCD lamp absorption system.

### Principle of absorption spectroscopy

Integral of absorption coefficient profile  $k(\nu)$  over the entire frequency range is theoretically given by the following equation

$$\int k(\nu) d\nu = \frac{\lambda^2 g_u AN}{8\pi g_l} \quad (1)$$

where  $\lambda$ : wavelength of absorption line,  $g_u$  and  $g_l$ : statistical weights of upper and lower levels,  $A$ : transition probability. Absorbance  $\alpha$  that can be experimentally determined is given by [1]

$$\alpha \equiv \frac{I_{in} - I_{out}}{I_{in}} = 1 - \frac{\int f_s(\nu) \exp[-k_0 f_a(\nu) l] d\nu}{\int f_s(\nu) d\nu} \quad (2)$$

where  $f_s(\nu)$  and  $f_a(\nu)$ : line profiles of light source and absorber,  $k_0$ : absorption coefficient at line center, i.e.,  $k(\nu) = k_0 f_a(\nu)$ . In low pressure sputtering condition, line profiles are approximated by Gaussian function with Doppler width  $\Delta\nu_D$ . Eventually, atom density is given by the equation

$$N = \left( \frac{8\pi g_l}{\lambda^2 g_u A_{ul}} \cdot \frac{\sqrt{\pi}}{2\sqrt{\ln 2}} \cdot \Delta\nu_D \right) k_0 \quad (3)$$

Figure 1 shows a relation between absorbance  $\alpha$  versus optical thickness  $k_0l$ , which was calculated on Zn I 307.6 nm line for various gas temperature of absorber when source gas temperature is fixed 300K. Since the absorption coefficient at line center  $k_0$  for the 307.6 nm line absorption is very small, we find that 10% absorption requires the Zn density of  $2 \times 10^{12} \text{ cm}^{-3}$  if the absorption length is 0.3 m. To lower the detection limit, we need to utilize the most sensitive absorption line at 213.9 nm.

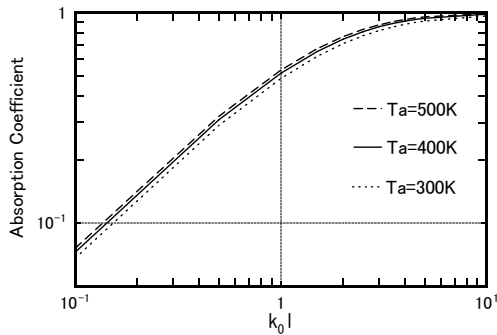


Fig.1 Relation between absorbance and optical thickness calculated for Zn I 307.6 nm line.

### Experimental

Preliminary measurement was done using a set up shown in Fig. 2. The light discharged from HCD Lamp is converted into the collimated beam with the lens of  $f=100\text{mm}$ , and it is made for plasma to pass through the quartz window, and focused again with a lens. After the focused light enters into the spectroscope by the optical fiber, and it converts it into an electric signal with the photoelectric multipliable tube, it is multiplied and recorded with the oscilloscope. Then the density is calculated by comparing the

transmitted light intensities of the HCD lamp for the presence of the electrical discharge for deposition.

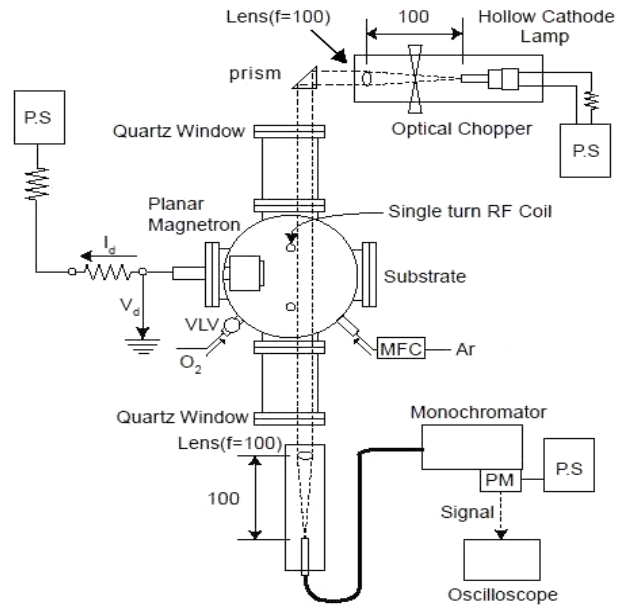


Fig.2 Experimental setup for the absorption measurement of sputtered zinc atoms using a hollow cathode lamp.

### Results

Absorption measurement was done using the Zn I 307.6 nm line for the condition of ICP-RF power of 200W, target RF power (target voltage times target current) of 100W, and working pressure of 30 mTorr. As a result, absorbance of about 6.5% was obtained, which corresponds to the zinc atom density of  $1.5 \times 10^{12} \text{ cm}^{-3}$ .

### Conclusions

Absorbance of about 6.5% was obtained, which corresponds to the zinc atom density of  $1.5 \times 10^{12} \text{ cm}^{-3}$ .

### References

- [1] A. Kono, S. Takashima, M. Hori, T. Goto: Pla. Phy. Lett. 76 (2000) 469.

## Observation of Arcing in DC Magnetron Sputtering of AZO Target

Kazuki Komine<sup>1</sup>, Masanori Shinohara<sup>2</sup>, Yoshinobu Matsuda<sup>2\*</sup>

<sup>1</sup>*Graduate School of Science and Technology, Nagasaki University,  
Bunkyo 1-14, Nagasaki 852-8521, Japan*

<sup>2</sup>*Department of Electrical and Electronic Engineering, Nagasaki University,  
Bunkyo 1-14, Nagasaki 852-8521, Japan*

\*Tel: +81-95-819-2540, Fax: +81-95-819-2540, E-mail: ymat@nagasaki-u.ac.jp

### Abstract

Arcing phenomena was investigated in DC magnetron sputtering of AZO target. Arc count was found to depend on discharge power and working pressure. The arc most frequently occurred at 5mTorr. Velocity of cathode spot was larger for higher pressure.

### Introduction

Mainstream of transparent conductive film has long been indium-doped tin oxide (ITO) in industry. However, the indium which is included in ITO is scarcity metal. Therefore, aluminum doped ZnO (AZO) attracts attention. Arcing (abnormal electrical discharge) to occur during deposition become a problem in sputtering. When the arcing occurs, target surface may melt and fly apart. It may change the thin film character.[1,2] Especially, the arcing is easy to occur on AZO target than ITO target. So we have observed cathode spot in DC magnetron sputtering with poisoning AZO target.

### Experimental

Figure 1 shows the experimental setup. We used a poisoning AZO target (diameter 76mm) so that the arc may easily occur. We used a planar magnetron, in which the center magnetic pole is S, the outside circle magnetic pole is N. Erosion area is a range of radius 8~23mm. We have investigated the discharge power dependence of arc count as a parameter of working pressure using an arc counter. We took a movie of cathode spot with the high speed digital video camera (CASIO EX-FH20BK) that is able to take 1000 frames per second. We took a movie with 420 frames per second in the experiment. The movie was analyzed by Irfan View (free software).

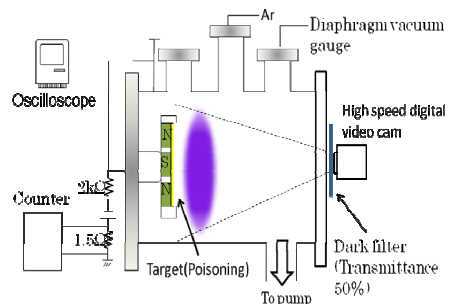


Fig1. Experimental setup

## Results

We found that the cathode spot moves in the direction of  $-\mathbf{J} \times \mathbf{B}$ . Figure 2 shows temporal change of arc count. The result indicates the arc count does not change so much with time. Figure 3 shows the discharge power dependence of arc count as a parameter of working pressure. The result indicates there are typical condition to cause arcing in power and working pressure. Figure 4 shows the discharge power dependence of arc velocity as a parameter of working pressure. The result indicates the arc velocity is larger for higher pressure.

## Conclusions

The cathode spot moves in the direction of  $-\mathbf{J} \times \mathbf{B}$ . Arc count does not change so much with time. Arc count depends on discharge power and working pressure. The arc velocity is larger for higher pressure.

## References

- [1] Andre Anders: Thin Solid Films 502 (2006) 22 – 28.
- [2] Allen L Garner: Appl. Phys. Letters 92, 011505 (2008).

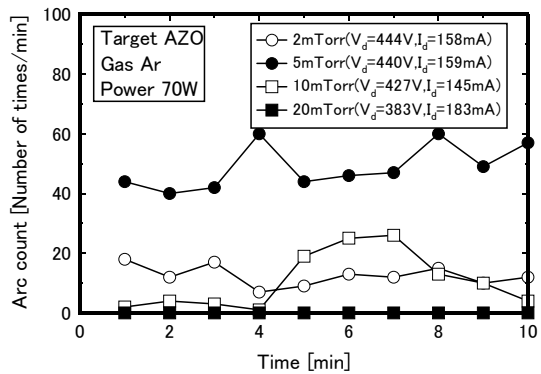


Fig2. Temporal change of arc count.

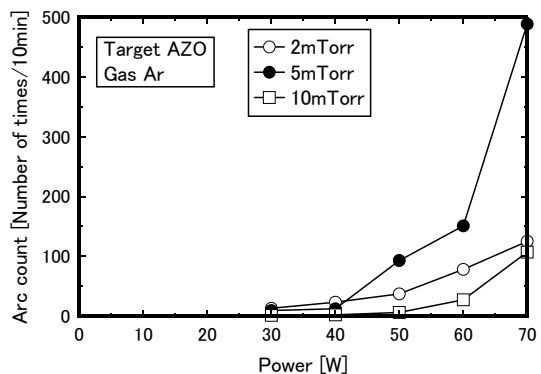


Fig3. Discharge power dependence of arc count as a parameter of working pressure.

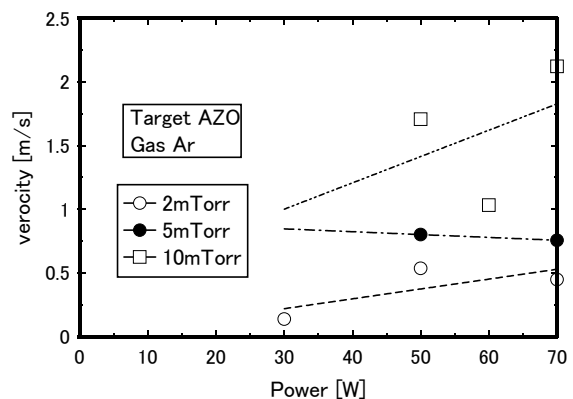


Fig4. Discharge power dependence of arc velocity as a parameter of working pressure.

## Inner Wall DLC Coating of Narrow Tubes by Using the 2<sup>nd</sup> Harmonic ECR Micro Plasma

K. Yan<sup>1</sup>, Y. Nitta<sup>3</sup>, T. Nakatani<sup>3</sup>, K. Okamoto<sup>3</sup>,  
M. Shinohara<sup>2</sup> and H. Fujiyama<sup>1\*</sup>

<sup>1</sup>Graduate School of Science and Technology, Nagasaki Univ.,

<sup>2</sup>Faculty of Engineering, Nagasaki Univ.,

<sup>3</sup>Toyo Advanced Technologies Co. Ltd

Nagasaki University, 1-14 Bunkyo, Nagasaki 852-8521, Japan

E-mail: [plasma@nagasaki-u.ac.jp](mailto:plasma@nagasaki-u.ac.jp)

### Abstract

For the inner surface DLC (Diamond Like Carbon) coating of narrow tubes, we have investigated on CVD & PVD hybrid process with the 2nd harmonic electron cyclotron resonance (ECR) plasmas. From the analysis of Raman spectrum, it was confirmed that DLC could be prepared on the substrate.

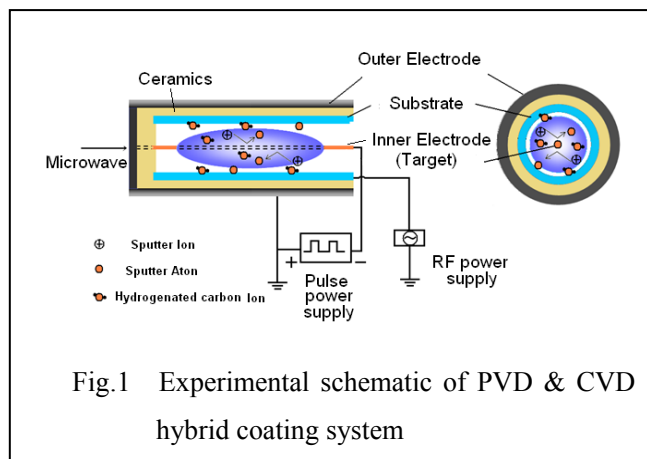
*Keywords:* Micro plasma, ECR, Inner coating, Narrow tube, Hybrid process

### Introduction

For the application to medical and biotechnology field, we are trying to deposit DLC films on an inner wall of narrow tubes with the 2nd harmonic ECR plasma. For the faster deposition, better homogeneity and adhesiveness of the films to the substrate, hybrid process simultaneous using the coaxial sputtering and PECVD was developed. In the present research, we challenged to coat DLC films in an inner wall of narrow tube by using this hybrid process, and analyzed a Raman spectrum of the films.

### Experimental

Figure 1 shows the experimental schematic of developed PECVD & PVD hybrid coating system. The inner electrode is carbon rod target. The outer electrode is electrically grounded. The narrow glass tube was set in contact with the outer electrode. Mixed gas (50%Ar+50%C<sub>2</sub>H<sub>4</sub>) were introduced into





the tube, the operational pressure was 7mTorr. 2.45GHz TEM mode microwave was applied to the inner electrode. Plasma can be generated between the inner and outer electrodes. The CVD process is operated when reactive C<sub>2</sub>H<sub>4</sub> gas is supplied. The coaxial sputtering process is operated when a negative pulse bias voltage is applied to the inner electrode. When the pulse bias voltage was applied in mixed gas, the CVD & PVD hybrid process could be realized simultaneously.

### Results and Discussions

Figure 2 shows the Raman spectrum for the condition of CVD process with RF bias=-30V. The Raman spectrum for the condition of CVD & PVD hybrid process (RF bias =-30V, Pulse bias=-700V) is also shown in Fig.3. From these results, it was found that DLC films could be prepared by the hybrid process.

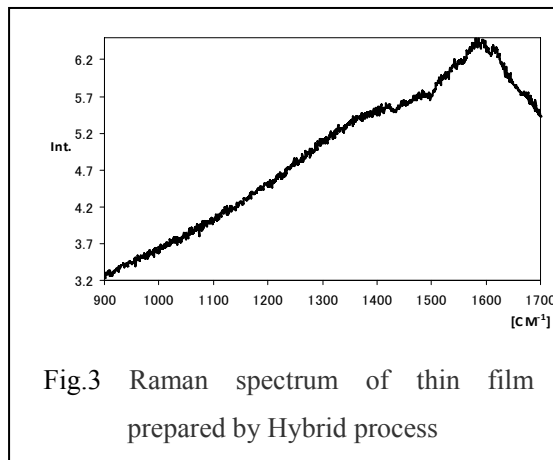
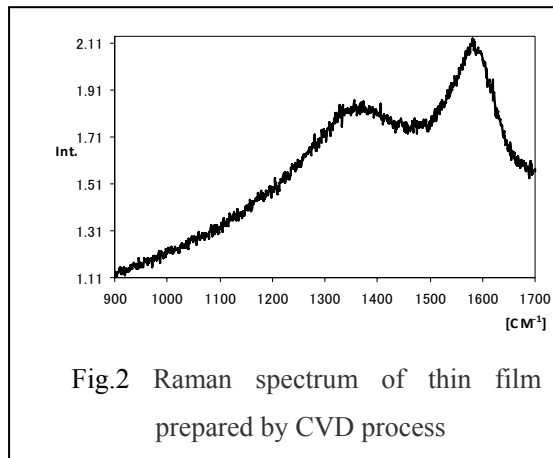
By comparison with both spectra, it is found that I<sub>D</sub>/I<sub>G</sub> ratio in Fig.3 is larger than that in Fig.2. In fact, sp<sup>3</sup> structure of the films by the present CVD & PVD hybrid process seems to be larger than that prepared by CVD process. Further study is needed to understand the reason why.

### Conclusions

We have developed new method for inner surface DLC coating of narrow tubes by using CVD & PVD hybrid process in the 2nd harmonic ECR plasmas. It was found that DLC film could be prepared by using CVD & PVD hybrid process.

### References

1. S.Yamamoto . Optics and Tribology, Vol.41, No.9, p.760(1996)



## CVD · PVD Hybrid DLC Coating to Extra Fine Wire by Quadrupole Magnetron Plasmas

○S. Yoshitsune<sup>1</sup>, S. Nishiyama<sup>2</sup>, N. Iwamoto<sup>2</sup>,  
Y. Tokunaga<sup>2</sup>, M. Shinohara<sup>3</sup> and H. Fujiyama<sup>1</sup>

<sup>1</sup>*Graduate School of Science and Technology, Nagasaki University.*

<sup>2</sup>*Japan Fine Steel Co., Ltd.,* <sup>3</sup>*Faculty of Engineering, Nagasaki University,*

*1-14 Bunkyo-machi, Nagasaki 852-8521, Japan*

*E-mail: d707049j@cc.nagasaki-u.ac.jp*

### Abstract

It was investigated that characteristics of DLC thin films deposited to extra fine wire by CH<sub>4</sub> gas, Ar gas and CH<sub>4</sub>/Ar gas mixtures. It was found that the characteristics of films are change depending on mixture rate of the gases.

### Key Words

DLC, Quadrupole magnetron plasmas, CVD · PVD Hybrid Process, Extra Fine Wire

### Introduction

We forward this experiment for following two purposes. First target is biocompatibility addition to surface of guide wire in medical field. Second target is making target wire for coating to inner wall of fine canal.

So, this experimental purpose is to deposit DLC thin film that has high hardness, smooth surface and biocompatible to extra fine wire of several hundred micro meters in diameter. We aim at improvement of adhesion and uniformity of film by using quadrupole magnetron plasmas and CVD · PVD hybrid coating method. quadrupole magnetron plasmas was developed by Professor H.Fujiyama and more for optical fiber coating. [1] CVD · PVD hybrid coating method is using by both CVD and PVD method. In this paper, we tried DLC coating to extra fine wire by changing gas mixing ratio of Ar and CH<sub>4</sub>.

### Experimental

Figure 1 shows electrode holder and electrode structure of the quadrupole magnetron plasmas. Four carbon electrodes (outer diameter ; 4mm) were arranged in the square, and the hole to pass the wire through the center of

square was opened. The four electrodes was applied 60Hz AC power supply. It is same voltage that the electrodes were arranged in the diagonal position. The wire (outer diameter ; 300  $\mu$  m , length ; 200mm) was treated mirror finish and caught be apply negative DC voltage. The chamber was twisted by solenoidal coil and the quadrupole magnetron plasmas were generated by 630 Gauss magnetic field. We deposited with this setup while changing gas mixing ratio as needed. In this paper, we report results of films by using PVD method by Ar, CVD method by CH<sub>4</sub> and Hybrid coating method by Ar/CH<sub>4</sub> gas mixture. The experimental condition is shown in Table.1.

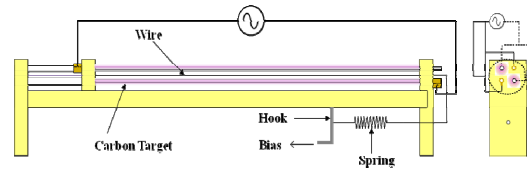


Fig.1 Coating Method for Extra Fine Wire Coating

Table.1 Experimental Condition

|                   |                 |           |
|-------------------|-----------------|-----------|
| Pressure          | 300[mTorr]      |           |
| Gas               | CH <sub>4</sub> | 100[sccm] |
|                   | Ar              |           |
| Discharge Voltage | 280[V]          |           |
| Bias Voltage      | -100[V]         |           |
| Magnetic Field    | 630[Gauss]      |           |
| Deposition Time   | 30[min.]        |           |

## Results and Discussions

Figure 2 shows raman spectra of films with hybrid coating system. It was found that DLC was deposited by CH<sub>4</sub>: 50sccm, Ar: 50sccm and CH<sub>4</sub>: 75, Ar: 25sccm. But it was found that Graphite was deposited by CH<sub>4</sub>: 25, Ar: 75sccm.

Figure 3 shows SEM image of film with hybrid coating system (CH<sub>4</sub>: 50sccm, Ar: 50sccm). It was found that the uniformity of the films with hybrid coating system is higher than the films with CVD and PVD.

## Conclusions

It was found that the characteristics of films are change depending on mixture rate of the gases. In this experiment, I think the high uniformity and high adhesion DLC coating method to extra fine wire is an advantage for hybrid coating system over CVD and PVD.

## Reference

[1] T. Kashima, Y. Matsuda and H. Fujiyama: *Materials Science & Engineering*, Vol.A139 pp.79-84 (1991).

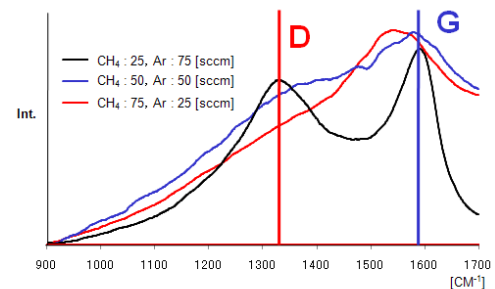


Fig.2 Raman Spectra of Films with Hybrid Coating System

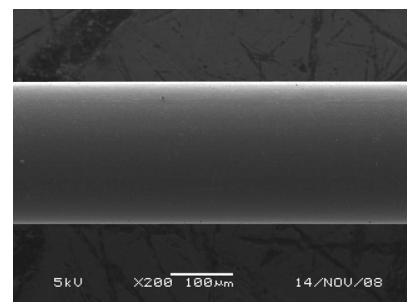


Fig.3 SEM Image of Film with Hybrid Coating System (CH<sub>4</sub>: 50sccm, Ar: 50sccm)

## Generation of Micro Plasma Surrounded by Solid Wall for Sub-ECR Condition

A.Yukishige<sup>1</sup>, H. Fujiyama<sup>1</sup> and M. Shinohara<sup>2</sup>

<sup>1</sup>Graduate School of Science and Technology

<sup>2</sup>Faculty of Engineering, Nagasaki University

*1-14 Bunkyo Nagasaki, 852-8521, Japan*

e-mail:d707240k@cc.Nagasaki-u.ac.jp

### Abstract

Microsize plasma sources for the sub ECR condition have been investigated at low-pressure range less than 0.1Torr. It is found that the 2.45GHz microwave discharge could easily occurred by the minimum ignition power at just below of ECR magnetic flux density in narrow space surrounded by solid wall.

**Keywords** Microplasma, Sub-ECR, Minimum Ignition Power

### Introduction

Low-pressure microplasma generation has been attempted to perform the inner coating of narrow tube by the sputtering process. We are developing the low-pressure microplasma to realize the inner coating of narrow tube by the sputter processing. In the present paper, we will report on the results of minimum Ignition power between the 2<sup>nd</sup> harmonic ECR and ECR conditions

### Experiments

Figure 1 shows the experimental setup. The Microwave source of 2.45GHz is emitted in the TEM mode. so that the microwave can propagate through metallic tube of any size.

The diameter of an inner electrode is 5mm, and the gap length has been kept by outer electrode of 16~9mm of diameter. And the plasma generation point is located about 25mm from

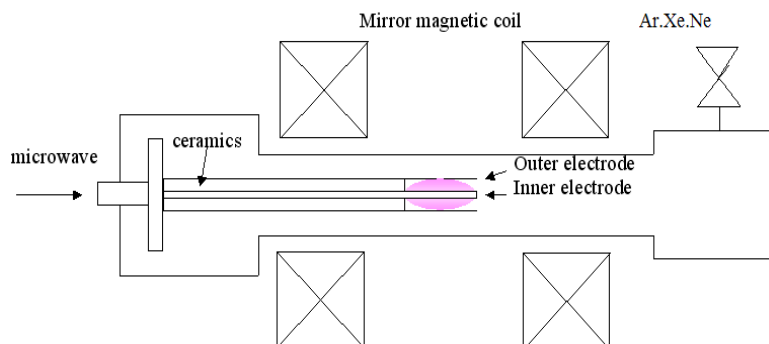


Fig1 experimental setup

the edge of the electrodes. It is located in the center of the mirror magnetic coil. A ceramics is inserted other than the portion of the plasma generation. The minimum ignition power was determined by plasma discharge measurements

## Results and Discussions

As a result of experiments, we succeeded the microplasma generation for the low pressure conditions of 10mTorr. Figure 2 shows that the magnetic field dependence of the minimum ignition power in Ar, Xe and Ne gases. The plasma has been mainly generated for the condition of Sub- ECR ( $\omega_c/\omega=0.8\sim0.9$ ). In the figure, it is found that the minimum ignition power is less than 5W in Sub-ECR condition. It seems that the determination of minimum ignition power was inferred the collision cross-section of each gas for high pressure condition, and the ionization energy of gas in low pressure condition.

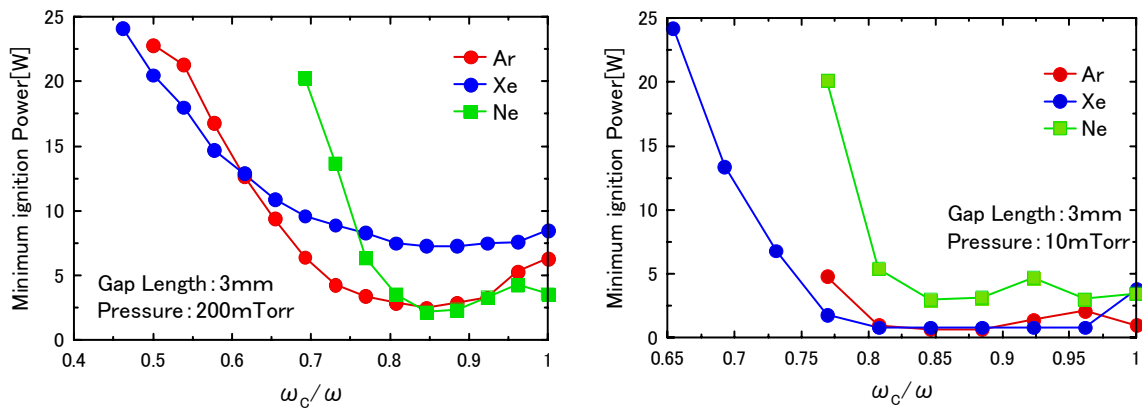


Fig.2 Magnetic flux density dependence of minimum Ignition in Ar, Xe and Ne gases for 200mTorr and 10mTorr.

## Conclusions

The purpose of this research is the low-pressure micro plasma generation for the inner coating of narrow tubes. As the result of the minimum ignition power measurement, for the gap length of 5.5~2.0mm, the minimum ignition power for plasma generation has been confirmed at Sub-ECR conditions ( $\omega_c/\omega=0.8\sim0.9$ ), rather than the second harmonic ECR or ECR conditions.

## Electrodeposition Process of Zn-Te Compound Semiconductors

Y. Kawanaka<sup>1</sup>, T. Ohgai<sup>2\*</sup>, K. Takao<sup>2</sup>, M. Mizumoto<sup>2</sup>, A. Kagawa<sup>2</sup>,  
Y. Tanaka<sup>3</sup> and S. Sumita<sup>3</sup>

<sup>1</sup>Graduate School of Science & Technology, <sup>2</sup>Department of Materials Science and Engineering,

<sup>1,2</sup>Nagasaki University, 1-14 Bunkyo-machi, Nagasaki 852-8521, JAPAN

<sup>3</sup>TDK Corporation, 2-15-7 Higashi-Ohwada, Ichikawa-shi, Chiba, 272-8558, JAPAN

\*Tel/Fax: +81-95-819-2638, E-mail: ohgai@nagasaki-u.ac.jp

### Abstract

Zn-Te compound semiconductors were synthesized in aqueous solution using electrodeposition technique. During the co-deposition of Zn and Te, under potential deposition (UPD) of Zn was observed. By rising the solution temperature up to 353 K, UPD of Zn was promoted by formation of Zn(OH)<sub>2</sub>. Band gap energy of Zn-Te films annealed at 573 K was close to 2.26 eV.

**Keywords:** Zn, Te, semiconductor, UPD, electrodeposition

### Introduction

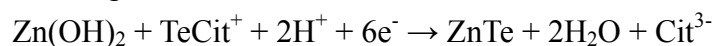
II-VI compound semiconductors (ZnO, ZnS, ZnSe, ZnTe, etc.) with wide band gap energy can be applied to the opto-electronic devices such as light emission devices and photovoltaic solar cells. Among of the II-VI compound semiconductors, ZnTe can be applied to green light emission devices (ca. 550 nm) and photovoltaic solar cells because the band gap energy of ZnTe is 2.26 eV. Te can be electrodeposited from acidic aqueous solution [1] and is not harmful elements such as As, Cd, Pb and Se. In this paper, electrodeposition process of Zn-Te compound semiconductors from acidic aqueous solution was studied.

### Experimental

Aqueous electrolytic solutions were synthesized from zinc sulfate, tellurium oxide and citrate acid (or malic acid). The solution pH was adjusted to 5.0 by adding sulfuric acid and sodium hydroxide and the solution temperature was kept to 353K. A glass sheet coated with ITO, a gold wire and Ag/AgCl electrode were used as a cathode, an anode and a reference electrode. Optimum condition for Zn-Te deposition was determined by the cathodic polarization curves measured at a wide potential range. Phase, structure and chemical composition of electrodeposited Zn-Te was investigated by using XRD and EDX. Band gap energy of Zn-Te electrodeposited on ITO was estimated by using UV spectrophotometer.

## Results and Discussions

Figure 1 shows cathodic polarization curves for Zn-Te electrodeposition. The polarization curves obtained from the solution containing  $\text{H}_3\text{BO}_3$  (No.2) and the solution bubbled by blowing  $\text{N}_2$  gas (No.3) are also shown in the figure.  $\text{H}_3\text{BO}_3$  in the solution acts as pH buffer substance and  $\text{N}_2$  gas in the solution prevents  $\text{TeCit}^+$  ions from oxidation. At the potential of ca.  $-0.2$  V,  $\text{H}^+$  ions began to be reduced. With increasing the current up to  $10^{-6}$  A, the potential polarized to around  $-0.5$  V and Te began to deposit. With increase in the current over  $10^{-5}$  A, the potential polarized from  $-0.5$  V to  $-1.0$  V. In the potential range, pH in the vicinity of cathode can increase up to around 6 due to the diffusion limit of  $\text{H}^+$  ions and  $\text{TeCit}^+$  ions, then  $\text{Zn}(\text{OH})_2$  forms in the vicinity of cathode [2]. Electrodeposition of ZnTe will proceed by Zn UPD due to the formation of  $\text{Zn}(\text{OH})_2$  as the following reaction.



Zn-Te films deposited in the potential range from  $-0.8$  V to  $-0.9$  V mainly contained ZnTe phase with stoichiometric composition. Furthermore, with increase in the current more than  $10^{-4}$  A, the potential polarized to less-noble than  $-1.0$  V. In the potential range, massive metallic Zn began to deposit from  $\text{Zn}^{2+}$  ions.

Band gap energy of as-deposited Zn-Te films was less than 1.5 eV. On the other hand, the band gap energy of Zn-Te films annealed at 573 K was close to 2.26 eV, which is ideal value of ZnTe.

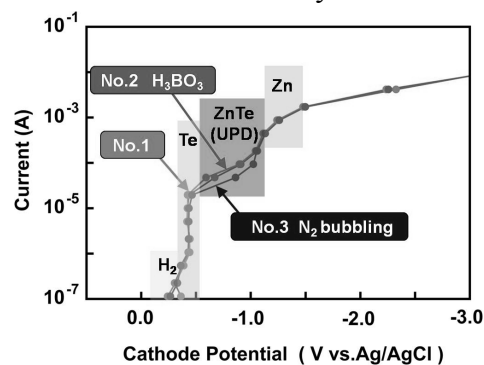


Fig.1. Cathodic polarization curves for Zn-Te electrodeposition. (No.1: standard solution, No.2: solution containing  $\text{H}_3\text{BO}_3$ , No.3: solution bubbled by blowing  $\text{N}_2$  gas.)

## Conclusions

Optimum deposition potential to obtain ZnTe single phase was determined to the range from  $-0.8$  V to  $-0.9$  V. Zn UPD due to the formation of  $\text{Zn}(\text{OH})_2$  promoted the electrodeposition of ZnTe with stoichiometric composition. By annealing the electrodeposited Zn-Te films, the band gap energy increased up to around 2.26 eV.

**Acknowledgements:** This work was supported in part by Japan Society for the Promotion of Science (Grant-in-aid for Scientific Research C : No.19560734), The President's Discretionary Fund of Nagasaki University, Yazaki Memorial Foundation for Science & Technology and TDK Corporation.

## References

- 1: T. Ohgai, L. Gravier, X. Hoffer and J.-Ph. Ansermet, *J. Appl. Electrochem.*, **35**, 479 (2005)
- 2: H. Nakano, T. Ohgai, H. Fukushima, T. Akiyama and R. Kammel, *METALL*, **55**, 676 (2001)

## Magnetic Property of Electrodeposited Ni-W, Ni-Mo and Ni-Cr Alloys

T. Fujimaru<sup>1</sup>, T. Ohgai<sup>2\*</sup>, K. Takao<sup>2</sup>, M. Mizumoto<sup>2</sup>, A. Kagawa<sup>2</sup>,  
Y. Tanaka<sup>3</sup> and S. Sumita<sup>3</sup>

<sup>1</sup>Graduate School of Science & Technology, <sup>2</sup>Department of Materials Science and Engineering,

<sup>1,2</sup>Nagasaki University, 1-14 Bunkyo-machi, Nagasaki 852-8521, JAPAN

<sup>3</sup>TDK Corporation, 2-15-7 Higashi-Ohwada, Ichikawa-shi, Chiba, 272-8558, JAPAN

\*Tel/Fax: +81-95-819-2638, E-mail: ohgai@nagasaki-u.ac.jp

### Abstract

Ni-W, Ni-Mo and Ni-Cr nano-crystalline alloys have been electrochemically fabricated from aqueous solution. With increasing in W, Mo and Cr content in deposit, the crystal grain size decreased and the lattice constant increased. The deposited alloys composed of nano-crystalline  $\gamma$  solid solution, which was thermodynamically non-equilibrium phase. With increase in W, Mo and Cr content in deposit, magnetic coercive force of the alloy decreased down to around 10 Oe.

**Keywords:** *electrodeposition, Ni, W, Mo, Cr, magnetic property, nano-crystal*

### Introduction

W, Mo and Cr alloys show excellent physical and chemical properties, which can be applied to excellent wear-resistance, heat-resistance and corrosion-resistance materials. Conventionally, the production process of W, Mo and Cr bulk alloys requires high temperature and high vacuum conditions. On the other hand, W, Mo and Cr can co-electrodeposit from an aqueous solution with the iron-group metals, such as Ni, Co, and Fe as fine crystalline alloys even in room temperature. Super fine crystalline or amorphous state alloys based on iron-group metals show an excellent magnetic property with high permeability, which can be applied to high sensitive magnetic field sensors [1, 2]. In this paper, the crystal structure and soft magnetic property of electrodeposited Ni-W, Ni-Mo and Ni-Cr alloys were studied.

### Experimental

Ni-W (Ni-Mo) alloy was electrodeposited from an aqueous solution containing NiSO<sub>4</sub>, Na<sub>2</sub>WO<sub>4</sub> (Na<sub>2</sub>MoO<sub>4</sub>) and citric acid, while Ni-Cr alloy was electrodeposited from an aqueous solution containing NiCl<sub>2</sub>, CrCl<sub>3</sub>, H<sub>3</sub>BO<sub>3</sub>, HCOONH<sub>4</sub> and H<sub>2</sub>NCH<sub>2</sub>COOH. was used as, while Cu sheet, Au wire and Ag/AgCl electrode were used as a cathode, an anode and a reference electrode. The alloy composition was determined by EDX and crystal structure of the alloy was analyzed by XRD. Magnetic hysteresis loops of the alloys were measured by VSM.



## Results and Discussions

XRD patterns obtained from electrodeposited pure Ni, Ni-Mo (a), Ni-W (b) and Ni-Cr (c) alloy films were shown in Fig.1. The main peaks in XRD patterns obtained from pure Ni corresponds to (111) reflection planes of fcc Ni phase composed of large crystals. The  $\gamma$  (111) peaks obtained from Ni-Mo, Ni-W and Ni-Cr alloys became broader and shifted to lower diffraction angle with an increase in Mo, W and Cr content in the alloy. These results suggest that the crystal grains are refined and the lattice constant is

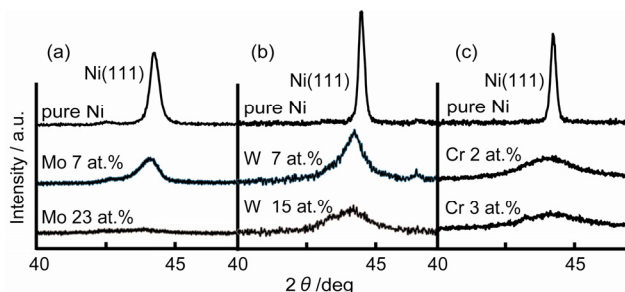


Fig.1. XRD patterns obtained from electrodeposited pure Ni, Ni-Mo, Ni-W and Ni-Cr alloys.

increased with increase in Mo, W and Cr content. Ni-23at%Mo, Ni-15at%W and Ni-3at%Cr alloys consisted of very small crystals with the diameter of several nano-meters.

Dependence of Mo, W and Cr content in the electrodeposited alloys on the magnetic coercive force is shown in Fig.2. With increasing in Mo, W and Cr content, the coersivity decreased down to around 10 Oe, while that of pure Ni was ca. 100 Oe.

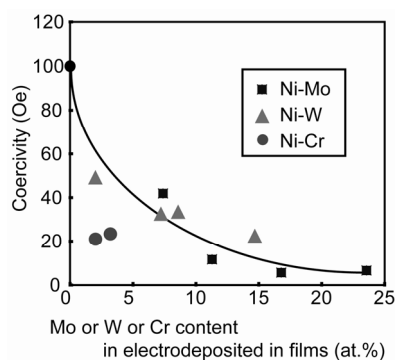


Fig.2. Relationship between Mo or W or Cr content in alloys and coercivity.

## Conclusions

With increasing W, Mo and Cr content in deposits, crystal grain size of Ni-W, Ni-Mo and Ni-Cr alloys decreased and the lattice constant increased. These alloys formed a  $\gamma$  solid solution with nano-crystals. Since the magneto-crystalline anisotropy energy decreased due to the decreasing crystal grain size, magnetic coercive force of these alloys decreased down to ca. 10 Oe with increase in W, Mo and Cr content.

**Acknowledgements:** This work was supported in part by Japan Society for the Promotion of Science (Grant-in-aid for Scientific Research C : No.19560734), The President's Discretionary Fund of Nagasaki University, Yazaki Memorial Foundation for Science & Technology and TDK Corporation.

## References

1. T. Ohgai, I. Enculescu, C. Zet, L. Westerberg, K. Hjort, R. Spohr and R. Neumann, *J. Appl. Electrochem.* **36**, 1157 (2006)
2. T. Ohgai, K. Hjort, R. Spohr and R. Neumann, *J. Appl. Electrochem.* **38**, 713 (2008)

## Electrochemical Synthesis of Zn-Al-based Layered Double Hydroxides Intercalated with 4-hydroxy-3-methoxy Cinnamic Acid as a UV-ray Absorbent

Naoyuki Hario<sup>1</sup>, Kai Kamada<sup>2</sup>, Takeo Hyodo<sup>1</sup>, Yasuhiro Shimizu<sup>2</sup>,  
and Makoto Egashira<sup>2</sup>

<sup>1</sup>Graduate School of Science and Technology

<sup>2</sup>Department of Materials Science and Engineering, Faculty of Engineering  
Nagasaki University, 1-14 Bunkyo-machi, Nagasaki 852-8521, Japan

\*Tel: 81-95-819-2645, Fax: 81-95-819-2643, E-mail: d708100k@nagasaki-u.ac.jp

### Abstract

One-step electrochemical synthesis of Zn-Al-based layered double hydroxides intercalated with 4-hydroxy-3-methoxy cinnamic acid as a UV-ray absorbent (Zn-Al/HMCA LDH) was attempted in this study. Among various preparation conditions, it was confirmed that HMCA was intercalated into the interlayers of Zn-Al-based layered double hydroxide (Zn-Al LDH) by potentiometric electrolysis at -1.5 V for 1 h at RT. The Zn-Al/HMCA LDH films prepared on a Pt plate showed an excellent UV-ray absorption property.

**Keywords:** Layered double hydroxide, intercalation, 4-hydroxy-3-methoxy cinnamic acid, UV-ray absorbent

### Introduction

Layered double hydroxides (LDH) are very promising in various fields such as catalysis, ion exchange and drug delivery systems [1]. Among them, Zn-Al LDH has received recently considerable attentions, because various functional organic molecules can be intercalated into the interlayers. Generally, LDH is prepared by co-precipitation with constituent metal salts in an aqueous solution. However, it is very difficult to synthesize Zn-Al LDH intercalated with functional organic molecules directly by such a chemical method. On the other hand, electrochemical synthesis may allow us one-step synthesis and compositional control of Zn-Al LDH intercalated with functional organic molecules. Therefore, electrochemical synthesis of Zn-Al/HMCA LDH films on a Pt working electrode has been attempted in this study.

### Experimental

Zn-Al/HMCA LDH films were electrochemically prepared on the surface of the Pt electrode (area:  $1 \times 1 \text{ cm}^2$ ) masked by masking tape as follows. After  $\text{Al}(\text{NO}_3)_3 \cdot 9\text{H}_2\text{O}$  and  $\text{Mg}(\text{NO}_3)_2 \cdot 6\text{H}_2\text{O}$  were dissolved in deionized water ( $\text{Al}^{3+}$ : 14.8 mM,  $\text{Mg}^{2+}$ : 7.4 mM), the solution was mixed with a 44.4 mM HMCA ethanol solution. The Zn-Al/HMCA LDH film was obtained by potentiostatic electrolysis at -1.5~-0.4 V for 1 h in the above mixed solution at RT, using a Pt counter electrode and a saturated Ag/AgCl reference electrode. As a reference, a LDH film without HMCA (Zn-Al LDH) was also prepared in a solution without HMCA. Crystalline structures of the samples obtained were analyzed by XRD, intercalation behavior of HMCA in the Zn-Al/HMCA LDHs was estimated by FT-IR, and their optical properties were measured by UV-VIS diffuse

reflectance spectroscopy.

## Results and Discussion

Figure 1 shows XRD patterns of Zn-Al LDH and Zn-Al/HMCA LDH films, which were prepared on a Pt electrode by electrolysis at -1.2 V and -1.5 V, respectively. The Zn-Al LDH had a developed layer structure with a basal spacing ( $d_{003}$ ) of ca. 0.86 nm, which corresponded to the sum of the thickness of ionic  $\text{NO}_3^-$  (0.38 nm) and that of a brucite-like layer (0.48 nm) [1]. On the other hand,  $d_{003}$  of Zn-Al/HMCA LDH was ca. 1.64 nm and thus the interlayer distance is ca. 1.16 nm, which is similar to the molecular length of HMCA. Figure 2 shows a FT-IR spectrum of Zn-Al LDH/HMCA. The spectrum was characterized with asymmetric and symmetric stretching vibrations of carboxyl group at 1511 and 1429  $\text{cm}^{-1}$ , respectively, along with O-H stretching of hydroxyl group and deformation vibration of  $\text{H}_2\text{O}$  at 3330 and 1637  $\text{cm}^{-1}$ , respectively. From these results, HMCA was suggested to be intercalated into the interlayer spaces of Zn-Al LDH.

UV-VIS diffuse reflectance spectra of Zn-Al LDH and Zn-Al/HMCA LDH are shown in Fig. 3. Zn-Al LDH could hardly absorb UV ray in the range of 250~400 nm. In contrast, Zn-Al/HMCA LDH showed an excellent UV-ray shielding ability, suggesting that HMCA was successfully fixed in the interlayer spaces of Zn-Al LDH.

## Conclusions

HMCA was intercalated into interlayer spaces of Zn-Al LDH by simple potentiometric electrolysis, and the ZnAl-LDH/HMCA film prepared on a Pt

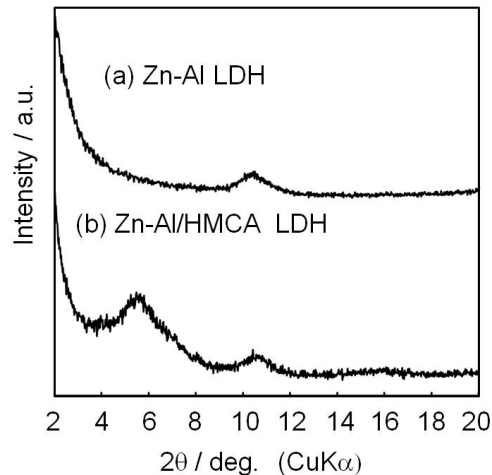


Fig. 1 XRD patterns of LDH thin films; (a) Zn-Al LDH prepared at -1.2 V and (b) Zn-Al/HMCA LDH prepared at -1.5 V.

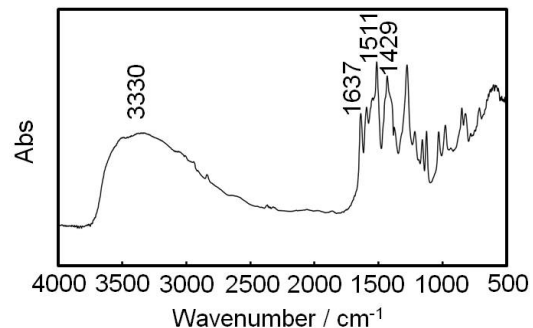


Fig. 2 FT-IR spectrum of a Zn-Al/HMCA LDH film.

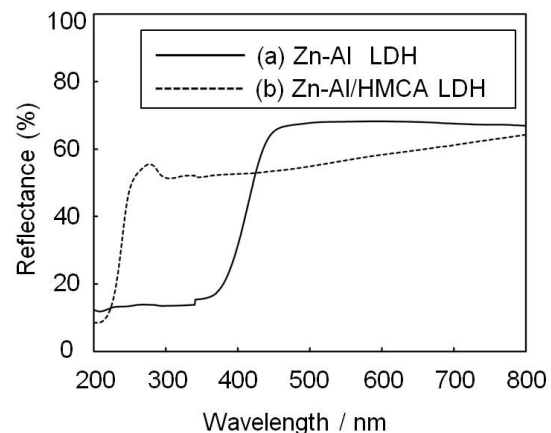


Fig. 3 UV-VIS diffuse reflectance spectra of (a) Zn-Al LDH and (b) Zn-Al/HMCA LDH films.

## Reference

1. W. Sun et al., *Mater. Chem. Phys.*, **107**, 261–265 (2008).